

General Disclaimer

One or more of the Following Statements may affect this Document

- This document has been reproduced from the best copy furnished by the organizational source. It is being released in the interest of making available as much information as possible.
- This document may contain data, which exceeds the sheet parameters. It was furnished in this condition by the organizational source and is the best copy available.
- This document may contain tone-on-tone or color graphs, charts and/or pictures, which have been reproduced in black and white.
- This document is paginated as submitted by the original source.
- Portions of this document are not fully legible due to the historical nature of some of the material. However, it is the best reproduction available from the original submission.

(NASA-CR-169670) MECHANISMS OF
DEVITRIFICATION OF GRAIN BOUNDARY GLASSY
PHASES IN Si₃N₄ MATERIALS Summary Technical
Report (Florida Univ.) 129 p HC A07/MP A01

N83-14177

CSSL 07D G3/25 Uclas
02282

Summary Technical Report

to

NASA-Lewis Research Center

MECHANISMS OF DEVITRIFICATION OF GRAIN BOUNDARY
GLASSY PHASES IN Si₃N₄ MATERIALS

NASA Grant #NSG 3254



Submitted by

L. L. Hench, Professor
Ceramics Division
Department of Materials Science and Engineering
University of Florida
Gainesville, Florida 32611

December 17, 1982

Summary Technical Report
to
NASA-Lewis Research Center

MECHANISMS OF DEVITRIFICATION OF GRAIN BOUNDARY
GLASSY PHASES IN Si_3N_4 MATERIALS

NASA Grant #NSG 3254

Submitted by

*L. L. Hench, Professor
Ceramics Division
Department of Materials Science and Engineering
University of Florida
Gainesville, Florida 32611*

December 17, 1982

TABLE OF CONTENTS

OVERVIEW.....	1
Si ₃ N ₄ GRAIN BOUNDARY PHASES.....	4
GRAIN-BOUNDARY PHASES IN HOT-PRESSED SILICON NITRIDE CONTAINING Y ₂ O ₃ AND CeO ₂ ADDITIVES.....	29
COMPOSITIONAL EFFECTS OF Si ₃ N ₄ FRACTURE SURFACES.....	40
ANALYSIS OF GRAIN BOUNDARY PHASE DEVITRIFICATION OF Y ₂ O ₃ AND Al ₂ O ₃ DOPED Si ₃ N ₄	60
EFFECTS OF DEVITRIFICATION OF THE AMORPHOUS PHASE OF Si ₃ N ₄ + Y ₂ O ₃ + Al ₂ O ₃ CERAMICS.....	68
EFFECT OF Y ₂ O ₃ AND Al ₂ O ₃ ON THE OXIDATION RESISTANCE OF Si ₃ N ₄	106

OVERVIEW

The objectives of this grant were: 1) to develop means for analyzing changes in the grain boundary (g.b.) phases of Si_3N_4 , 2) to determine the effects of composition and thermal history on devitrification of the g.b. phases, and 3) relate devitrification of the g.b. phases of Si_3N_4 to mechanical behavior and oxidation sensitivity of the material. The series of six papers submitted for publication presented in this Summary Report describe our progress towards achieving our three objectives.

The first paper is a thorough review of the phase relationships that occur within the grain boundaries of Si_3N_4 containing various densification aids. Comparisons of the effects of MgO , Y_2O_3 , CeO_2 , and $\text{Y}_2\text{O}_3 + \text{Al}_2\text{O}_3$ are made in terms of the phase equilibria of the $\text{Si}_3\text{N}_4 + \text{SiO}_2 + \text{additive}$ compositional system. Two new equilibrium phase diagrams for the $\text{Si}_3\text{N}_4\text{-SiO}_2$ and Y_2O_3 and $\text{Si}_3\text{N}_4\text{-SiO}_2\text{-Ce}_2\text{O}_3$ systems are presented in this work.

An experimental comparison of the effects of Y_2O_3 vs CeO_2 densification aids on the fracture surfaces of Si_3N_4 is made in the second paper. Auger electron spectroscopy showed that both oxides are concentrated within the fracture surface. Scanning electron microscopy showed evidence that Si_3N_4 with CeO_2 formed an intergranular structure of fine grained oxynitride reaction products, as predicted by phase equilibria, whereas the Y_2O_3 containing sample showed evidence of an intergranular glassy phase.

Several surface analysis methods were used in the third paper to show that Si_3N_4 fracture surfaces with Y_2O_3 possess a higher concentration of oxygen than the bulk and increasing concentrations of Y_2O_3 and Al_2O_3 increases the oxygen content of the intergranular phase. This paper provides direct evidence from fracture surfaces that certain compositions

of $\text{Si}_3\text{N}_4 + \text{Y}_2\text{O}_3 + \text{Al}_2\text{O}_3$ result in an amorphous grain boundary phase which is resistant to devitrification whereas other compositions devitrify more easily.

It was shown in the fourth paper of this series that devitrification of the amorphous g.b. phase of $\text{Si}_3\text{N}_4 + 15\% \text{Y}_2\text{O}_3 + 2\% \text{Al}_2\text{O}_3$ could be achieved by increasing the vacuum heat treating temperature to 1200°C . A new analytical method, Fourier transform infrared reflection spectroscopy (FTIRRS), was developed to analyze post-fracture surfaces in order to achieve this result.

A comparison of the effects of various levels of Al_2O_3 additions to the $\text{Si}_3\text{N}_4 + \text{Y}_2\text{O}_3$ system on sensitivity to grain boundary phase devitrification is presented in the fifth paper. It was shown that heat treatment at 1000°C produced some crystallization of $\text{Y}_2\text{Si}_2\text{O}_7$ in samples containing 2, 4, and 6% Al_2O_3 whereas material with 8% Al_2O_3 developed considerably more $\text{Y}_2\text{Si}_2\text{O}_7$ and some 10-9-1 phase. A 1200°C heat treatment produced more devitrification for all compositions. However, the 6% Al_2O_3 samples showed the most $\text{Y}_2\text{Si}_2\text{O}_7$ and 10-9-1 phases with the 2% Al_2O_3 sample second. The 4% Al_2O_3 additions result in the most resistance to devitrification.

FTIRRS analyses of the heat treated series showed that there is little shift of the spectra of the fracture surfaces of the 4% Al_2O_3 material whereas fracture surfaces of the 2% Al_2O_3 samples were affected considerably by devitrification. Little differences were noted for fracture surfaces of the 6 and 8% Al_2O_3 samples due to devitrification. However, the results that show splitting of primary Si-N molecular stretching vibration peaks of fracture surfaces confirm that crystallization is occurring in the grain boundary phase.

Both the compositional changes and the heat treatments affect room temperature and high temperature strengths of these materials. Heat

treatment of the 8% Al_2O_3 at 1200°C produced the highest room temperature (113,280 psi) and elevated temperature (20,010 psi) strengths of the series studied.

Finally, in the sixth paper of the series the oxidation sensitivity of $\text{Si}_3\text{N}_4 + 15 \text{ w/o } \text{Y}_2\text{O}_3$ materials with 2, 4, 6, and 8% Al_2O_3 are compared at temperatures as low as 1000°C . It was found that concentrations of $\text{Al}_2\text{O}_3 > 4\%$ greatly retard the rate of oxidation and alter the mechanism of surface attack by promoting the surface formation of a glassy layer which contains mixed oxynitride bonds. The glassy layer retards heterogeneous oxidation attack and reduces the effect of an oxidation transition temperature between 1000°C and 1100°C for these materials.

Si_3N_4 GRAIN BOUNDARY PHASES

J. P. Cuha
University of Missouri at Rolla
Department of Ceramic Engineering
Rolla, MO 65401

L. L. Hench
Ceramics Division
Department of Materials Science and Engineering
University of Florida
Gainesville, FL 32611

Introduction

In order to fabricate fully dense hot-pressed Si_3N_4 , currently a prime candidate for heat engine and gas turbine components, additives are required for sintering or hot-pressing. During the last several years, considerable experimental efforts have been made to improve the high-temperature properties of Si_3N_4 by: 1) synthesizing high-purity $\alpha\text{-Si}_3\text{N}_4$ powders for use as starting materials; 2) using oxide additives which would allow the formation of refractory grain boundary phases, and 3) modifying processing techniques to improve product homogeneity. The use of high-purity Si_3N_4 powder improves high-temperature properties as well as increases oxidation resistance by eliminating undesirable impurity constituents such as SiO_2 , CaO and alkaline oxides, and to a lesser extent Al_2O_3 and Fe_2O_3 . This results in an increase in the refractoriness of the grain boundary phases formed during densification at elevated temperatures. However, the production of high-purity Si_3N_4 powder in bulk quantities may not be cost effective. Also, high-temperature properties, although improved, are still limited by the reaction products formed by the additives being used in densification. Thus, it is especially important to understand the behavior of additives which can simultaneously promote densification and enhance the refractoriness of the grain boundary phases.

Early attempts to hot-press Si_3N_4 to full density used a small amount of MgO as a densification aid which resulted in formation of a liquid phase at moderately high temperatures and promoted densification

of the sample. However, a major problem preventing the widespread use of MgO as a densification aid was the decrease in strength of the hot-pressed material above 1000°C. Evidence obtained with commercially hot-pressed Si_3N_4 containing MgO indicated that the decrease in strength was primarily due to the formation of the grain boundary glassy phase developed during hot-pressing. The viscosity of a silicate glassy phase decreases rapidly with increasing temperature and, as a result, the liquid starts to flow at elevated temperatures causing grain boundary sliding and ultimate mechanical failure of the Si_3N_4 material. Further understanding of the nature, distribution and characteristics of the grain boundary glassy phase has led to the conclusion that impurities in Si_3N_4 powders, particularly, CaO and alkaline oxides, decrease the viscosity and lower the softening temperature of the grain boundary phase.

Other oxides besides MgO which are known to be effective in hot-pressing or sintering Si_3N_4 include Y_2O_3 . The improved properties of hot-pressed Si_3N_4 with Y_2O_3 have been attributed to the formation of highly refractory grain-boundary phases identified as yttrium silicon oxynitrides. However, addition of certain compositional ranges of Y_2O_3 degrade the oxidation resistance of Si_3N_4 materials. This undesirable effect on oxidation resistance can be eliminated by the use of CeO_2 or combined $\text{Y}_2\text{O}_3+\text{Al}_2\text{O}_3$ mixtures.

Because of the broad range of oxides studied as densification aids it is becoming important to establish the principles governing their behavior. The purpose of this article is to summarize the findings of the characteristics of the grain-boundary phase in dense Si_3N_4 based

materials and relate those characteristics to the phase equilibria of the systems. It will be shown that certain phase equilibria principles can be used to improve the refractoriness of the grain boundaries of these materials. For a review of other aspects of Si_3N_4 processing and properties the reader is referred to Messier and Croft⁽¹⁾.

MgO Additives

Hot-pressing of Si_3N_4 with MgO as an additive is one of the earliest approaches taken to produce dense Si_3N_4 materials⁽²⁾. Early attempts of understanding the densification mechanisms of Si_3N_4 containing MgO have been made by Wild et. al⁽³⁾ and Terwillinger and Lange⁽⁴⁾. These workers found that at 1 atm. of N_2 pressure, MgO reacts with SiO_2 present in the starting materials or formed by the decomposition of Si_3N_4 during hot-pressing at moderately high temperatures, to form forsterite, Mg_2SiO_4 . The silicate phase becomes a liquid at hot-pressing temperatures and promotes densification of Si_3N_4 by a solution-reprecipitation process. This conclusion was confirmed by direct observation by Drew and Lewis⁽⁵⁾ of the glassy phase in the grain-boundaries of Si_3N_4 containing MgO using transmission electron microscopy (TEM).

Hot-pressing of Si_3N_4 with 5% MgO at higher nitrogen pressure (>10 atm) was performed by Mitomo⁽⁶⁾ with a view to suppress thermal decomposition of Si_3N_4 , thereby permitting higher densification temperatures. He proposed that densification proceeds in two stages, namely, by initial particle rearrangement followed by a solution-reprecipitation process. Soon thereafter phase relations in the system Si_3N_4 - SiO_2 -MgO and their significance to strength and oxidation resistance of Si_3N_4

were investigated by Lange⁽⁷⁾ who observed that the high temperature strength of Si_3N_4 containing MgO is strongly dependent on the MgO/SiO₂ molar ratio. It is this molar ratio which determines the amount of liquid phase present as predicted by the eutectics within the ternary compositional system.

The role of alkaline-doped MgSiO_3 on the densification process of Si_3N_4 has been studied by Kossowsky⁽⁸⁾ who reported that the alkaline content should be kept below 50-100 ppm for optimum strength. Kossowsky's study used Auger electron spectroscopy (AES) to show that impurity constituents such as Ca, Mg, Na and K concentrated in the grain-boundaries of commercially hot-pressed Si_3N_4 . Similar findings were reported by Hofmann et. al⁽⁹⁾ using AES to study the fracture surfaces of hot-pressed Si_3N_4 containing MgO. Powell and Drew⁽¹⁰⁾ also carried out AES studies on fracture surfaces of an Si_3N_4 -7% MgO hot-pressed material and observed the presence of significant amounts of Ca, Mg and oxygen at the grain-boundaries. They estimated the probable chemical composition of the intergranular glassy phase to be 0.03 CaO: +0.1 MgO: +2 SiO₂ and attributed the reduction of strength of the hot-pressed material at temperatures above 1000°C to the decrease in viscosity of the grain boundary phase due to the presence of CaO.

A critical review of viscosity of glasses in the system CaO-MgO-Al₂O₃-SiO₂ was reported by Turkdogan and Bills⁽¹¹⁾ who observed that the viscosity of a CaO: Mg: 2 SiO₂ melt decreases rapidly within the temperature range between 1200° and 1600°C. Measurements of the viscosity of the grain boundary glassy phase in hot-pressed Si_3N_4 containing MgO and CaO by and internal friction technique by Mosher et. al⁽¹²⁾ confirm

that high temperature deformation occurs by this mechanism. The effect of impurity phases, particularly CaO, alkaline oxides, Al_2O_3 and Fe_2O_3 on the high-temperature mechanical properties of 5% MgO fluxed hot-pressed Si_3N_4 was also studied by Iskoe et. al⁽¹³⁾. These workers observed that CaO, Na_2O and K_2O reduce the high-temperature strength of Si_3N_4 but Al_2O_3 and Fe_2O_3 have little effect.

Direct observations of the intergranular glassy phase in hot-pressed Si_3N_4 by transmission electron microscopy (TEM) have been carried out by several workers^(5,14-17). Clarke and Thomas⁽¹⁴⁾ used a lattice fringe imaging technique with TEM to identify the intergranular phases and reported that the second phase does not exist as a continuous wetting layer at the grain boundaries, but is generally localized at some of the multiple grain junctions and, occasionally, as a very thin layer ($<10 \text{ \AA}$) between the grains. This observation, however, contradicts the findings of Lou et. al⁽¹⁵⁾ who reported that a continuous grain boundary glassy layer exists in the commercially hot-pressed Si_3N_4 . The discrepancy was attributed by Lou et. al⁽¹⁶⁾ to the difference in the TEM techniques used by the two groups of workers. Krivanek et. al⁽¹⁷⁾ employed several analytical techniques to study the nature, distribution and composition of the grain-boundary phases in commercially hot-pressed Si_3N_4 and confirmed that a thin intergranular glassy layer exists at most grains and interphase boundaries. Further, the concentration of various impurity constituents, particularly CaO, in the glass exceeds several times their overall concentration so that even small amounts of impurity elements can have a disproportionately large influence on the properties of the glassy intergranular phase.

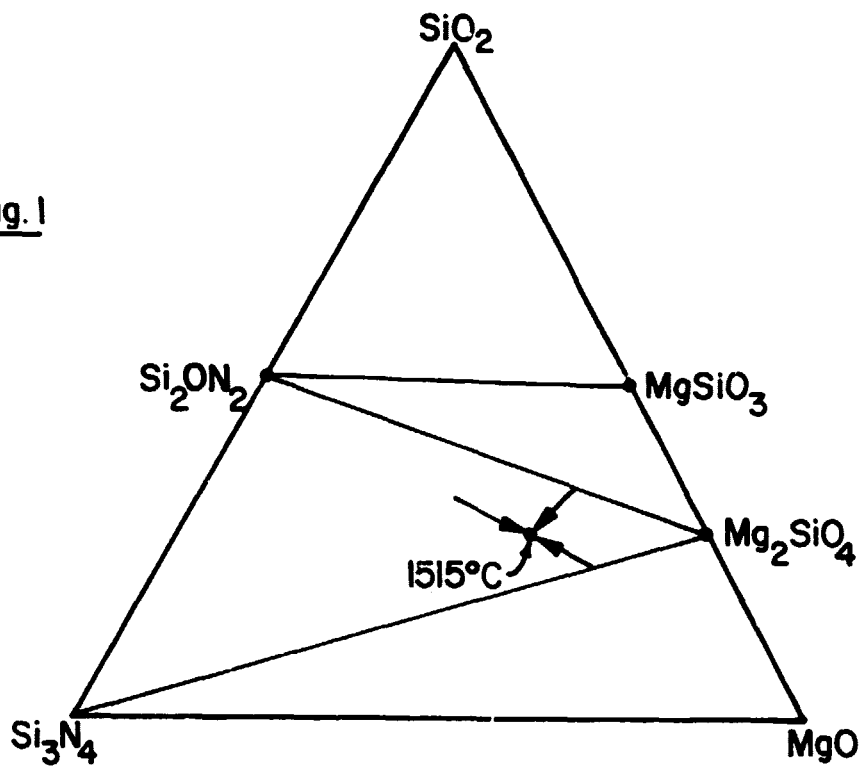
Lange⁽¹⁸⁾ extended his phase equilibria work⁽⁷⁾ to include the melting behavior of several compositions in the subsystem Si_3N_4 - $\text{Si}_2\text{N}_2\text{O}$ - Mg_2SiO_4 in which a ternary eutectic close to Mg_2SiO_4 was proposed as shown in Fig. 1. The temperature of the ternary eutectic was determined to be 1515°C. The presence of CaO as an impurity phase results in the further lowering of the melting temperature of the intergranular glassy phase to 1325°C. However, in a recent publication, Clarke et al.⁽¹⁹⁾ examined the intergranular phases in MgO fluxed hot-pressed Si_3N_4 using several complementary TEM techniques and report that the composition of the intergranular non-crystalline phase can not be related to the ternary eutectic composition studied by Lange⁽¹⁸⁾ but corresponds to a composition in the $\text{Si}_2\text{N}_2\text{O}$ - SiO_2 - MgSiO_3 phase field near the MgO- SiO_2 tie-line. On subsequent examination of the non-crystalline intergranular phase, Clarke et al.⁽²⁰⁾ further observed that it undergoes phase separation and possible crystallization to $\text{Si}_2\text{N}_2\text{O}$ and MgSiO_3 . The compositional range determined for the phase separation is close to the known miscibility gap existing in the pseudobinary system MgO- SiO_2 .

Y_2O_3 Additive

The effectiveness of Y_2O_3 as an additive for hot-pressing Si_3N_4 has been discussed by several workers⁽²¹⁻²⁵⁾. Reaction between Si_3N_4 and Y_2O_3 was studied by Tsuge et al.⁽²²⁾ who identified a crystalline phase of composition $\text{Si}_3\text{N}_4 \cdot \text{Y}_2\text{O}_3$ in the hot-pressed samples and tentatively postulated the existence of another phase of composition $\text{Si}_3\text{N}_4 \cdot 2\text{Y}_2\text{O}_3$. Preliminary property measurements at 1315°C reported by Gazza⁽²³⁾ showed that the high-temperature mechanical properties of Si_3N_4 can be significantly

ORIGINAL PAGE IS
OF POOR QUALITY

Fig. 1



improved by using Y_2O_3 as a densification aid. Rae et al⁽²⁴⁾ observed that densification of Si_3N_4 in presence of Y_2O_3 is enhanced by the formation of a transient silicon yttrium oxynitride melt at elevated temperatures and further reaction with more Si_3N_4 allows the formation a refractory silicon yttrium oxynitride phase, $Y_2(Si_2O_3N_4)$ which can accommodate impurity constituents into its structure that would otherwise degrade the high-temperature properties of Si_3N_4 .

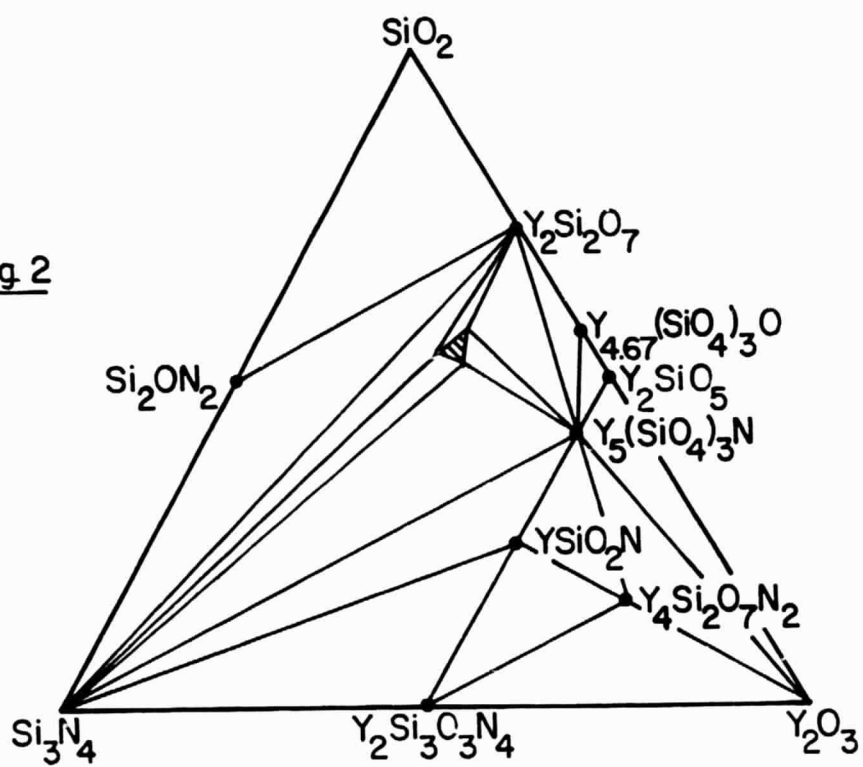
In an effort to establish the existence various silicon yttrium oxynitrides and their significance to hot-pressing of Si_3N_4 with Y_2O_3 additives, phase equilibria in the system $Si_3N_4-SiO_2-Y_2O_3$ have been investigated by several groups⁽²⁶⁻²⁹⁾. Although some disagreement still exists on the number and compositions of the various compounds occurring in the system, it is generally accepted that there are four pseudo-ternary compounds with compositions of $Y_2Si_3O_3N_4$, $YSiO_2N$, $Y_4Si_2O_7N_2$ and $Y_{10}(SiO_4)_6N_2$. The crystal structure of $Y_2Si_3O_3N_4$ was determined by Horiuchi and Mitomo⁽³⁰⁾ who reported that the compound is isostructural with the melilite silicates: akermanite, $Ca_2MgSi_2O_7$ having a tetragonal symmetry. The crystal structure of $YSiO_2N$ was related to the α -wollastonite, $CaSiO_3$, by Jack⁽²⁷⁾ and the powder X-ray diffraction pattern has been indexed by Morgan et al⁽³¹⁾ on the basis of the hexagonal pseudowollastonite structure. The compound $Y_4Si_2O_7N_2$ was reported by Wills et al⁽²⁶⁾ to be isostructural with the silicates of wohlerite-cuspidine, $Ca_4Si_2O_7F_2$, having a monoclinic structure. The compound $Y_{10}(SiO_4)_6N_2$ was reported to be isostructural with hexagonal fluorapatite, $Ca_5(PO_4)_3F$, by Thompson⁽³²⁾ and the indexed X-ray powder diffraction pattern of the compound was presented by Wills et al⁽²⁶⁾.

With the available data on compound formation and compatibility relations existing between the various phases in the pseudo-ternary system $\text{Si}_3\text{N}_4\text{-SiO}_2\text{-Y}_2\text{O}_3$, a phase diagram has been deduced as shown in Fig. 2. Partial data on the liquid formation in the system are due to Gauckler et al⁽²⁹⁾ who observed two-liquid forming regions at 1550°C. The first is in the SiO_2 -rich region within the compatibility-triangle $\text{Si}_2\text{N}_2\text{O-Y}_2\text{Si}_2\text{O}_7\text{-SiO}_2$ where compositions exhibited signs of bloating during annealing. A similar effect has been reported by Wills et al⁽²⁶⁾. The second liquid forming region was located in the compatibility-triangle $\text{Si}_3\text{N}_4\text{-Y}_2\text{Si}_2\text{O}_7\text{-Y}_{10}(\text{SiO}_4)_6\text{N}_2$. Melting behavior of compositions within this area showed liquid formation at a temperature between 1480° and 1520°C.

The liquids in both the regions which form during hot-pressing become glass when cooled. From the phase equilibria data, it is generally understood that during hot-pressing Y_2O_3 reacts with Si_3N_4 and surface SiO_2 to form a liquid which allows densification of the materials. As the reaction proceeds, the liquid combines with excess Si_3N_4 to give one or more of the refractory silicon-yttrium-oxynitrides. Unreacted liquid cools to give a glass which remains in the grain-boundaries and impairs the high-temperature strength of Si_3N_4 . TEM studies on identification and characterization of grain boundary phases in hot-pressed Si_3N_4 with 10% Y_2O_3 additive have been reported by Clarke and Thomas⁽³³⁾. Detailed microstructural analysis has revealed that, in addition to the yttrium silicon oxynitride phase located at the multiple Si_3N_4 grain junctions, there exists a thin, probably noncrystalline

ORIGINAL PAGE IS
OF POOR QUALITY

Fig. 2



boundary phase separating the Si_3N_4 and the oxynitride grains. However, Clarke and Thomas could not determine the composition of this third phase and suggested that the presence of the amorphous film between the Si_3N_4 and crystalline yttrium silicon oxynitride grains is probably responsible for the decrease of the mechanical strength of the hot-pressed material.

The effect of the grain-boundary oxynitride phases on the oxidation resistance of Si_3N_4 has also been studied⁽²⁸⁾. Lange et al⁽²⁸⁾ observed that compositions within the Si_3N_4 - $\text{Y}_2\text{Si}_2\text{O}_7$ - Y_2O_3 phase field exhibited relatively poor oxidation resistance at 1000°C and above. The problem was attributed to the accelerated linear oxidation behavior of the grain boundary yttrium silicon oxynitride phases, particularly, $\text{Si}_3\text{Y}_2\text{O}_3\text{N}_4$. At temperatures of 1000°C and above, the oxynitrides rapidly form non-protective and porous oxide scales causing catastrophic degradation and eventual disintegration of the material. In contrast, compositions within the compatibility triangle Si_3N_4 - $\text{Si}_2\text{N}_2\text{O}$ - $\text{Y}_2\text{Si}_2\text{O}_7$, in which none of the quaternary oxynitride compounds occur, exhibit excellent oxidation resistance. It was suggested that this was due to the compatibility of SiO_2 , the oxidation product of Si_3N_4 , with the secondary phases, $\text{Y}_2\text{Si}_2\text{O}_7$ and $\text{Si}_2\text{N}_2\text{O}$ and the relatively high melting temperature of the eutectic in this compositional area. However, Weaver and Lucek⁽³⁴⁾ disagreed with this finding and stress the need for property optimization through composition variation in hot-pressed Si_3N_4 with Y_2O_3 additives. These workers report that no deterioration of strength or oxidation resistance could be observed if the Y_2O_3 content was kept below a certain critical

limit. Based on their experimental data, it was suggested that 8% Y_2O_3 addition represents an optimized compositional level in which substantial improvements in both the strength and oxidation resistance have been observed.

CeO₂ Additive

The use of CeO₂ as a hot-pressing aid for densifying Si₃N₄ powder has been reported by several workers⁽³⁵⁻³⁹⁾. It is generally agreed that the addition of CeO₂ significantly enhances densification of Si₃N₄ with improvements in high-temperature properties. In these studies it was assumed that CeO₂ and SiO₂ thus formed further combine with Si₃N₄ to give several quaternary cerium silicon oxynitrides. The existence of a compound having the chemical formula $3Ce_2O_3 \cdot 2Si_3N_4$ has been first reported by Wills and Cunningham⁽⁴⁰⁾ who assigned an orthorhombic structure for the compound. However, Morgan and Carroll⁽⁴¹⁾ and Thompson⁽⁴²⁾ re-examined the X-ray diffraction pattern for the compound and reported that the correct chemical composition of the compound is CeSiO₂N having a pseudo-hexagonal structure similar to YSiO₂N⁽³¹⁾.

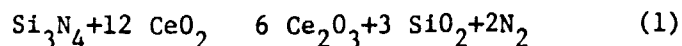
Mah et al⁽⁴³⁾ studied the densification behavior of Si₃N₄ with both CeO₂ and Ce₂O₃ additives and suggest that a nitrogen containing cerium orthosilicate, $Ce_{4.67}(SiO_4)_3O$, which forms as a grain-boundary glassy phase, was mainly responsible for the densification of Si₃N₄. Two cerium silicon oxynitrides, Ce₂Si₆O₃N₈ and Ce₄Si₂O₇N₂ were identified and the X-ray powder diffraction data for the compounds have been

presented. Guha et al⁽⁴⁴⁾ hot-pressed Si_3N_4 with CeO_2 additive at temperatures between 1400° and 1750°C and identified a nitrogen containing apatite phase, $\text{Ce}_5(\text{SiO}_4)_3\text{N}$ analogous to $\text{Y}_5(\text{SiO}_4)_3\text{N}$ and the previously reported compound CeSiO_2N as reaction products. Evidence obtained by X-ray powder diffraction of the hot-pressed compositions indicated that both the oxynitrides constitute pseudo-binary tie-lines with Si_3N_4 in the system $\text{Si}_3\text{N}_4\text{-SiO}_2\text{-Ce}_2\text{O}_3$. The crystallographic data proposed by Mah et al⁽⁴³⁾ for the compound $\text{Ce}_4\text{Si}_2\text{O}_7\text{N}_2$ have been re-examined by Morgan⁽⁴⁵⁾ and Guha⁽⁴⁶⁾ both of whom have concurrently assigned a monoclinic cuspidine type ($\text{Ca}_4\text{Si}_2\text{O}_7\text{F}_2$) unit-cell for the compound.

Subsolidus phase relations in the system Ce-Si-O-N have been reported by Jack⁽⁴⁶⁾ who proposed four quaternary cerium oxynitrides that are isostructural with the yttrium analogues plus an additional phase, $\text{Ce}_2\text{O}_3 \cdot 2\text{Si}_3\text{N}_4$ which has no yttrium analogue. Lange^(48,49) has also proposed a tentative phase diagram for the pseudo-ternary system $\text{Si}_3\text{N}_4\text{-SiO}_2\text{-Ce}_2\text{O}_3$ but failed to mention the compound $\text{Ce}_2\text{O}_3 \cdot 2\text{Si}_3\text{N}_4$ and did not observe the compound $\text{Ce}_2\text{Si}_3\text{O}_3\text{N}_4$ and $\text{Ce}_4\text{Si}_2\text{O}_7\text{N}_2$ although these are expected in the diagram. The exact composition of the nitrogen apatite phase represented by Lange⁽⁴⁹⁾ in the diagram as $\text{Ce}_{10}(\text{SiO}_{3.67}\text{N}_{0.33})_2$ (Ref. 47) and $\text{Ce}_5(\text{SiO}_4)_3\text{N}$ still remains uncertain. However, the existence of a new group of silicon lanthanide oxynitrides of the general formula $\text{Ln}_5(\text{SiO}_4)_3\text{N}$ which are isostructural with the hexagonal fluorapatite, $\text{Ca}_5(\text{PO}_4)_3\text{F}$ has been confirmed by Hamon et al⁽⁵⁰⁾ and the crystal structure of nitrogen apatites with particular reference to $\text{Y}_5(\text{SiO}_4)_3\text{N}$ was

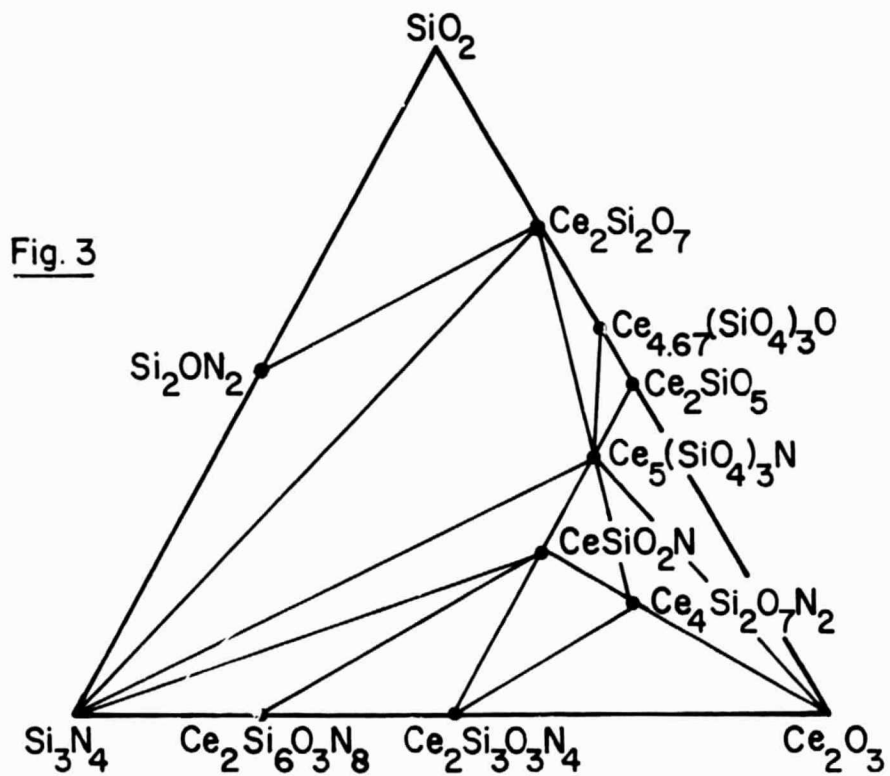
discussed by Jack⁽⁵¹⁾. The nitrogen containing Ce-apatite phase, $Ce_5(SiO_4)_3N$ has been prepared by Guha⁽⁵²⁾ using solid state reaction techniques and the X-ray powder diffraction data for the compound which are similar to those of $Y_5(SiO_4)_3N$ were presented.

Based on the foregoing data on the chemical composition of the various phases in the pseudo-ternary system $Si_3N_4-SiO_2-Ce_2O_3$ and the compatibility relations between them, a phase diagram is deduced as shown in Fig. 3. As mentioned by the previous workers^(47,48), the close resemblance between this and $Si_3N_4-SiO_2-Y_2O_3$ systems suggests that the densification behavior and ultimate properties of Si_3N_4 hot-pressed with ceria will be similar to those with yttria. The results obtained so far on the hot-pressing behavior of Si_3N_4 with Y_2O_3 and CeO_2 additives appear to confirm this supposition. Thus, it is now known that during hot-pressing, both of these oxides form a nitrogen containing apatite oxynitride phase which eventually allows the formation of a liquid phase in the grain-boundaries of Si_3N_4 and promotes densification of the material. Further reaction of the liquid with more Si_3N_4 yields one or more grain boundary refractory oxynitride phases which leads to improvement in high-temperature properties of the densified material. However, the advantage of CeO_2 over Y_2O_3 as an additive is that for each mole of CeO_2 added, corresponding molar proportions of Ce_2O_3 and SiO_2 will be formed according to the reaction:



Thus, the reaction of Si_3N_4 with CeO_2 allows the formation of the nitrogen containing Ce-apatite phase through reaction with the intermediate Ce_2O_3 phase. The Ce-apatite phase, in turn, will form the liquid phase

ORIGINAL PAGE IS
OF POOR QUALITY



required for densification of Si_3N_4 . Further, due to the compositional limit for SiO_2 which is always present in all the compositions containing CeO_2 , the quaternary oxynitrides located on the $\text{Si}_3\text{N}_4\text{-Ce}_2\text{O}_3$ join cannot be formed. This is in contrast to the case of Y_2O_3 in which the oxynitride $\text{Si}_3\text{N}_4\cdot\text{Y}_2\text{O}_3$ is known to be mainly responsible for the catastrophic oxidation of Si_3N_4 at 1000°C . Therefore, for the same concentrations of additive, Si_3N_4 densified with CeO_2 should be much more oxidation resistant than Si_3N_4 densified with Y_2O_3 .

$\text{Y}_2\text{O}_3/\text{Al}_2\text{O}_3$ Additive

Silicon nitride densified with $\text{Y}_2\text{O}_3/\text{Al}_2\text{O}_3$ mixtures develops an extensive intergranular glassy phase which is very effective for obtaining highly dense products with excellent flexural strength. Early attempt to sinter Si_3N_4 with Y_2O_3 in which Al_2O_3 was incorporated as an impurity phase during ball milling was made by Tsuge et al⁽⁵³⁾. They obtained a higher flexural strength for the material than previously reported data for Si_3N_4 containing MgO . The extensive glassy phase formed at high temperatures crystallized to refractory grain-boundary phases containing $\beta\text{-Si}_3\text{N}_4$ and $\text{Si}_3\text{N}_4\cdot\text{Y}_2\text{O}_3$ during cooling. Wills⁽⁵⁴⁾ has investigated the reaction of Si_3N_4 with Y_2O_3 and Al_2O_3 and suggested that a new phase exists with the probable composition $5\text{Y}_2\text{O}_3\cdot\text{Si}_3\text{N}_4\cdot\text{Al}_2\text{O}_3$ content in the mixtures he studied, Morgan⁽⁵⁵⁾, however, has disagreed with the occurrence of any new phase in the system and emphasizes that a solid solution series, $\text{Y}_4\text{Al}_{2-x}\text{Si}_x\text{O}_{9-x}\text{N}_x$ exists instead.

Venables et al⁽⁵⁶⁾ used 10% of the eutectic composition of Y_2O_3 - Al_2O_3 as an additive and reported excellent sintering characteristics of Si_3N_4 due to the formation of a large volume of liquid glassy phase which completely wetted the solid and migrated rapidly through the Si_3N_4 grains. Jack⁽⁴⁷⁾ supported these findings and postulated a wide range of solid solution depicted as β -sialon in the pseudo-ternary system Si_3N_4 - Y_2O_3 - Al_2O_3 . Compositions within the solid solution range showed none of the catastrophic oxidation at 1000°C experienced with some of the Si_3N_4 - Y_2O_3 compositions without Al_2O_3 . It was further suggested that the lowest liquidus in the Y_2O_3 - SiO_2 - Al_2O_3 system is at approximately 1350°C above which the oxidation of yttrium sialons involves liquid formation and hence becomes more pronounced. Milberg and Miller⁽⁵⁷⁾ prepared a composition containing 53% Si_3N_4 , 27% Al_2O_3 and 20% Y_2O_3 by sintering for 3 hrs at 1600°C in an argon atmosphere. The XRD pattern showed the presence of β -sialon lines superimposed on a halo typical of a noncrystalline substance. When the same material was heated at 1200°C for 185 hr., the diffraction pattern showed the presence of $Y_2Si_2O_7$ which indicated that a glassy phase initially present in the material devitrified to yttrium disilicate during the heat-treatment. The preparation of Si-Y-Al-O-N glasses was reported by Shillito et al⁽⁵⁸⁾ and hardness values obtained for these glasses were comparable to those of a Si-Y-Al-O glass.

An extensive study of the effect of Al_2O_3 on the mechanical properties of Si_3N_4 containing Y_2O_3 (or CeO_2) has been performed by Smith and Quackenbush⁽⁵⁹⁾. They found that Al_2O_3 preferentially goes into

the liquid phase formed at the sintering or hot-pressing temperatures and suppresses crystallization, thereby promoting glass formation. At elevated temperatures, this glassy phase causes structural degradation by slow crack growth and intergranular fracture. When phase purity is maintained, the decrease in Al_2O_3 content enhances crystallization of refractory grain-boundary phases containing $\text{Y}_2\text{Si}_2\text{O}_7$ and $\text{Y}_5(\text{SiO}_4)_3\text{N}$ which were mainly responsible for the substantial improvement in the high-temperature strength of the Si_3N_4 material. In a concurrent publication, Quackenbush and Smith⁽⁶⁰⁾ reported the oxidation behavior of Si_3N_4 with Y_2O_3 and Al_2O_3 additives and observed that the Al_2O_3 bearing materials show good oxidation resistance at 1000°C . Above this temperature, oxidation of the materials follow parabolic kinetics and is controlled by oxygen diffusion through the surface silicate layer.

In a recent study, Hench et al⁽⁶¹⁾ have employed several surface analytical techniques (XRD, IRRS and AES) to examine the fracture surfaces of Si_3N_4 hot-pressed with Y_2O_3 and Al_2O_3 densification aids. These workers have observed that the fracture occurs preferentially within the oxygen enriched grain boundaries. An increase in Y_2O_3 content increased the concentration of oxygen within the fracture surface. Additions of 13 to 15% Y_2O_3 and 6% Al_2O_3 to Si_3N_4 enhanced the formation of an amorphous grain-boundary phase which failed to devitrify when heat-treated for 10 hrs. at 1000°C in vacuum

In a related study Hench, et al⁽⁶²⁾ investigated the oxidation resistance of Si_3N_4 containing 15 w/o Y_2O_3 and 2, 4, 6 and 8% Al_2O_3 . Oxidation was followed at temperatures as low as 1000°C by use of

infrared reflection spectroscopy. It was found that Al_2O_3 additions of 4% or greater significantly retard oxidation of $\text{Si}_3\text{N}_4+15\% \text{Y}_2\text{O}_3$ even though this composition is in the field where the destructive $\text{Si}_3\text{Y}_2\text{O}_3\text{N}_4$ phase can form. The oxidation protection is due to formation of a surface layer containing mixed silicon oxynitride bonds which retard a heterogeneous mode of attack of the Si_3N_4 structure. The mechanisms and the Al_2O_3 compositional effect are the same at both 1000°C and 1100°C confirming the previous conclusion⁽⁶⁰⁾ that development of surface glassy phases greatly reduce the importance of an oxidation transition temperature for these materials.

Acknowledgements

The authors gratefully acknowledge partial financial support of NASA Grant #NS63254.

References

1. D. R. Messier and W. J. Croft, Silicon Nitride, Army Materials and Mechanics Research Center, Watertown, Mass. 02172, AMRC TR 82-42 (1982).
2. G. G. Deely, J. M. Herbert and N. C. Moore, "Dense Silicon Nitride", Powder Met., No. 8, 145-151 (1961).
3. S. Wild, P. Grieveson, K. H. Jack and M. Latimer, "The Role of MgO in Hot-Pressed Si_3N_4 ", in Special Ceramics 5, P. Popper, ed., British Ceramic Research Association, 1972, pp. 377-384.
4. G. R. Terwilliger and F. F. Lange, "Hot-Pressing Behavior of Si_3N_4 ", J. Am. Ceram. Soc. 57(1), 25-29 (1974).
5. P. Drew and M. H. Lewis, "The Microstructures of Si_3N_4 Ceramics During Hot-Pressing Transformations", J. Mater. Sci. 9(2), 261-269 (1974).
6. M. Mitomo, "Pressure Sintering of Si_3N_4 ", J. Mater. Sci. 11, 1103-1107 (1976).
7. F. F. Lange, "Phase Relations in the System Si_3N_4 - SiO_2 -MgO and Their Interrelation with Strength and Oxidation", J. Am. Ceram. Soc. 61(1-2) 53-56 (1978).
8. R. Kossowsky, "The Microstructure of Hot-Pressed Si_3N_4 ", J. Mater. Sci., 8(11), 1603-1615 (1973).
9. S. Hofmann and L. J. Ganckler, "A Study of Fracture Surfaces of Hot-Pressed Si_3N_4 by Auger Electron Spectroscopy", Powder Met. Inst., 6, 90-92 (1974).
10. E. D. Powell and P. Drew, "The Identification of a Grain-Boundary Phase in Hot-Pressed Si_3N_4 by Auger Electron Spectroscopy", J. Mater. Sci., 9(11), 1867-1870 (1974).
11. E. T. Turkdogan and P. M. Bills, "A Critical Review of Viscosity of CaO-MgO- Al_2O_3 - SiO_2 Melts", Am. Ceram. Soc. Bull., 39(11), 682-687 (1960).
12. D. R. Mosher, R. Raj and R. Kossowsky, "Measurement of Viscosity of the Grain-Boundary Phase in Hot-Pressed Si_3N_4 ", J. Mater. Sci., 11(1), 49-53 (1976).
13. J. L. Iskoe, F. F. Lange and E. S. Diaz, "Effect of Selected Impurities on the High Temperature Mechanical Properties of Hot-Pressed Si_3N_4 ", J. Mater. Sci., 11(5), 908-912 (1976).
14. D. R. Clarke and G. Thomas, "Grain Boundary Phases in a Hot-Pressed MgO Fluxed Si_3N_4 ", J. Am. Ceram. Soc., 60(11-12), 491-495 (1977).

15. L. K. V. Lou, T. E. Mitchell and A. H. Heuer, "Impurity Phases in Hot-Pressed Si_3N_4 ", J. Am. Ceram. Soc., 61(9-10), 392-396 (1978).
16. L. K. V. Lou, T. E. Mitchell and A. H. Heuer, "Discussion of Grain Boundary Phases in a Hot-Pressed MgO Fluxed Si_3N_4 ", J. Am. Ceram. Soc., 61(9-10), 462-464 (1978).
17. O. L. Krivanek, T. M. Shaw and G. Thomas, "The Microstructure and Distribution of Impurities in Hot-Pressed and Sintered Si_3N_4 ", J. Am. Ceram. Soc., 61(11-12), 585-589 (1979).
18. F. F. Lange, "Eutectic Studies in the System Si_3N_4 - $\text{Si}_2\text{N}_2\text{O}$ - Mg_2SiO_4 ", J. Am. Ceram. Soc., 62(11-12), 617-619 (1979).
19. D. R. Clarke, N. J. Taluzec and R. W. Carpenter, "The Intergranular Phase in Hot-Pressed Si_3N_4 , I. Elemental Composition", J. Am. Ceram. Soc., 64(10), 601-607 (1981).
20. D. R. Clarke, N. J. Taluzec and R. W. Carpenter, "The Intergranular Phase in Hot-Pressed Si_3N_4 , II. Evidence for Phase Separation and Crystallization", J. Am. Ceram. Soc., 64(10), 608-611 (1981).
21. G. E. Gazza, "Hot-Pressed Si_3N_4 ", J. Am. Ceram. Soc., 56(12), 662 (1973).
22. A. Tsuge, H. Kudo and K. Komeya, "Reaction of Si_3N_4 with Y_2O_3 in Hot-Pressing", J. Am. Ceram. Soc., 57(6), 269-270 (1974).
23. G. E. Gazza, "Effect of Y_2O_3 Additions on Hot-Pressed Si_3N_4 ", Am. Ceram. Soc. Bull., 54(9), 778-781 (1975).
24. A.W.J.M. Rae, D. P. Thompson, N. J. Pipkin and K. H. Jacki, in Special Ceramics 6, P. Popper, ed., British Ceramic Research Association, Stoke-on-Trent, England, 1975, pp. 347-360.
25. K. H. Jack, "Review: Sialons and Related Nitrogen Ceramics," J. Mater. Sci., 11(6), 1135-1158 (1976).
26. R. R. Wills, S. Holmquist, J. M. Wimmer and J. A. Cunningham, "Phase Relations in the System Si_3N_4 - Y_2O_3 - SiO_2 ", J. Mater. Sci., 11(7), 1305-1309 (1976).
27. K. H. Jack, in Nitrogen Ceramics, F. L. Tiley, ed., Noordhoff International, Reading Mass, 1977, pp. 109-128.
28. F. F. Lange, S. C. Singhal and R. C. Kuznicki, "Phase Relations and Stability Studies in the Si_3N_4 - SiO_2 - Y_2O_3 Pseudoternary System", J. Am. Ceram. Soc., 60(5-6), 249-252 (1977).
29. L. J. Ganckler, H. Hohnke and T. Y. Tiers, "The System Si_3N_4 - SiO_2 - Y_2O_3 ", J. Am. Ceram. Soc., 63(1-2), 35-38 (1980).

30. S. Horiuchi and M. Mitomo, "Crystal Structure of $\text{Si}_3\text{N}_4\text{-Y}_2\text{O}_3$ Examined by a LMV High-Resolution Electron Microscope," *J. Mater. Sci.*, 14, 2543-2546 (1979).
31. P.E.D. Morgan, P. J. Carroll and F. F. Lange, "Crystal Structure of YSiO_2N and a Reappraisal of the 'Vaterite' Type, YBO_3 ", *Mater. Res. Bull.*, 12(3), 251-259 (1977).
32. D. P. Thompson, in Special Ceramics 6, P. Popper, ed., British Ceramic Research Association, England, 1972, pp. 358.
33. D. R. Clarke and G. Thomas, "Microstructure of Y_2O_3 Fluxed Hot-Pressed Si_3N_4 ," *J. Am. Ceram. Soc.*, 61(3-4), 114-118 (1978).
34. G. Q. Weaver and J. W. Lucek, "Optimization of Hot-Pressed $\text{Si}_3\text{N}_4\text{-Y}_2\text{O}_3$ Materials", *Am. Ceram. Soc. Bull.*, 57(12), 1131-1136 (1978).
35. I. C. Huseby and G. Petzow, "Influence of Various Densifying Additives on Hot-Pressed Si_3N_4 ", *Powder Metall. Int.* 6(1), 17-19 (1974).
36. K. S. Mazdidasni and C. M. Cooke, "Consolidation, Microstructure and Mechanical Properties of Si_3N_4 Doped with Rare-Earth Oxides", *J. Am. Ceram. Soc.*, 57(12), 536-537 (1974).
37. H. F. Priest, G. L. Priest and G. E. Gazza, "Sintering of Si_3N_4 Under High Nitrogen Pressure," *J. Am. Ceram. Soc.*, 60(1-2), 81 (1977).
38. G. N. Babini, A. Bellosi and P. Vincenzini, "Hot Pressing of Silicon Nitride with Ceria Additions," *Ceramurgia Int.*, 6(3), 91-98 (1980).
39. A. Arias, "Effect of CeO_2 , MgO and Y_2O_3 Additions on the Sinterability of a Milled Si_3N_4 with 145 wt % SiO_2 ", *J. Mater. Sci.*, 16, 787-799 (1981).
40. R. R. Wills and J. A. Cunningham, "Silicon Cerium Oxynitride", *J. Mater. Sci.*, 12(1), 208-210 (1977).
41. P.E.D. Morgan and P. J. Carroll, "Crystal Structures of CeSiO_2N and LaSiO_2N ", *J. Mater. Sci.*, 12(11), 2343-2349 (1977).
42. D. P. Thompson, "Comments on Silicon Cerium Oxynitride", *J. Mater. Sci.*, 12(11), 2344-2345 (1977).
43. T. Mah, K. J. Mazdidasni and R. Ruh, "The Role of Cerium Orthosilicate in the Densification of Si_3N_4 ", *J. Am. Ceram. Soc.*, 62(1-2), 12-16 (1979).
44. J. P. Guha, P. Goursat and M. Billy, "Hot-Pressing and Oxidation Behavior of Silicon Nitride with Ceria Additive", *J. Am. Ceram. Soc.*, 63(1-2), 119-120 (1980).

45. P.E.D. Morgan, "Comment on the Structures of $Ce_4Si_2O_7N_2$, $La_4Si_2O_7N_2$, $Ce_2O_3 \cdot 2Si_3N_4$ and $La_2O_3 \cdot 2Si_3N_4$ ", *J. Amer. Ceram. Soc.*, 62(11-12), 636 (1979).
46. J. P. Guha, "The Crystal Structure of the Silicon Cerium Oxynitride, $Ce_4Si_2O_7N_2$ ", *J. Mater. Sci.*, 15(1), 262-263 (1980).
47. K. H. Jack, "The Fabrication of Dense Nitrogen Ceramics" in Materials Science Research, Vol. III, H. Palmour, R. F. Davis and T. M. Hare, eds., Plenum Press, NY, 1978, pp. 501-578.
48. F. F. Lange, "Dense Silicon Nitride Ceramics: Fabrication and Interrelations with Properties", in Materials Science Research, Vol. III, H. Palmour, R. F. Davis and T. M. Hare, eds., Plenum Press, NY, 1978, pp. 597-614.
49. F. F. Lange, " Si_3N_4 - Ce_2SiO_2 Materials: Phase Relations and Strength", *Am. Ceram. Soc. Bull.*, 59(2), 239-249 (1980).
50. C. Hamon, R. Marchand, M. Maunaye, J. Gande and J. Guyadr, "Compounds Having an Apatite Structure: III", *Rev. Khim. Miner.*, 12(3), 259-267 (1975).
51. K. H. Jack, "Review: Sialons and Related Nitrogen Ceramics", *J. Mater. Sci.*, 11(6), 1135-1158 (1976).
52. J. P. Guha, "The Silicon Cerium Oxynitride $Ce_5(SiO_4)_3N$ with Fluorapatite Structure", *J. Mater. Sci.*, 15, 521-522 (1980).
53. A. Tsuge, K. Nishida and M. Komatsu, "Effect of Crystallizing the Grain-Boundary Glass Phase on the High Temperature Strength of Hot-Pressed Si_3N_4 Containing Y_2O_3 ", *J. Am. Ceram. Soc.*, 58(7-8), 323-326 (1975).
54. R. R. Wills, "Reaction of Si_3N_4 with Al_2O_3 and Y_2O_3 ", *J. Am. Ceram. Soc.*, 58(7-8), 335 (1975).
55. P.E.D. Morgan, "Comments on 'Reaction of Si_3N_4 with Al_2O_3 and Y_2O_3 ' and 'Silicon Yttrium Oxynitrides' by R. R. Wills", *J. Am. Ceram. Soc.*, 59(1-2), 86, (1976).
56. J. D. Venables, D. K. McNamera and R. G. Lye, in Nitrogen Ceramics, Proc. NATO Advanced Study Institute, Canterbury, England, 1976.
57. M. E. Milberg and W. M. Miller, "Observation of a Non-Crystalline Phase in Sintered Si_3N_4 - Al_2O_3 - Y_2O_3 ", *J. Am. Ceram. Soc.*, 61(3-4), 179 (1978).
58. K. R. Shillito, R. R. Wills and R. B. Bennett, "Silicon Metal Oxynitride Glasses", *J. Am. Ceram. Soc.*, 61(11-12), 537 (1978).
59. J. T. Smith and C. L. Quackenbush, "Phase Effects in Si_3N_4 Containing Y_2O_3 and Ce_2O_3 : I. Strength", *Am. Ceram. Soc. Bull.*, 59(5), 529-537 (1980).

60. C. L. Quackenbush and J. T. Smith, "Phase Effects in Si_3N_4 Containing Y_2O_3 or CeO_2 : II Oxidation", Am. Ceram. Soc. Bull., 59(5), 533-537 (1980).
61. L. L. Hench, F. Ohuchi, P. N. Vaidyanathan and S. Dutta, "Compositional Effects on Si_3N_4 Fracture Surface", to be published.

GRAIN-BOUNDARY PHASES IN HOT-PRESSED
SILICON NITRIDE CONTAINING Y_2O_3 and CeO_2 ADDITIVES

J. P. Guha
Department of Ceramic Engineering
University of Missouri-Rolla
Rolla, MO 65401

L. L. Hench
Ceramics Division
Department of Materials Science and Engineering
University of Florida
Gainesville, FL 32611

Introduction

The high-temperature strength and oxidation resistance of Si_3N_4 hot-pressed with Y_2O_3 ⁽¹⁻⁶⁾ and rare-earth oxides, particularly, CeO_2 ⁽⁷⁻¹¹⁾ have been the subject of numerous studies. It has been generally recognized that the usefulness of these oxides as an effective hot-pressing additive is largely dependent on the formation and stability of several intergranular phases identified as yttrium/cerium silicon oxynitrides which form during hot-pressing. Although the nature and characteristics of the individual oxynitride compounds have been widely reported, there is still much to learn of the composition of the grain-boundary phases that result from particular hot-pressing sequences and their overall effect on the high-temperature properties of Si_3N_4 . Recently, direct microstructural analysis of the grain-boundary phases in Y_2O_3 fluxed hot-pressed Si_3N_4 by lattice fringe imaging using transmission electron microscopy⁽¹²⁾ has emerged as an useful technique for identifying various amorphous and crystalline phases and for demonstrating their overall distribution in the grain-boundaries of Si_3N_4 . This technique in conjunction with selected area electron diffraction and energy dispersive X-ray microanalysis has been used to determine the composition of intergranular phases in Si_3N_4 sintered with Y_2O_3 additive⁽¹³⁾. However, the heterogeneous distribution of the grain boundary phase in these materials makes quantitative analyses of their chemical composition difficult because of the small sampling volume in the TEM methods. Also, the large sampling depth usually makes TEM compositional analysis of fracture surfaces ambiguous because of the thin layer of grain

boundary phase on the fracture surface. Because of the surface sensitivity of Auger electron spectroscopy it has been used by several workers⁽¹⁴⁻¹⁶⁾ to analyze the fracture surface of MgO doped Si_3N_4 hot-pressed materials and to estimate the chemical composition of the grain-boundary glass phase. The work described in this communication uses a combination of Auger electron spectroscopy and scanning electron microscopy to analyze the grain boundary phases of Y_2O_3 and CeO_2 doped Si_3N_4 hot-pressed materials. It demonstrates that the additives predominantly concentrate in the grain-boundaries of Si_3N_4 in the form of various oxynitrides phases.

Materials and Methods

Samples were prepared from high-purity Si_3N_4 powder to which 5 - 20 wt% Y_2O_3 and CeO_2 were added separately. The mixtures were blended for 24 hrs. in polyethylene containers using Si_3N_4 milling media to avoid contamination. The samples were uniaxially hot-pressed in a graphite mold coated with BN at 1700°C for 2 hrs. in a purified N_2 atmosphere at a pressure of 28 MN/m^2 , allowed to cool to room temperature inside the furnace in flowing N_2 and then machined to remove BN from the surfaces. A portion from each sample was crushed to fine powder and analyzed by X-ray powder diffraction (XRD) using $\text{CuK}\alpha$ radiation to identify the crystalline phases present. The grain boundary phases in the hot-pressed samples were analyzed by Auger electron spectroscopy (AES). Thin sections cut from the hot-pressed samples were fractured at room temperature and directly mounted in the AES with the fracture surface facing upward. For comparison, a portion of the bulk sample was metallographically

polished, cleaned and dried and mounted alongside the fractured specimen. The whole assembly was evacuated to 10^{-9} Torr. for 24 hrs. Prior to focusing the primary electron beam to the specimens, the surfaces, particularly, those of the polished specimens were sputtered with an Argon ion beam to remove the contamination due to handling and exposure to the atmosphere. AES was performed with the sputtering switched off but a partial pressure of Argon (4×10^{-5} Torr.) was maintained throughout the analysis. A beam current of $40 \mu\text{A}$ and primary beam energy of 3KeV provided the optimum conditions for the resolution of the characteristic Auger peaks for both yttrium and cerium. The fracture surfaces of the hot-pressed samples were also examined by scanning electron microscopy (SEM) and secondary electron images were obtained.

Results

X-ray powder diffraction analysis of the hot-pressed samples of Si_3N_4 with Y_2O_3 additive revealed mainly $\beta\text{-Si}_3\text{N}_4$ as the major phase with two additional crystalline phases identified as $\text{Y}_2\text{Si}_3\text{O}_3\text{N}_4$ and YSiO_2N . The presence of the latter phase was detected only in those samples which contained a high-proportion of Y_2O_3 . From the available phase equilibria data⁽¹⁷⁾ for the system $\text{Si}_3\text{N}_4\text{-SiO}_2\text{-Y}_2\text{O}_3$, it is evident that the surface SiO_2 present in the starting Si_3N_4 has shifted the overall composition within the compatibility triangle $\text{Si}_3\text{N}_4\text{-Y}_2\text{Si}_3\text{O}_3\text{N}_4\text{-YSiO}_2\text{N}$.

Samples hot-pressed with CeO_2 additive, on the other hand, were found to contain $\beta\text{-Si}_3\text{N}_4$ as the major phase with two crystalline phases identified as CeSiO_2N and the nitrogen containing apatite-type $\text{Ce}_5(\text{SiO}_4)_3\text{N}$.

As already known^(9,11) CeO_2 decomposes to Ce_2O_3 in presence of Si_3N_4 with Ce_2O_3 and SiO_2 allows the formation of the quaternary oxynitride phases. Thus, it is apparent that the formation of SiO_2 during hot-pressing has resulted in shifting the overall composition within the compatibility triangle Si_3N_4 - CeSiO_2N - $\text{Ce}_5(\text{SiO}_4)_3\text{N}$ in the system Si_3N_4 - SiO_2 - Ce_2O_3 .

Scanning electron micrographs of the fracture surfaces of hot-pressed Si_3N_4 doped with Y_2O_3 and CeO_2 are shown in Fig. 1. Previous workers⁽¹⁴⁻¹⁶⁾ have reported that the fracture in hot-pressed Si_3N_4 is predominantly intergranular and hence is expected to show a high proportion of grain-boundary area. In this study hot-pressed specimens which were fractured at room temperatures and then examined by SEM revealed a combination of inter- and intragranular fracture for both the Y_2O_3 and CeO_2 doped Si_3N_4 samples. As shown in Fig. 1(A), a SEM photomicrograph of a Y_2O_3 doped Si_3N_4 hot-pressed sample at high magnification exhibits large grains of Si_3N_4 sintered together. In a few isolated areas, however, elongated pores preferentially located between the Si_3N_4 grains show evidence of the presence of an intergranular liquid phase. In contrast, SEM examination of CeO_2 -doped Si_3N_4 hot-pressed samples, Fig. 1(B), revealed numerous areas in which the reaction between Si_3N_4 and the additive oxide can be demonstrated. Fig. 1(B) shows the morphology of the reaction zone which primarily consists of large Si_3N_4 grains surrounded by a porous and fine-grained layer containing the oxynitride phases formed as reaction products.

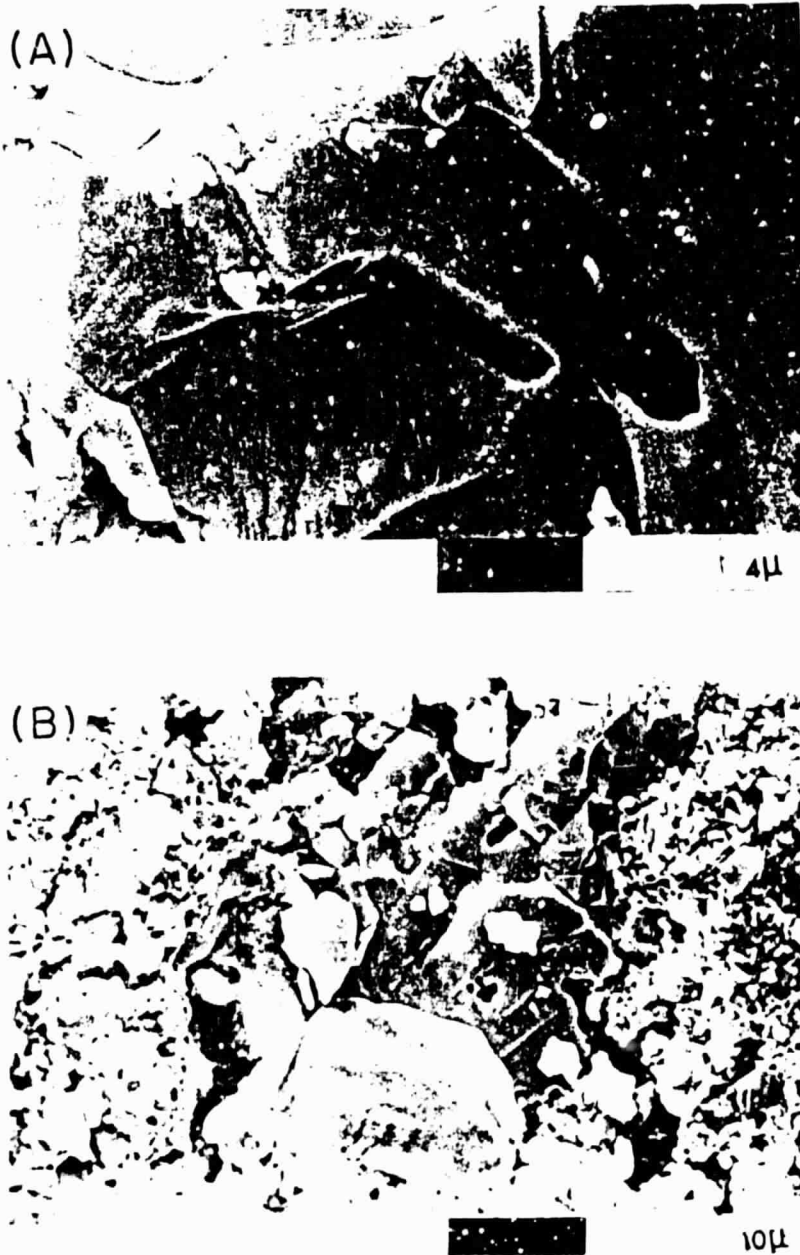


Fig. 1. Scanning electron micrographs of fracture surfaces of hot-pressed Si_3N_4 containing (A) 10 wt % Y_2O_3 and (b) 10 wt % CeO_2 .

Auger electron spectra obtained for both polished and fracture surfaces showed characteristic peaks for silicon, nitrogen and oxygen. The surfaces were found to be free from any detectable impurities or inclusions except for carbon which was present in significant quantities in all samples. The characteristic oxygen peak observed in the polished samples which persisted even after prolonged sputtering can be attributed to the presence of an oxide phase, presumably surface SiO_2 associated with the starting Si_3N_4 material. No peaks for either yttrium or cerium could be detected in the polished samples which confirms the earlier findings⁽³⁾ that there is no solubility of these oxides in Si_3N_4 .

In contrast, the characteristic spectra obtained from fracture surfaces showed the presence of yttrium and cerium in the respective samples. Typical Auger spectra of the fracture surfaces of hot-pressed Si_3N_4 doped with Y_2O_3 and CeO_2 are shown in Fig. 2 (A) and (B) respectively. The peak to peak amplitudes for oxygen (503 eV) and nitrogen (379 eV) varied significantly between the polished and the fracture surfaces. In general, a high oxygen content observed in the fracture surfaces is consistent with the existence of an oxygen enriched phase in the grain-boundaries. Furthermore, the presence of yttrium and cerium in the fracture surfaces and an overall increase in the O/N ratio imply that the additive oxides are predominantly concentrated in the intergranular phases. Thus the AES analysis used in conjunction with XRD and SEM techniques appear to be very effective in the identification and characterization of the grain-boundary phases in hot-pressed Si_3N_4 with

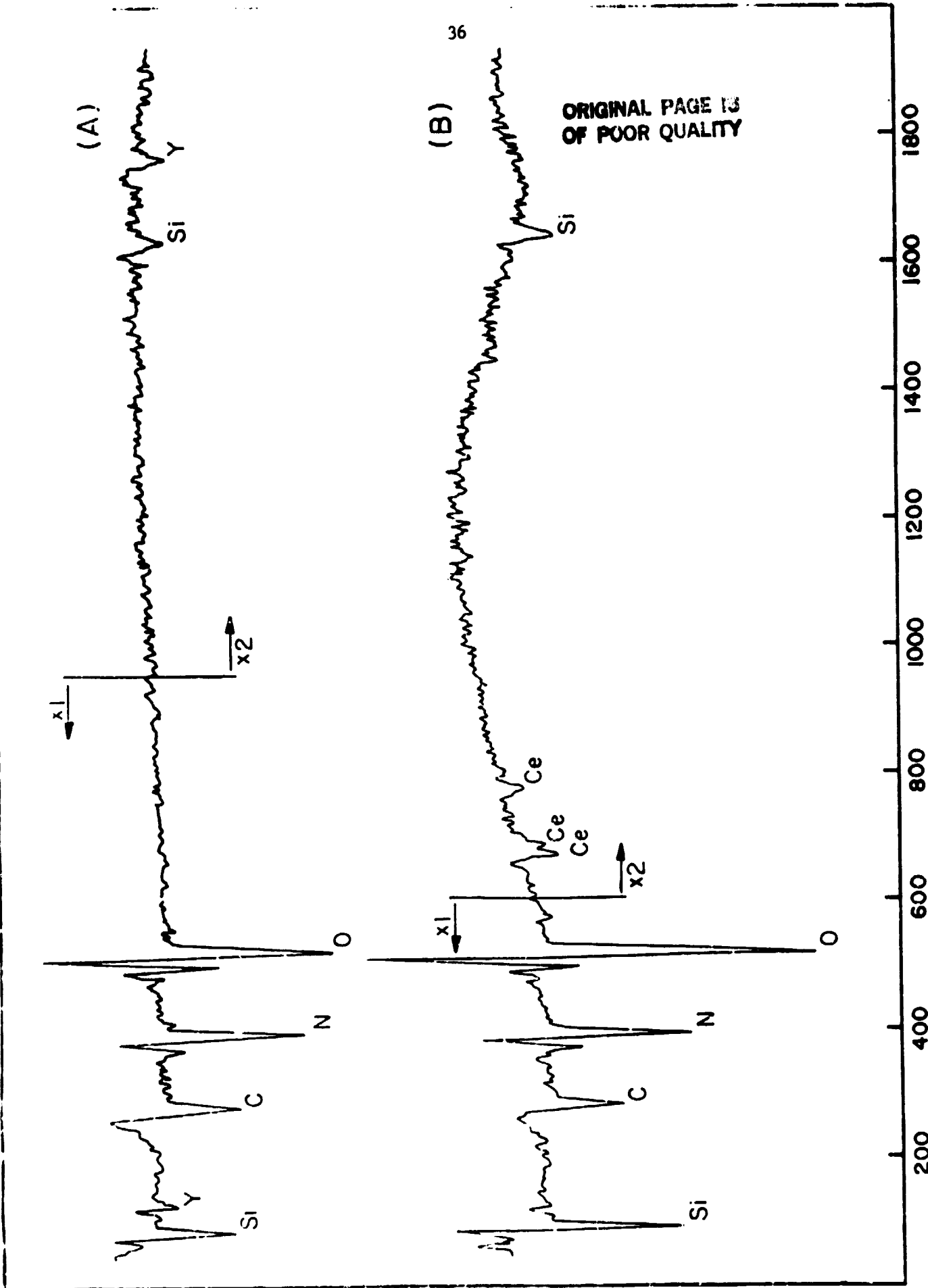


Fig. 2. Auger spectra of fracture surfaces of Si_3N_4 hot-pressed with (A) 10 wt % Y_2O_3 and (B) 10 wt % CeO_2 .

Y_2O_3 and CeO_2 additives. Although no attempt was made in this study to perform quantitative analysis of the grain-boundary phases, an effort is now in progress to locate the area of interest in the sample and to carry out point by point Auger electron analysis using scanning AES to obtain a two dimensional mapping of the concentration of selected surface elements.

Acknowledgements

The authors wish to thank Susan Hofmiester for the Auger electron analysis and Professor Paul H. Holloway for helpful discussions. Partial financial support of NASA Grant #NS6 3254 is also gratefully acknowledged.

REFERENCES

1. A. Tsuge, H. Kudo and K. Komeya, "Reaction of Si_3N_4 and Y_2O_3 in Hot-Pressing", *J. Am. Ceram. Soc.*, 57(6) 269-70 (1974).
2. G. E. Gazza, "Effect of Yttria additions on Hot-Pressed Si_3N_4 ", *Am. Ceram. Soc. Bull.*, 54(9) 778-81 (1975).
3. A. W. J. M. Rae, D. P. Thompson, N. J. Pipkin and K. H. Jack, pp. 347-60 in *Special Ceramics 6*, Edited by P. Popper, British Ceramic Research Association, Stoke-on-Trent, England 1975.
4. R. R. Wills, S. Holmquist, J. M. Wimmer and J. A. Cunningham, "Phase Relationships in the System Si_3N_4 - Y_2O_3 - SiO_2 ", *J. Mater. Sci.*, 11(7) 1305-09 (1976).
5. F. F. Lange, S. C. Singhal and R. C. Kuznicki, "Phase Relations and Stability Studies in the Si_3N_4 - SiO_2 - Y_2O_3 Pseudoternary Systems", *J. Am. Ceram. Soc.*, 60(5-6) 249-52 (1977).
6. G. Q. Weaver and J. W. Lucek, "Optimization of Hot-Pressed Si_3N_4 - Y_2O_3 Materials", *Am. Ceram. Soc. Bull.*, 57(12) 1131-36 (1978).
7. K. S. Mazdizasni and C. M. Cooke, "Consolidation, Microstructure, and Mechanical Properties of Si_3N_4 Doped with Rare-Earth Oxides," *J. Am. Ceram. Soc.*, 57(12) 536-37 (1974).
8. H. F. Priest, G. L. Priest and G. E. Gazza, "Sintering of Si_3N_4 under High Nitrogen Pressure", *ibid.*, 60(1-2) 81 (1977).
9. T. I. Mah, K. S. Mazdizasni and R. Ruh, "The Role of Cerium Orthosilicate in the Densification of Si_3N_4 ", *ibid.*, 62(1-2) 12-16 (1979).
10. J. P. Guha, P. Goursat and M. Billy, "Hot-Pressing and Oxidation Behavior of Silicon Nitride with Ceria Additive," *ibid.*, 63(1-2) 119-20 (1980).
11. F. Lange, " Si_3N_4 - Ce_2O_3 - SiO_2 Materials: Phase Relations and Strength", *Am. Ceram. Soc. Bull.*, 59(2) 239-49 (1980).
12. D. R. Clarke and G. Thomas, "Microstructure of Y_2O_3 Fluxed Hot-Pressed Silicon Nitride", *J. Am. Ceram. Soc.*, 61(3-4) 114-18 (1978).
13. O. L. Krivanek, T. M. Shaw and G. Thomas, "The Microstructure and Distribution of Impurities in Hot-Pressed and Sintered Silicon Nitride", *ibid.*, 62(11-12) 585-90 (1979).
14. R. Kossowsky, "The Microstructure of Hot-Pressed Silicon Nitride," *J. Mater. Sci.*, 8(11) 1603-15 (1973).

15. B. D. Powell and P. Drew, "The Identification of a Grain-Boundary Phase in Hot-Pressed Silicon Nitride by Auger Electron Spectroscopy", *ibid.*, 9(11) 1867-70 (1974).
16. S. Hoffmann and L. J. Gauckler, "A Study of Fracture Surfaces of Hot-Pressed Silicon Nitride by Auger Electron Spectroscopy", *Powder Met. Int.*, 6(2) 90-92 (1974).
17. L. J. Gauckler, H. Hohnke and T. Y. Tien, "The System $\text{Si}_3\text{N}_4\text{-SiO}_2\text{-Y}_2\text{O}_3$ ", *J. Am. Ceram. Soc.*, 63(1-2) 35-37 (1980).

Figure Captions

- Figure 1. Scanning electron micrographs of fracture surfaces of hot-pressed Si_3N_4 containing (A) 10 wt % Y_2O_3 and (B) 10 wt % CeO_2 .
- Figure 2. Auger spectra of fracture surfaces of Si_3N_4 hot-pressed with (A) 10 wt % Y_2O_3 and (B) 10 wt % CeO_2 .

COMPOSITIONAL EFFECTS ON Si_3N_4 FRACTURE SURFACES

L. L. Hench
University of Florida
Ceramics Division
Department of Materials Science and Engineering
Gainesville, Florida 32611

F. Ohuchi
E.I. duPont de Nemours and Company
Experimental Station
Central Research & Development Department
Wilmington, DE. 19898

P. N. Vaidyanathan
Manchester Division
The Warner and Swasey Company
5142 Manchester Road
Akron, OH. 44319

S. Dutta
NASA Lewis Research Center
Mail Stop 49-3
2100 Brookpark Road
Cleveland, OH. 44135

November 23, 1982

Introduction

Studies of dense Si_3N_4 show that the extent of an intergranular amorphous silicate phase is a function of the concentration and type of densification aids such as MgO ^(1,2), Y_2O_3 ^(3,4), CeO_2 ⁽⁵⁾ and Al_2O_3 ^(5,6). It has also been shown that the high temperature mechanical strength is also a function of the same compositional variables^(4,5) leading to the conclusion that the intergranular amorphous phase controls the thermal limits of performance. This conclusion is reinforced with evidence that crystallization of the grain boundary phase significantly improves high temperature mechanical strength⁽⁷⁾.

Although there have been efforts to analyze the intergranular phase on Si_3N_4 fracture surfaces^(8,9) the effects of densification aids and thermal history on extent of crystallinity of the fracture surface is still to be established. Smith and Quackenbush⁽⁵⁾, for example, showed that sintered Si_3N_4 containing Y_2O_3 and Al_2O_3 additions exhibited a 1400°C fracture surface containing many pullouts indicative of easy slippage between grains. Samples without Al_2O_3 showed much more transgranular fracture at both room temperature and 1400°C. However, identification of the intergranular phase responsible for these differences is extremely difficult since the thickness of the phase must be very small (100-200 Å) and may or may not be homogeneously distributed^(2,6,10).

The objectives of this investigation are twofold, (1) determine whether several surface analysis techniques (x-ray, IRRS, AES, etc.) can detect similar differences between fracture and non-fracture surfaces of dense Si_3N_4 and (2) establish whether variations in densification

additives or a crystallization heat treatment can alter the fracture surface analysis.

In understanding surfaces and interfaces it is important to recognize that analytical techniques sample to different depths within a surface. Secondary ion mass spectroscopy, ion scattering spectroscopy, and Auger electron spectroscopy (AES) obtain data from the near surface of a sample at a depth of 5-50 Å. The middle surface of the sample can be analyzed by using infrared reflection spectroscopy (RRS) to a depth of 0.5 μm. Standard scanning electron microscopy with energy dispersive x-ray analysis and electron microprobe techniques, penetrate to depths as large as 1.5 μm and such measurements are termed to be from the far surface⁽⁷⁾.

Hence the techniques chosen were IRRS, AES and x-ray so that information could be obtained from the near to the far surface.

Materials

Three series of Si_3N_4 samples containing various concentrations of densification aids were compared in this study. Bars containing 8% (by weight) Y_2O_3 and very low (<1%) Al_2O_3 (1" x 1/4" x 1/8") were hot pressed at NASA Lewis Research Center. A GTE SN402 amorphous Si_3N_4 powder was used with Y_2O_3 blended by dry milling. Samples were first cold pressed into compacts followed by hot pressing at 1760°C for 3 hrs. and 5000 psi. The other two series of samples were from commercial lots of sintered Si_3N_4 : 13-15% Y_2O_3 , 6% Al_2O_3 (GTE SN 2502) and 20% Y_2O_3 , 6% Al_2O_3 (GTE SN 3502). All samples were ground and polished to a final surface finish of 1 μm diamond paste.

Selected samples of each composition were also heat treated at 1000°C for 10 hrs. in vacuum, after densification, in order to alter the crystallization of the grain boundary phase.

Results

X-ray analysis

Standard powder diffraction analysis was performed on the samples before and after the 1000°C/10 hr. heat treatment. Figure 1 shows considerable difference in the phases present for the three materials. The sample with only 8% Y_2O_3 and little Al_2O_3 (Fig. 1A) shows $\beta-Si_3N_4$ similar to the results of Smith and Quackenbush for $Si_3N_4+6 Y_2O_3$ with no Al_2O_3 ⁽⁵⁾, and as predicted from the compatibility diagram of Wills et. al⁽¹²⁾.

Increasing the Y_2O_3 content to 13-15% and addition of 6% Al_2O_3 resulted in only $\beta-Si_3N_4$ appearing (Fig. 1B), again similar to the results of Smith and Quackenbush⁽⁵⁾ when Al_2O_3 was added to their $Si_3N_4+6 Y_2O_3$ samples. The absence of minor phases in the diffraction pattern indicates that the intergranular phase developed during densification is retained as an amorphous phase. However, when sufficient Y_2O_3 is present (20%) the Al_2O_3 addition does not suppress crystallization of the intergranular phase and a significant quantity of the 10.9.1 phase appears (Fig. 1C).

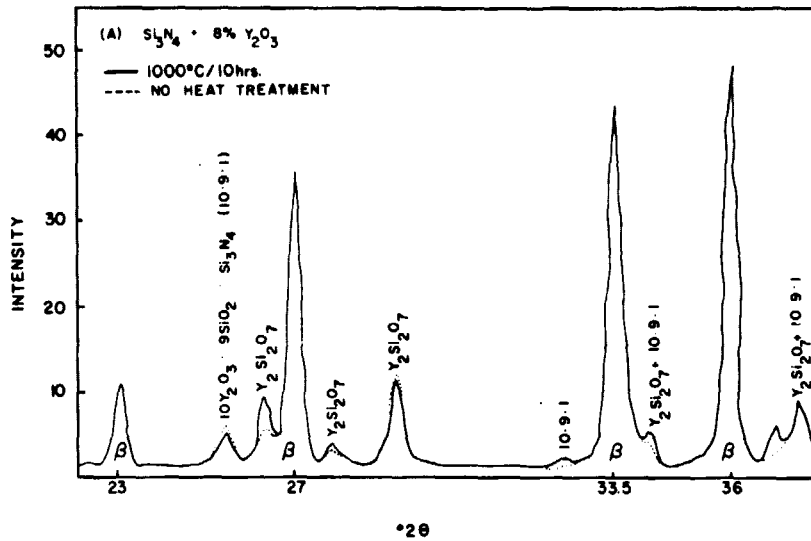


Fig. 1A. X-ray diffraction pattern of $\text{Si}_3\text{N}_4 + 8\% \text{Y}_2\text{O}_3$.

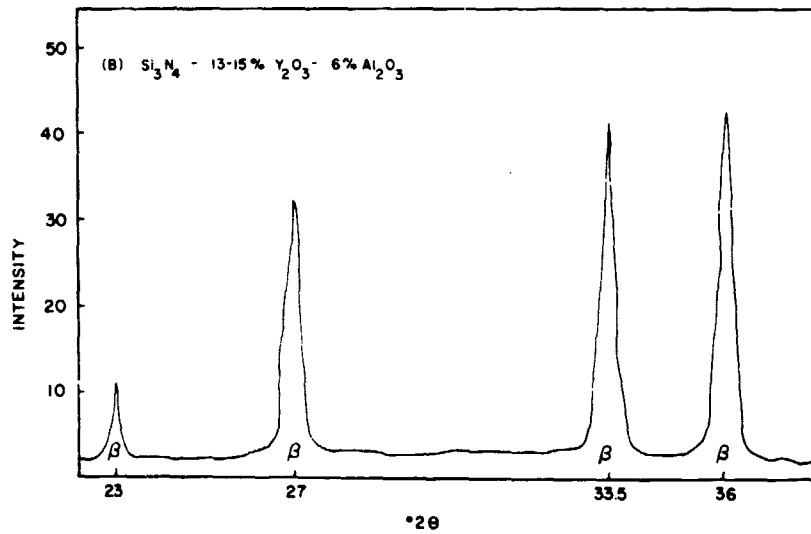


Fig. 1B. X-ray diffraction pattern of $\text{Si}_3\text{N}_4 + 13-15\% \text{Y}_2\text{O}_3 + \text{Al}_2\text{O}_3$.

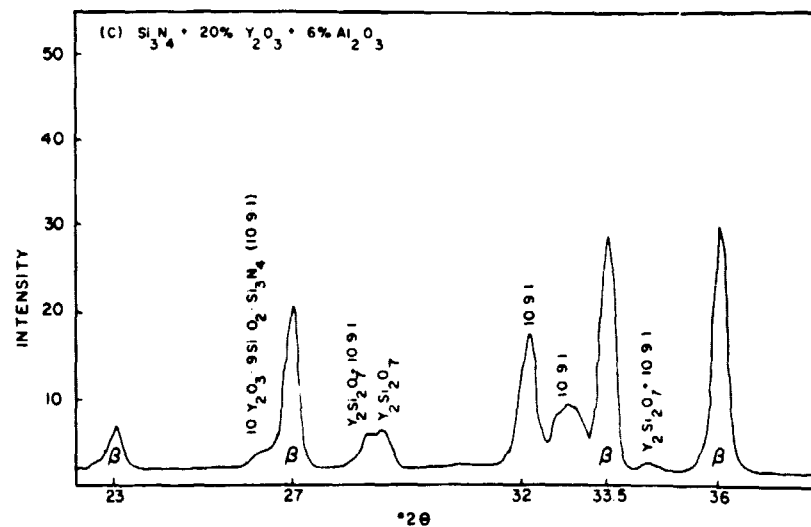


Fig. 1C. X-ray diffraction pattern of $\text{Si}_3\text{N}_4 + 20\% \text{Y}_2\text{O}_3 + 6\% \text{Al}_2\text{O}_3$.

A 10 hours heat treatment in vacuum at 1000°C shows a small effect on the extent of the minor phases for the 8% Y_2O_3 sample (Fig. 1A). There is an increase in both the $Y_2Si_2O_7$ and 10.9.1 phases. No differences were detected for the phases in the 15% and 20% Y_2O_3 samples after heat treatment (Figs. 1B, 1C).

Infrared Reflection Spectroscopy (IRRS) Analysis

Samples from the three compositional series before and after heat treatment were fractured in three point bending. The purpose of the three point bending fracture was to obtain a clean fracture surface that could be analyzed. The fracture surfaces were compared with polished surfaces using infrared reflection spectroscopy (IRRS). The technique was developed for the analysis of vitreous silicates⁽¹³⁾ and recently applied to studies of the oxidation and processing of Si_3N_4 ⁽¹⁴⁾. In this analytical method a double beam IR spectrometer is used in either of two modes. The specimen for analysis can be placed on one aperture and a spectrum obtained in comparison with a highly polished reflective metal mirror. The spectrum that results is termed a single beam spectrum because the purpose of the mirror is simply to eliminate the errors associated with air scattering and instrumental variations. However, for very precise analytical work, or the elimination of certain complex features from spectra, it is possible to compare the surface of the unknown placed on the specimen aperture with a reference standard. The spectrum that results is called a difference spectra. The advantage of a difference spectrum is that it is possible to compare samples with and without various environmental changes in the surface of the sample⁽¹⁴⁾.

As the incident IR beam penetrates only 0.2-0.5 μm of the surface of the sample the measurements are sensitive to surface films present on the sample. Consequently, if the Si_3N_4 fracture surfaces have an increased concentration of amorphous silicate phase over that of the bulk, the difference should appear in the comparison of spectra of a fracture surface versus a polished surface.

A single beam IRRS spectrum of vitreous SiO_2 is compared to that of a polished surface of dense $\text{Si}_3\text{N}_4 + 8\% \text{Y}_2\text{O}_3$ in Figure 2. Two major peaks due to Si-O-Si bonds appear in the vitreous SiO_2 spectrum. The (S) peak at 1110 cm^{-1} is due to the molecular stretching vibration of the Si-O-Si bonds and the (R) peak at 470 cm^{-1} is due to molecular rocking vibrations of the same bonds⁽⁸⁾. Because of disorder in the structure of vitreous SiO_2 there is considerable broadening of both of these reflection peaks.

The IRRS spectrum of Si_3N_4 shows two Si-N-Si molecular stretching vibrations (SN_1 and SN_2) located at 1020 cm^{-1} and 900 cm^{-1} respectively. Three Si-N-Si molecular rocking vibrations (SNR_1 , SNR_2 , SNR_3) are also present at 570 cm^{-1} , 430 cm^{-1} , and 370 cm^{-1} . The relationship between these vibrational modes with Si_3N_4 structures^(15,16,17) are still being established.

Single beam IRRS spectra of Si_3N_4 fracture surfaces (Fig. 2) show a loss of most of the reflected intensity which is due to the roughened surface of the fracture. Nearly all of the intensity of the SN_1 peak

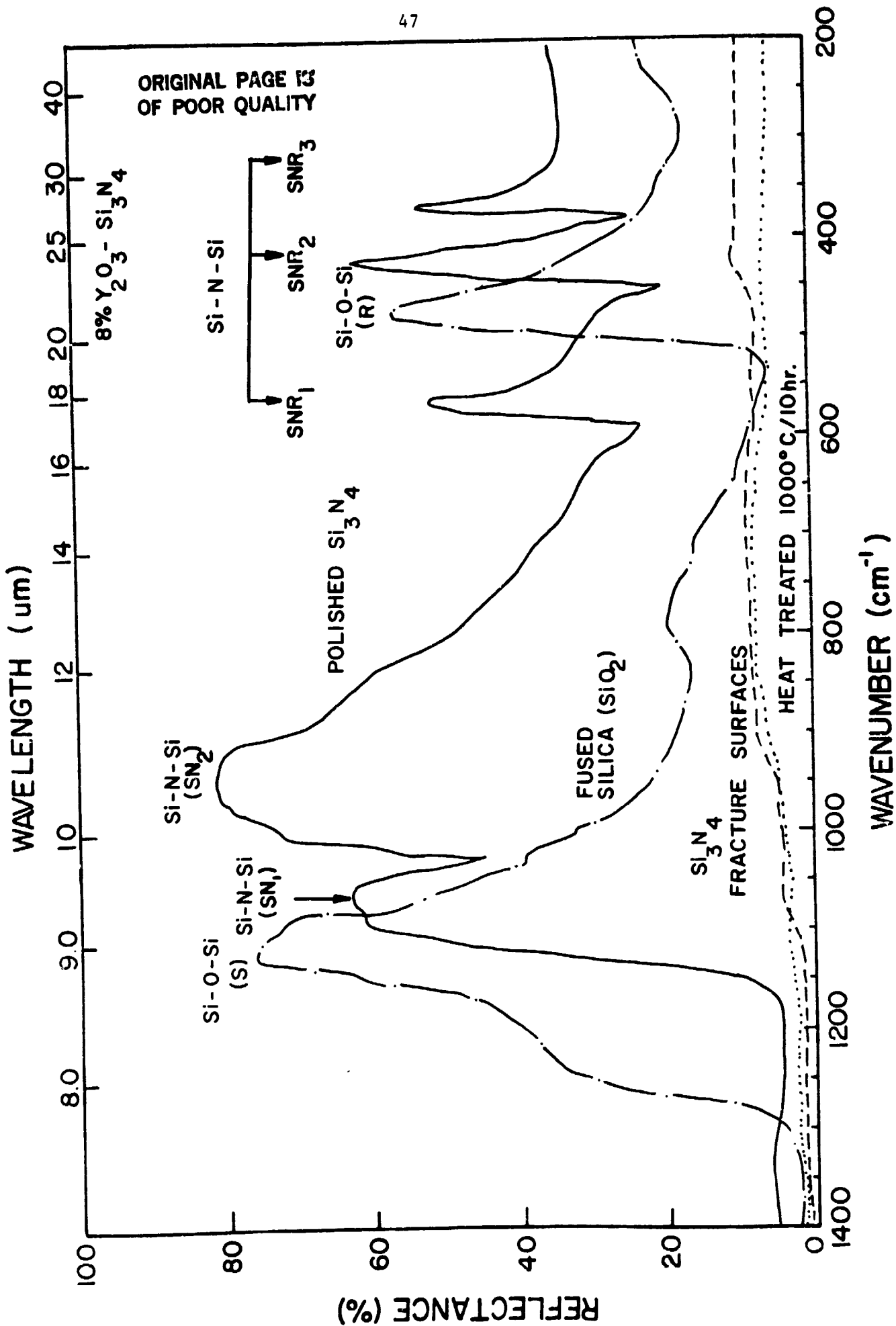


Fig. 2. Infra Red Spectra of Si₃N₄ + 8% Y₂O₃

is gone whereas some reflection intensity at the location of the SN_2 peak is still present. This suggests that there may be some variation in the composition of the fracture surface compared with the non-fractured material. Only a small difference between samples with and without the $1000^\circ\text{C}/10$ hr. heat treatment is detected.

In order to emphasize the spectral differences between the polished and the fracture surfaces, a second set of IRRS spectra was obtained using the difference spectroscopy method⁽¹⁰⁾. In this method only the molecular vibrations within the surface layer of the fractured vs non-fractured samples that are different are plotted as a function of the wavelength of the incident radiation.

Fig. 3A shows the IRRS difference spectra for the 8% Y_2O_3 sample with and without the $1000^\circ\text{C}/10$ hr. heat treatment. Before heat treatment some differences exist in the molecular vibrations in the $1400\text{--}1150$ cm^{-1} region for the fracture vs. non-fractured surfaces. This is the spectral region where Si-O-Si vibrations are intense (see Fig. 2) and indicates a larger concentration of Si-O bonds within the fracture surface than in the polished surface. Heat treatment eliminates these differences which indicates that there is less preferential fracture within the intergranular phase after 10 hrs. at 1000°C .

Increasing the concentration of oxide densification aids increases the magnitude of the difference spectra in the 1100 cm^{-1} to 1300 cm^{-1} range (Figs. 3B and 3C). This indicates that more Si-O bonds are present in the fracture surface of the samples containing the higher concentrations of Y_2O_3 . This is as expected if the densification aids are concentrating

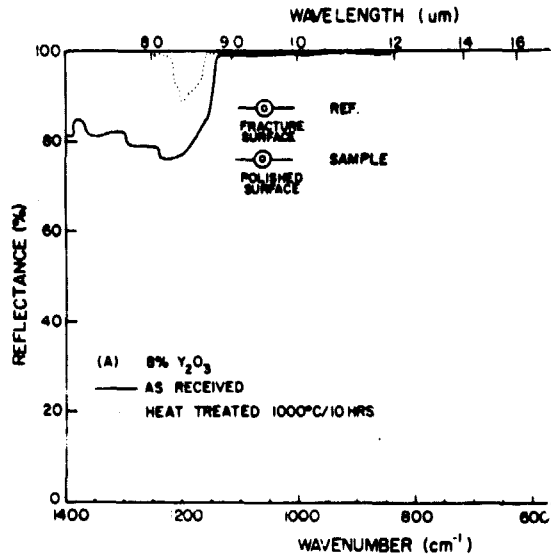


FIG 3A IR DIFFERENCE SPECTRA OF $Si_3N_4 + 8\% Y_2O_3$

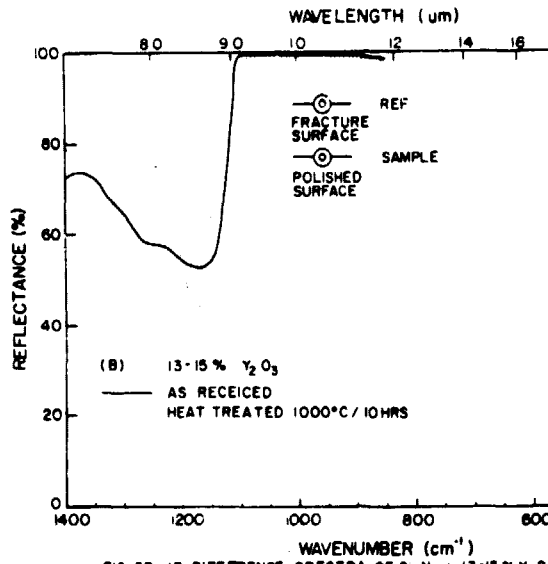


FIG 3B IR DIFFERENCE SPECTRA OF $Si_3N_4 + 13-15\% Y_2O_3$

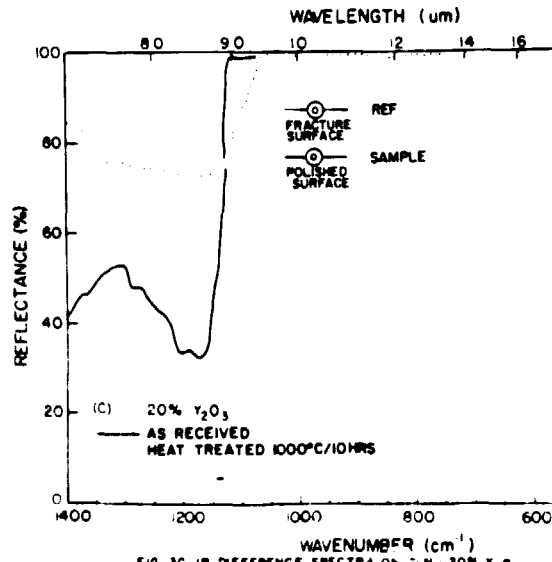


FIG 3C IR DIFFERENCE SPECTRA OF $Si_3N_4 + 20\% Y_2O_3$

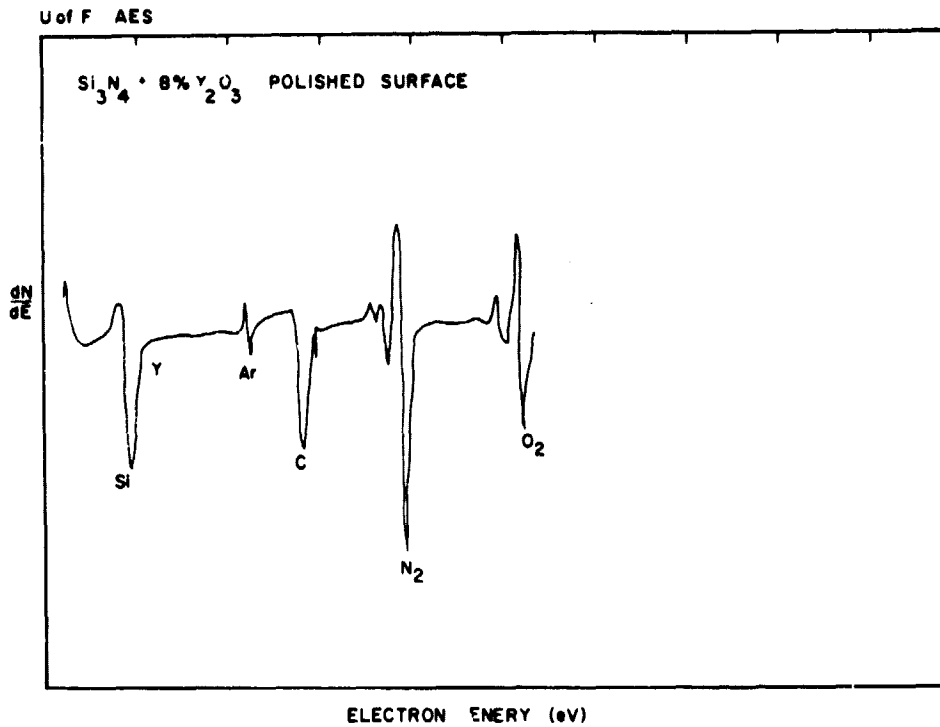
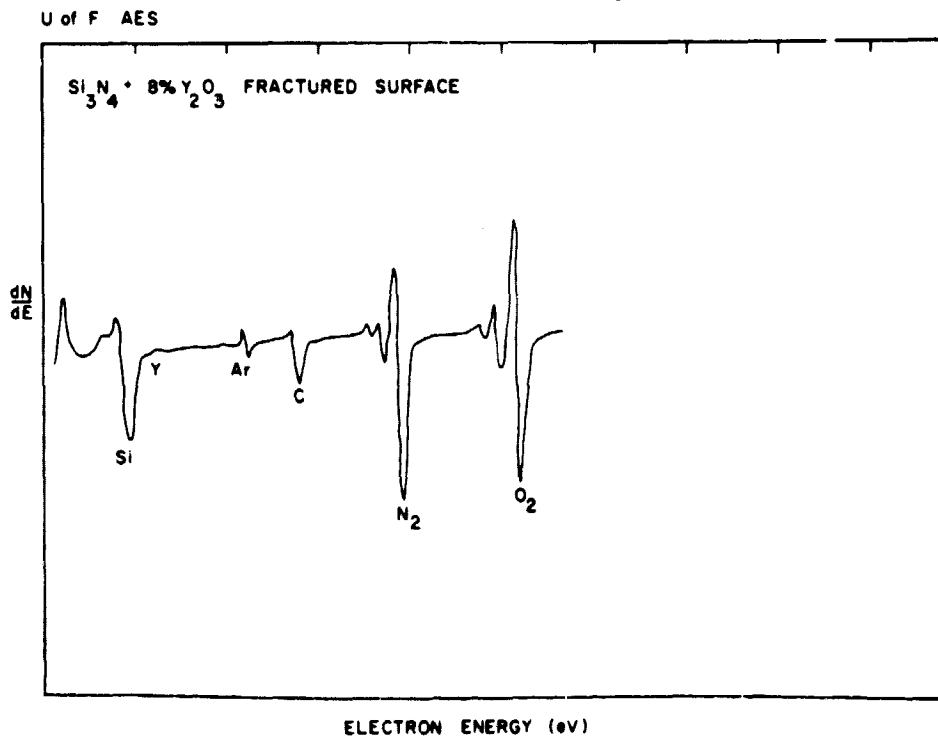
ORIGINAL PAGE IS
 OF POOR QUALITY

in the grain boundaries and fracture occurs preferentially through the g.b. phase. Heat treatment at 1000°C decreases the spectral difference between fracture and polished surfaces for both the 13-15% Y_2O_3 and the 20% Y_2O_3 samples. However, the phase on the fracture surface of the 13-15% Y_2O_3 samples is more resistant to heat treatment and therefore is indicative of a vitreous phase more resistant to devitrification.

Auger Electron Spectroscopy

Auger electron spectroscopy (AES) was used to determine the composition differences of the fractured versus polished surfaces of the Si_3N_4 samples. The experimental techniques employed in AES are well established⁽¹⁸⁾ and will not be discussed here. The Auger analysis was made with a single path cylindrical mirror analyzer (CMA15-110, Perkin-Elmer, Physical Electronics Div., Eden Prairie, MN) incorporating a scanning electron gun. The primary electron beam was incidental 35-45° to the fractured surface of the specimen. The primary energy of 5 K eV with the beam current density of 2×10^{-1} A/cm² was used throughout the experiments. The derivative of the energy distribution of the secondary electrons was plotted using standard techniques. The modulation signals were kept constant at 3 eV peak to peak up to 550 eV in the Auger spectrum and at 15 eV after 550 eV.

Figure 4 shows typical spectra after Ar sputter cleaning of the surfaces from the Si_3N_4 -8% Y_2O_3 series. The oxygen content of the fracture surface (Fig. 4B) is considerably enhanced over that of the polished surface (Fig. 4A). There is almost a factor of 2x higher O/N ratio for the fracture surface. As the percentage of densification aid

Fig. 4A. Auger spectra of $\text{Si}_3\text{N}_4 + 8\% \text{Y}_2\text{O}_3$ - polished surface.Fig. 4B. Auger spectra of $\text{Si}_3\text{N}_4 + 8\% \text{Y}_2\text{O}_3$ - fractured surface.

is increased (Table I) the O/N ratio increased in the polished surface of the Si_3N_4 samples but even more so in the fracture surface and grain boundary phase.

Vacuum heat treatment of the samples at 1000°C produced quite variable results in the AES analysis (Table 1). The O/N ratio of the 8% Y_2O_3 sample increased with heat treatment and the fracture and polished surfaces became more alike. This change is consistent with the spectral differences in the IRRS analysis. Heat treating the 20% Y_2O_3 samples produced similar changes, i.e. the O/N ratio increases with heating and there is less difference between polished and fracture surfaces. However, the 15% Y_2O_3 material showed a decrease in O/N ratio upon heating and a larger difference between fracture and polish surfaces, for unknown reasons.

The above results confirmed the presence of an oxygen enriched phase at the fracture surfaces of the Si_3N_4 samples similar to the findings of Powell and Drew⁽⁸⁾ and Kosowsky⁽⁹⁾. These results also show that the addition of larger quantities of Y_2O_3 enhanced the concentration of oxygen within the fracture surface. Heat treatment at 1000°C changed the oxygen content of both fracture and non-fracture surfaces. However these findings yield little additional understanding regarding the crystalline versus glassy nature of the fracture surface.

Therefore, another experiment was performed using the rate of Si dissociation from the fracture surface as an index of the amorphous versus crystalline nature of the fracture phase(s). Thomas⁽¹⁹⁾ showed that under conditions of electron bombardment Si dissociated from the

TABLE I
 Auger Electron Spectroscopic (AES) Analysis of
 Oxygen/Nitrogen Peak Height Ratios of Si_3N_4 Polished
 and Fracture Surfaces

	<u>(O/N) Polished Surface</u>	<u>O/N Fractured Surface</u>
	<u>8% Y_2O_3</u>	
No Heat Treatment	0.6	1.1
Heat Treated 1000°C/10 hrs	1.7	2.0
	<u>15% Y_2O_3</u>	
No Heat Treatment	1.6	2.2
Heat Treated 1000°C/10 hrs	0.8	3.0
	<u>20% Y_2O_3</u>	
No Heat Treatment	1.2	1.7
Heat Treated 1000°C/10 hrs	3.8	3.1

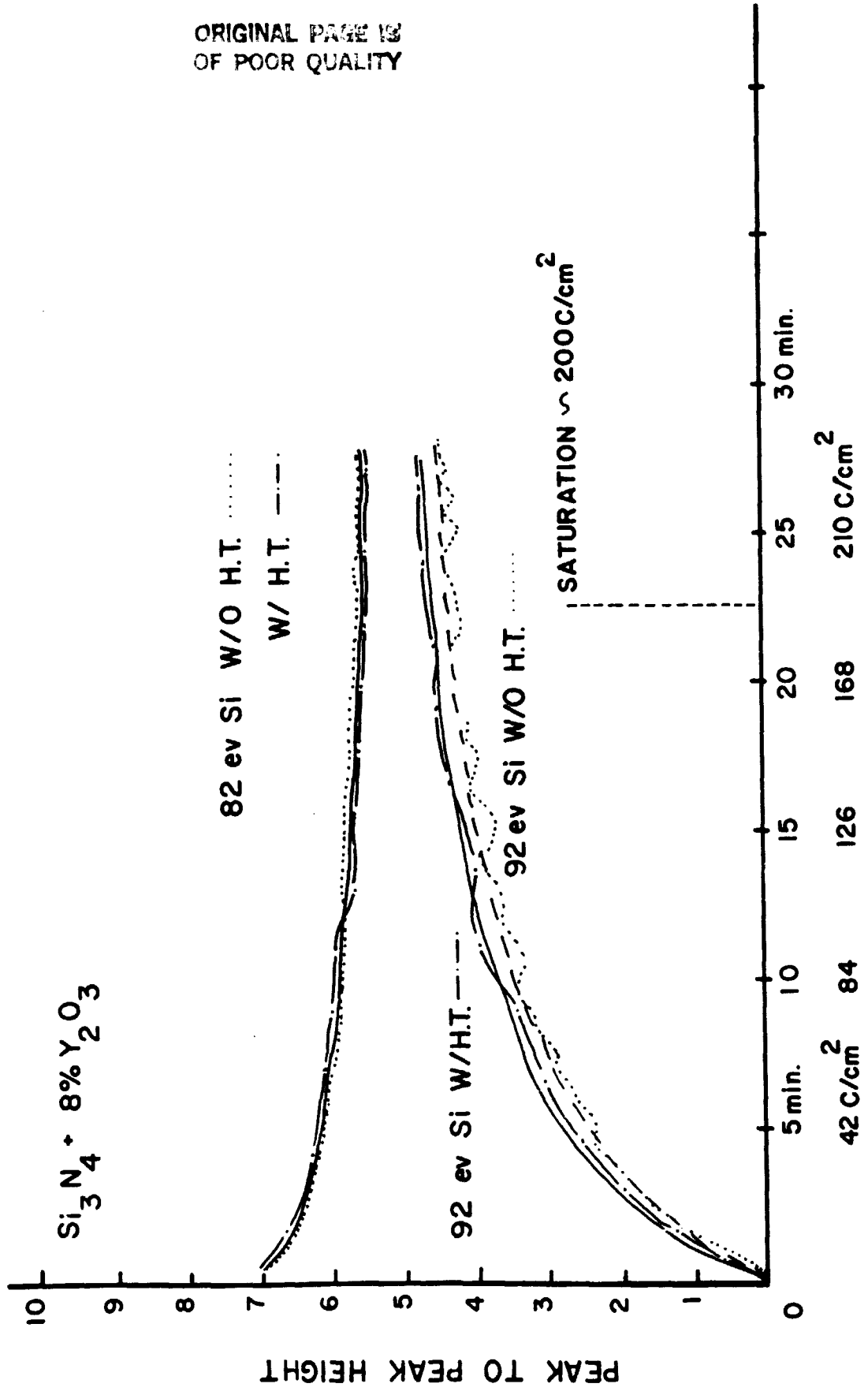
surface of quartz much more rapidly than from the surface of vitreous silica. Therefore, it was hypothesized that if an oxygen enriched Si_3N_4 fracture surface is amorphous, the rate of Si dissociation should be more rapid than from a devitrified fracture surface. Thus, a difference in the rate of dissociation may be associated with amorphous phase formation at the grain boundaries.

Samples of 8% Y_2O_3 - Si_3N_4 , before and after heat treatment, were fractured in-situ at 10^{-9} Torr in an Auger electron spectrometer. The decay of the 82 eV Si peak (characteristic of chemically bonded Si) and increase in the 92 eV Si peak (characteristic with elemental silicon) were monitored as a function of incident electron beam current (Fig. 5). Saturation was observed at approx. 200 c/cm^2 . No effect of the $1000^\circ \text{C}/10 \text{ hr.}$ heat treatment was observed.

A similar Si dissociation experiment was performed on the fracture surface of the Si_3N_4 sample containing 13-15% $\text{Y}_2\text{O}_3 + \text{Al}_2\text{O}_3$. Saturation occurred at approx. 600 C/cm^2 . Figure 6 compares results from the two compositions. The Si dissociation from the 8% Y_2O_3 fracture surface (10^{-9} Torr) was much more rapid (3x) than dissociation from the 15% Y_2O_3 fracture surface. No effect of the $1000^\circ\text{C}/10 \text{ hr.}$ heat treatment was observed in either sample.

Therefore, these results support the conclusion that the fracture surface of the 8% Y_2O_3 - Si_3N_4 material. However, they do not provide additional evidence regarding crystallization of the grain boundaries with the $1000^\circ\text{C}/10 \text{ hr.}$ heat treatment.

FIG. 5
RATE OF DISSOCIATION
OF Si



ORIGINAL PAGE IS
OF POOR QUALITY

ORIGINAL PAGE IS
OF POOR QUALITY

SUMMARY OF AES STUDY

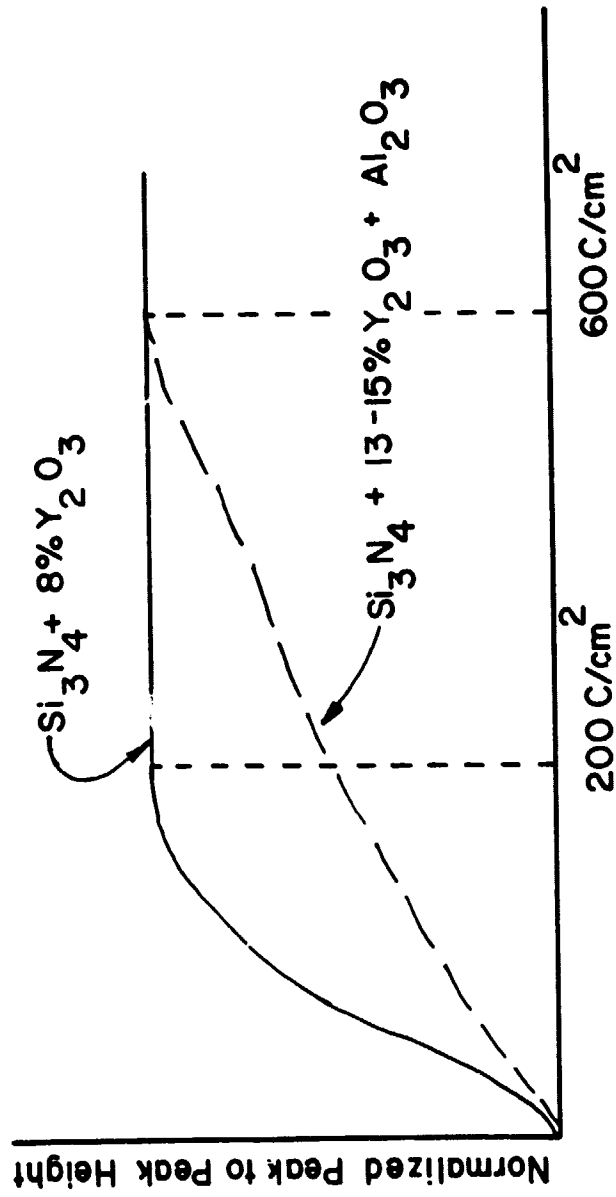


FIG. 6

Conclusions

Several surface analysis techniques (X-ray, IRRS, AES) applied to the same samples, show that fracture surfaces of Si_3N_4 with Y_2O_3 densification aids possess a higher concentration of oxygen than the bulk. Thus, the oxide densification aids concentrate in the grain boundaries and even low temperature fracture appears to occur preferentially within the oxygen enriched grain boundaries. Increasing concentrations of Y_2O_3 and Al_2O_3 increase the oxygen content of the fracture surface. A range of 13-15% Y_2O_3 +6% Al_2O_3 produces an amorphous g.b. phase which is resistant to devitrification. Fracture occurs through the amorphous phase with a 1000°C heat treatment having little effect on the amorphous phase.

Acknowledgment

The authors acknowledge partial financial support of NASA Grant #NSG3254 and helpful discussions with Prof. Paul Holloway.

References

1. S. Wild, P. Grieveson, K. H. Jack and M. J. Latimer, "Role of Magnesia in Hot-Pressed Si_3N_4 ", pp. 377-84 in Special Ceramics 5. Edited by P. Popper, British Ceramic Research Assn., Stokeon-Trent, England 1972.
2. L. K. V. Lou, T. E. Mitchell, and A. H. Heuer, "Discussion of Grain Boundary Phases in a Hot-Pressed MgO Fluxed Silicon Nitride," J. Am. Ceram. Soc., 61(9-10) 462-64 (1978).
3. G. E. Gazza, "Effect of Yttria Additions on Hot-Pressed Si_3N_4 ", Am. Ceram. Soc. Bull., 54(9) 778-81 (1975).
4. A. Tsuge, H. Kudo, and K. Komeya, "Reaction of Si_3N_4 and Y_2O_3 in Hot-Pressing", J. Am. Ceram. Soc. 57(6) 269-70 (1974).
5. J. Thomas Smith & Carr Lane Quackenbush "Phase Effects in Si_3N_4 Containing Y_2O_3 or CeO_2 ", American Ceramic Society Bulletin 59(5) 529-532 (1980).
6. R. E. Loehman and D. J. Rowcliffe, "Sintering of Si_3N_4 - Y_2O_3 - Al_2O_3 ", J. Am. Ceram. Soc. Vol. 63, (3-4) 144-148 (1980).
7. A. Tsuge, K. Nishida, and M. Komatsu, "Effects of Crystallizing the Grain-Boundary Glass Phase on the High Temperature Strength of Hot-Pressed Si_3N_4 Containing Y_2O_3 ", 58(7-8) 323-26 (1975).
8. B. D. Powell and P. Drew "The Identification of a grain boundary Phase in Hot-Pressed Silicon Nitride by Auger Electron spectroscopy", J. Mat. Sci., 9 1867-1870 (1974).
9. R. Kossowsky, "The microstructure of Hot-Pressed Si_3N_4 ", J. Mat. Sci. 8, 1603 (1973).
10. P. Drew and M. H. Lewis "The Microstructures of Silicon Nitride Ceramics During Hot-Pressing Transformations", J. Mat. Sci. 9, 261-269 (1974).
11. L. L. Hench, "Surface Characterization of Glass", in Characterization of Materials in Research, Ceramics and Polymers, U. Weiss and J. J. Burke, eds., Syracuse Univ. Press, Syracuse, N.Y. 211-251 (1975).
12. R. R. Wills, S. Holmquist, J. M. Wimmer, and J. A. Cunningham, "Phase Relations in the System Si_3N_4 - Y_2O_3 - SiO_2 ", J. Mater. Sci., 11(7) 1305-1309 (1976).
13. D. M. Sanders, W. B. Person, and L. L. Hench, "Quantitative Analysis of Glass Structure with the Use of Infrared Reflection Spectra", Appl. Spectro., 28(3) 247-255 (1974).

14. L. L. Hench, "Use of New Surface Physics For Controlling The Physical Properties of Ceramics", Proceedings Science of Ceramics 10, September 2-4, Munich, Germany (1979).
15. D. Hardie and K. H. Jack, "Crystal Structure of Silicon Nitride", Nature, 180, 332-333 (1957).
16. D. S. Thompson and P. L. Pratt, "The Structure of Silicon Nitride" Science of Ceramics 3, G. H. Stewart, ed. Academic Press 33-51 (1967).
17. D. R. Messier, "The Alpha/Beta Silicon Nitride Phase Transformation, Army Materials and Mechanics Res. Center, Watertown, MA. AMMRC TR 77-15 (1977).
18. Paul H. Holloway, "Fundamentals and Applications of Auger Electron Spectroscopy", Advances in Electronics and Electron Physics, Vol. 54, 241-298 (1980).
19. S. Thomas, "Electron Irradiation Effect in Auger Analysis of SiO_2 ", J. of Appl. Phy. 45(1) 161-166 (1974).

ANALYSIS OF GRAIN BOUNDARY PHASE DEVITRIFICATION
OF Y_2O_3 AND Al_2O_3 DOPED Si_3N_4

L. L. Hench and P. N. Vaidyanathan*

Ceramics Division
Department of Materials Science and Engineering
University of Florida
Gainesville, Florida 32611

*Presently at Manchester Division, Warner and Swasey Co.,
5142 Manchester Rd., Akron, OH 44319.

Introduction

A number of studies have shown that $Y_2O_3 + Al_2O_3$ additions to Si_3N_4 enhance densification and produce an amorphous grain boundary phase. (1-5)

It has also been shown that thermal treatments can be used to devitrify the grain boundary phase and thereby improve the high temperature mechanical properties. (4) Because of the very small scale of intergranular phases and their heterogeneous distribution it is difficult to follow devitrification processes. Previous studies have shown however that surface analysis method such as Auger electron spectroscopy (AES) can be used to analyze compositional differences between fracture surfaces and bulk, polished surfaces. (6-9)

Differences due to extent of crystallinity are difficult to assess though since AES is primarily a method sensitive to differences in elemental compositions of the surface. It also has been shown that infrared reflection spectroscopy (IRRS) can be used in a difference method to compare the fracture surface vs polished surface of Si_3N_4 samples. (9,10) However, it is often difficult to interpret details of the difference spectra.

The objective of the present communication is to show that use of a Fourier transform IR spectrometer in a single beam reflection mode can be used for direct comparison of fracture vs non-fractured Si_3N_4 surfaces. This is possible because the FTIR method permits a digital summation of nearly 1000 scans of the fracture surface. Consequently even though the fracture surface is rough and scatters the incident IR beam there is sufficient intensity per scan to produce a reliable summation spectrum of the surface. Therefore, changes in the fracture surface resulting from devitrification of the grain boundary phase are observable.

Materials and Methods

The samples used in this study were obtained from NASA Lewis Research Center, Cleveland, Ohio. Commercial grade Si_3N_4 , Y_2O_3 and Al_2O_3 were used. The sample contained 15% Y_2O_3 and 2% Al_2O_3 by weight. Mixtures for 100g batches were wet milled in polyethylene bottles for 17-20 hrs using high alumina grinding media and ethanol. The starting compositions were adjusted for Al_2O_3 pick up. After the powders were milled, the slurry was dried and sieved through a 60 mesh sieve to break up agglomerates. The powders were cold pressed at 414 MN/m^2 and sintered at 1750°C for 2 hrs under 1 atm nitrogen atmosphere. The specimens were then machined into test bars (2.54 by 0.64 by 0.32 inches) and the surfaces were subsequently ground to a surface finish of 10-15 μm .

The samples were heat treated in a vacuum induction heating furnace at either 1000°C for 10 hrs or 1200°C for 10 hrs each. The vacuum was maintained at 10^{-5} Torr. The samples were mounted on boron nitride dies during the heat treatment, to prevent contamination. The furnace was allowed to cool for 7 hrs before the samples were retrieved. The samples were analyzed by x-ray diffraction analysis (XRD) and by Fourier transform infrared reflection spectroscopic (FTIR) analysis. ⁽¹¹⁾

Results

The x-ray diffraction data of the non-heat treated and the heat treated samples are shown in Fig. 1. In the non-heat treated samples only the β -silicon nitride peaks are seen. However an amorphous hump is also observed indicating the presence of a glassy phase. When heat treated at 1000°C for 10 hrs, one additional peak is seen. However, after heat-treating at 1200°C for 10 hrs, several additional peaks are observed

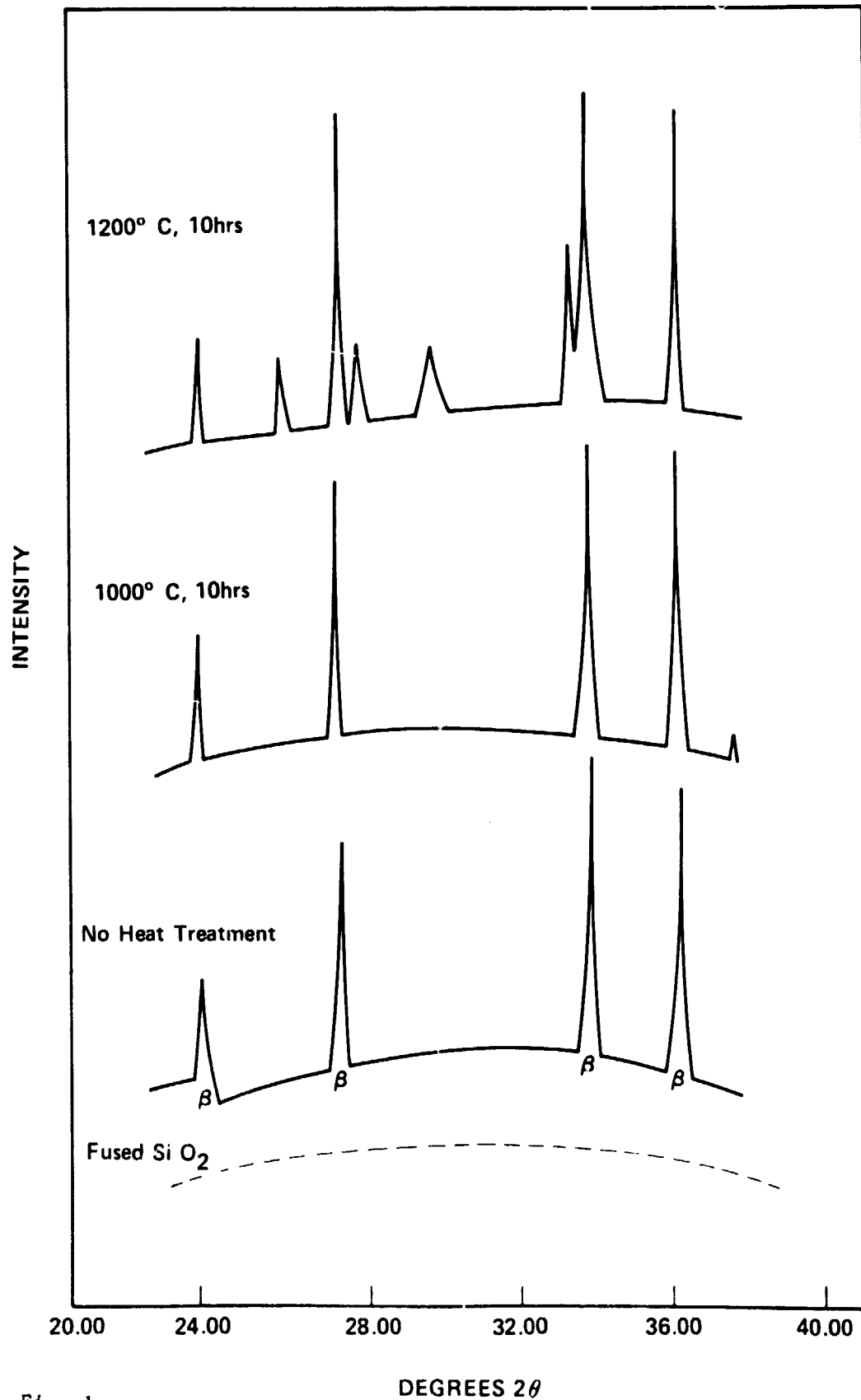
X-RAY DIFFRACTION PATTERNS OF $\text{Si}_3\text{N}_4 + 15\% \text{Y}_2\text{O}_3 + 2\% \text{Al}_2\text{O}_3$ 

Fig. 1

indicating the presence of crystalline phases. The amorphous hump is also decreased, suggesting that the glassy phase has crystallized and thus given rise to the new peaks.

The samples were analyzed by the FTIR method which involved a computer summation of 960 spectral scans. In addition to analyzing the polished surfaces, the samples were fractured in three point bending and the fracture surfaces were also analyzed by mounting the broken end of the sample over the 3 mm specular reflection aperture. The results are presented in Fig. 2.

The dotted curve in Fig. 2 is the IRRS spectrum of vitreous, fused silica used for a standard of comparison of Si-O stretching bonds at 1120 cm^{-1} vs Si-N stretching bonds. As discussed previously^(9,10) there are two primary Si-N molecular stretching vibrations in Si_3N_4 , SN_1 at 1050 cm^{-1} and SN_2 at 900 cm^{-1} . The dashed curves in Fig. 2 show that there is very little change in the SN_1 peak during heat treatment at either 1000°C or 1200°C . However there is a sharpening of the SN_2 peak, especially after the 1200°C treatment. This change is similar to that observed in the devitrification of $\text{Li}_2\text{O}-2\text{SiO}_2$ glasses.⁽¹²⁾

The FTIRRS spectra of the fracture surfaces of the unheat treated sample and the $1000^\circ\text{C}/10\text{ hr}$ sample are noisy in spite of averaging 960 scans. In both cases there is a considerable difference in the breadth and location of the SN_1 peak. The larger number of vibrational species in the $1100-1050\text{ cm}^{-1}$ region is characteristic of the presence of a considerable number of Si-O bonds in the fracture surface. After 10 hrs heat treatment at 1200°C the spectra of the fracture surface and the polished surface are nearly identical. The fracture surface is both smoother and the Si-O bonds present in the other samples no longer dominate the SN_1 peak.

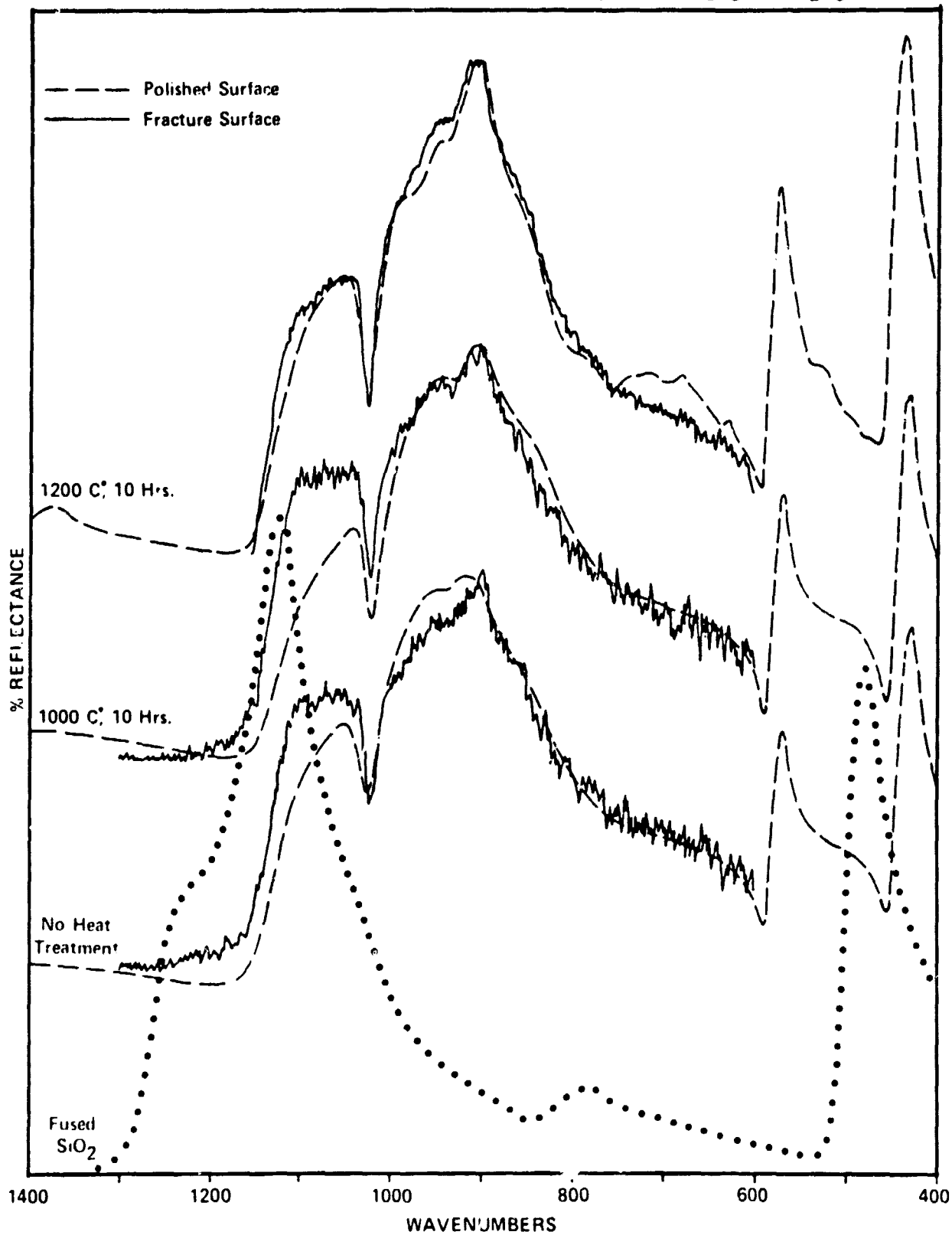
FOURIER TRANSFORM INFRARED SPECTRA OF $\text{Si}_3\text{N}_4 + 15\%\text{Y}_2\text{O}_3 + 2\%\text{Al}_2\text{O}_3$ 

Fig. 2

Discussion

The x-ray diffraction results indicate that crystallization occurred during heat treatment, especially at 1200°C. Even though the x-ray data was obtained from the bulk material, it can be assumed that the crystallization is at the grain boundary phase which is glassy before the heat treatment process.

The FTIRRS analysis shows that the devitrification did occur within the grain boundary phase. Prior to heat treatment the fracture surface shows spectral features characteristic of Si-O as well as Si-N bonds. This is direct evidence of preferential fracture through a phase of different composition than the bulk composition. After heat treatment there is no distinction between the fracture and non-fractured surface.

Conclusion

Use of Fourier transform IR reflection spectroscopy (FTIRRS) and x-ray diffraction shows that 10 hrs at 1200°C is sufficient to densify the amorphous grain boundary phase of Si_3N_4 containing 15% Y_2O_3 + 2% Al_2O_3 densification aids.

Acknowledgments

The authors acknowledge the assistance of Sunil Dutta of NASA Lewis Research Center in obtaining the Si_3N_4 samples and partial financial support of NASA Grant NSG 3254.

References

1. G. E. Gazza, "Effect of Yttria Additions on Hot-Pressed Si_3N_4 ," Am. Ceram. Soc. Bull., 54(9), 778-781 (1975).
2. A. Tsuge, H. Kudo and K. Komeya, "Reaction of Si_3N_4 and Y_2O_3 in Hot-Pressing," J. Am. Ceram. Soc., 57(6), 269-270 (1974).
3. J. Thomas Smith and Carr Lane Quackenbush, "Phase Effects in Si_3N_4 Containing Y_2O_3 or CeO_2 ," Am. Ceram. Soc. Bull., 59(5), 529-532 (1980).
4. A. Tsuge, K. Nishida and M. Komatsu, "Effects of Crystallizing the Grain-Boundary Glass Phase on the High Temperature Strength of Hot-Pressed Si_3N_4 Containing Y_2O_3 ," 58(7-8), 323-326 (1975).
5. R. E. Loehman and D. J. Rowcliffe, "Sintering of Si_3N_4 - Y_2O_3 - Al_2O_3 ," J. Am. Ceram. Soc., 63(3-4), 144-148 (1980).
6. B. D. Powell and P. Drew, "The Identification of a Grain Boundary Phase in Hot-Pressed Silicon Nitride by Auger Electron Spectroscopy," J. Mater. Sci., 9, 1867-1870 (1974).
7. R. Kossowsky, "The Microstructure of Hot-Pressed Si_3N_4 ," J. Mater. Sci., 8, 1603 (1973).
8. J. P. Guha and L. L. Hench, "Grain Boundary Phases in Hot-Pressed Silicon Nitride Containing Y_2O_3 and CeO_2 Additives," to be published.
9. L. L. Hench, F. Ohuchi, P. N. Vaidyanathan, and S. Dutta, "Compositional Effects on Si_3N_4 Fracture Surfaces," to be published.
10. L. L. Hench, "Use of New Surface Physics for Controlling the Physical Properties of Ceramics," Proceedings Science of Ceramics 10, Sept. 2-4, 1979, Munich, Germany.
11. L. L. Hench, G. LaTorre and H. Yamanaka, "Use of Fourier Transform IR Reflection Spectroscopy in Non-Destructive Surface Analysis of Ceramics and Glasses," to be published.
12. W. McCracken, D. E. Clark and L. L. Hench, "Aqueous Durability of Lithium Disilicate Glass-Ceramics," Am. Ceram. Soc. Bull., 61(11), 1218-1223 (1982).

EFFECTS OF DEVITRIFICATION OF THE
AMORPHOUS PHASE OF $\text{Si}_3\text{N}_4 + \text{Y}_2\text{O}_3 + \text{Al}_2\text{O}_3$ CERAMICS

L. L. Hench
University of Florida
Ceramics Division
Department of Materials Science and Engineering
Gainesville, Florida 32611

P. K. Vaidyanathan
Manchester Division
The Warner and Swasey Company
5142 Manchester Road
Akron, OH 44319

S. Dutta
NASA Lewis Research Center
Mail Stop 49-3
2100 Brookpark Road
Cleveland, OH 44135

Previous studies have shown the effectiveness of Y_2O_3 as a densification aid for Si_3N_4 ceramics.⁽¹⁻⁶⁾ It has also been demonstrated that addition of Al_2O_3 with Y_2O_3 greatly improves oxidation resistance of these materials.⁽³⁾ However, Al_2O_3 also significantly affects the relative proportion of amorphous phase produced during high temperature densification.⁽³⁾ Because the grain boundary amorphous phase is widely implicated in the degradation of mechanical properties of Si_3N_4 at high temperatures,⁽⁴⁾ it is important to understand the effect of varying the Al_2O_3 concentration on the extent of glassy phase. Also, since it has been shown that devitrification of the grain boundary phase can improve high temperature mechanical properties,⁽⁴⁾ it is also important to understand the effect of Al_2O_3 on control of grain boundary devitrification. Both of these topics are investigated in this paper.

Fully densified Si_3N_4 bodies were prepared by sintering at 1750°C in N_2 with 15% Y_2O_3 and 2, 4, 6 or 8% Al_2O_3 as the densification aid. Machined bars were then fractured at room temperature and 1370°C and phase analyses made of polished surfaces and fracture surfaces using X-ray diffraction (XRD) and Fourier transform infrared reflection spectroscopy (FTIRRS). Bars from the same compositions were also heat treated in vacuum at 1000°C or 1200°C for 10 hrs to promote devitrification of the grain boundary (g.b.) glassy phase. Phase analyses of polished and fracture surfaces were also made of these samples. Thus, the primary objective of this study is to relate the changes in room temperature and elevated temperature mechanical strength with the composition and extent of devitrification of the g.b. glassy phase.

Materials and Methods

The compositions were formulated to have a constant amount of 15% Y_2O_3 and varying amounts of Al_2O_3 . Table I summarizes the nominal compositions produced.

Commercial grade Si_3N_4 , Y_2O_3 , and Al_2O_3 powder (see Table II for sources) were used in the fabrication. An impurity analysis of the "as-received" powders is shown in Table II. Si_3N_4 and Al_2O_3 powders were a higher purity with respect to metal contaminants. Y_2O_3 powder contained Al, Si, and Fe as major impurities. The Si_3N_4 powder had an oxygen content of 2.7 wt % and a specific surface area of 11.84 m/g (3-point BET method). The Si_3N_4 powder was totally amorphous; the powder particles are spherical and often agglomerated (Fig. 1), with individual particle sizes ranging from 0.05 to 1.0 μm . Mixtures for 100 g batches were wet milled in polyethylene bottles for 17-20 h using high alumina grinding media and ethanol. The starting compositions were adjusted to allow for pick up of Al_2O_3 from the mills. After the powders were milled, the slurry was dried on a heated aluminum plate and sieved through a 60 mesh sieve to break up agglomerates. Seventeen grams of mixed powder was cold die pressed into rectangular blocks 7.6 x 2.5 x 0.64 cm followed by cold isostatic pressing at a total pressure of 414 MN/m^2 . The compacts were pressureless sintered in a "cold-wall" furnace at 1750°C for 2 h under nitrogen pressure of 1 atm.

Sintered specimens were machined into test bars (2.54 x 0.64 x 0.32 cm), and the surfaces were subsequently ground with a 220-grit wheel to a final surface roughness of 10-15 $\mu in rms$.

TABLE I. MATERIALS COMPOSITIONS FOR $\text{Si}_3\text{N}_4 - \text{Y}_2\text{O}_3 - \text{Al}_2\text{O}_3$ MIXTURE

COMPOSITION	WEIGHT PERCENT
SNYAL-2%	$\text{Si}_3\text{N}_4 - 15 \text{Y}_2\text{O}_3 - 2 \text{Al}_2\text{O}_3$
SNYAL-4%	$\text{Si}_3\text{N}_4 - 15 \text{Y}_2\text{O}_3 - 4 \text{Al}_2\text{O}_3$
SNYAL-6%	$\text{Si}_3\text{N}_4 - 15 \text{Y}_2\text{O}_3 - 6 \text{Al}_2\text{O}_3$
SNYAL-8%	$\text{Si}_3\text{N}_4 - 15 \text{Y}_2\text{O}_3 - 8 \text{Al}_2\text{O}_3$

TABLE II - TRACE IMPURITY ANALYSIS OF
RAW POWDERS (ppm)

Element	Si ₃ N ₄ [*] SN402	Al ₂ O ₃ ⁺	Y ₂ O ₃ ⁺⁺
Al	--	Major	640
Co	50	-----	---
Cu	--	-----	---
Cr	--	-----	90
Fe	70	70	160
Mg	--	110	90
Mn	--	-----	---
Mo	--	-----	---
Ni	--	-----	---
Si	Major	154	230
Ti	--	-----	---
V	--	-----	---
W	--	-----	---
Zr	--	-----	---

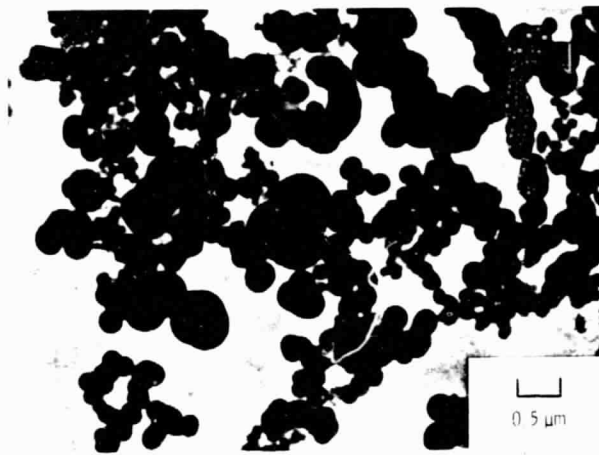
----- = not determined

*GTE, Sylvania, Towanda, PA

+Linde A, Union Carbide Corporation, New York, NY

++United Mineral & Chemical Corporation, New York, NY

ORIGINAL PAGE IS
OF POOR QUALITY



(a) SN402.

Figure 1. Transmission micrograph of commercial silicon nitride powder.

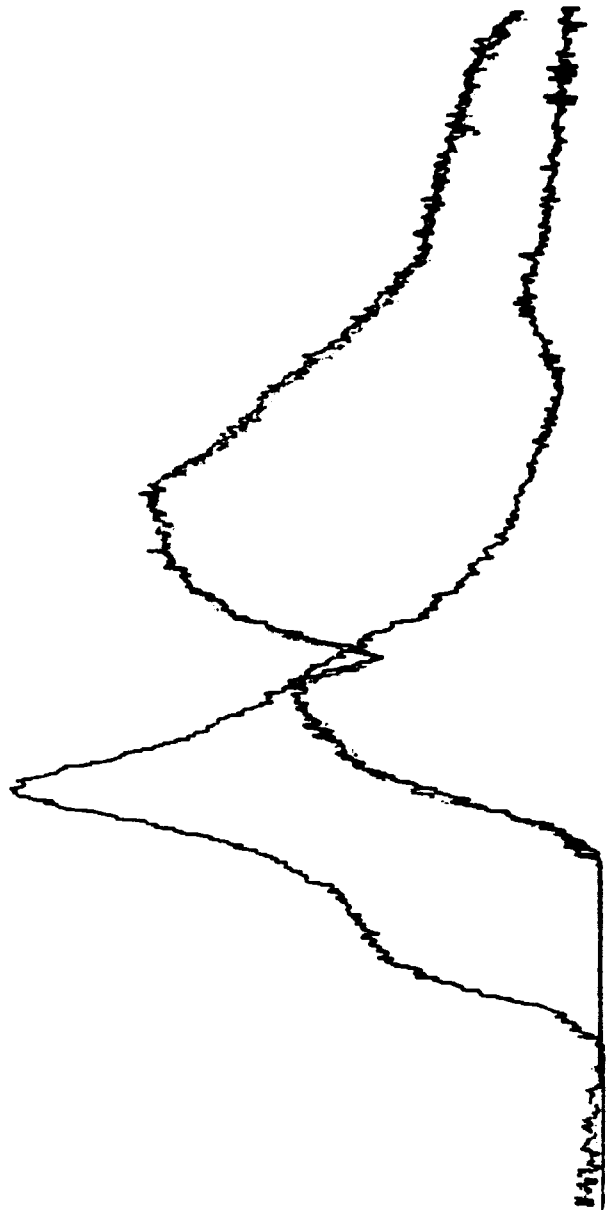
In order to ensure that all samples were homogeneous, infrared reflection analyses were made on 3 or 4 areas on each side of each sample using a 3 mm aperture. Nearly all samples showed no more than $\pm 1\%$ variation in intensity of the SN_1 and SN_2 peaks. Figure 2 illustrates the results of the homogeneity test for 4 samples, SNYAL-2% Al_2O_3 , SNYAL-3% Al_2O_3 , SNYAL-4% Al_2O_3 , and SNYAL-8% Al_2O_3 . The data were obtained with a grating IR spectrometer run on medium scan rate. A vitreous silica standard was also run along with each sample as well in order to normalize the data. Previous studies using this method showed very large variations in the microstructure and IRRS spectra for reaction bonded Si_3N_4 . The conclusions from the present homogenization study are that the samples prepared by sintering with the $Y_2O_3 + Al_2O_3$ are uniformly dense regardless of the percentage of Al_2O_3 in the composition.

Two-thirds of the samples from the SNYAL composition series were selected at random for a 10 hour thermal treatment in vacuum induction heating furnace at either 1000°C or 1200°C. The vacuum was maintained at 10^{-5} Torr. During heat treatment the samples were mounted on BN dies to prevent contamination. The furnace was cooled to room temperature during a seven hour period.

Fracture of the samples with and without heat treatment was done on an Instron testing machine in four point bending using SiC loading platens for the 1370°C tests and tool steel for the room temperature fracture. A 3/8" gauge length was used in both cases and a cross heat speed of 0.02"/min. Both low and high temperature fracture was done in air resulting in approximately 5 minutes exposure at 1370°C and 1.5 hours for the high temperature thermal cycle.

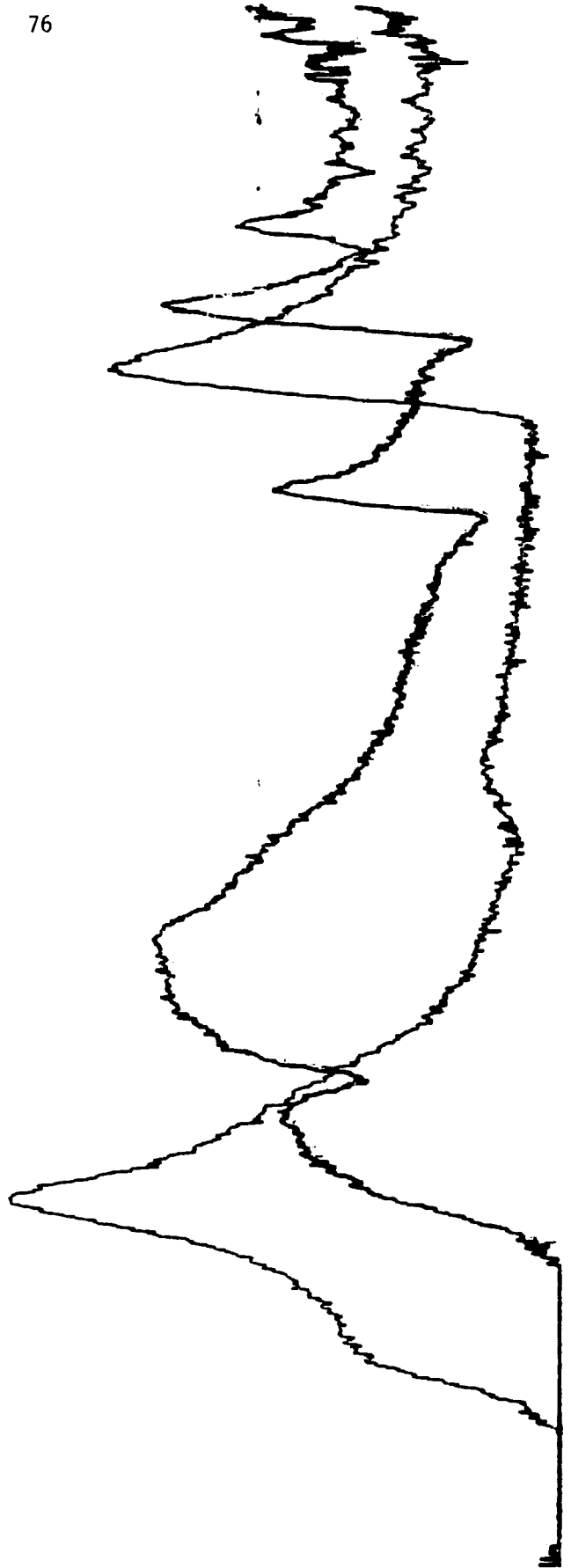
ORIGINAL PAGE IS
OF POOR QUALITY

Fig. 2A. SNYAL-1



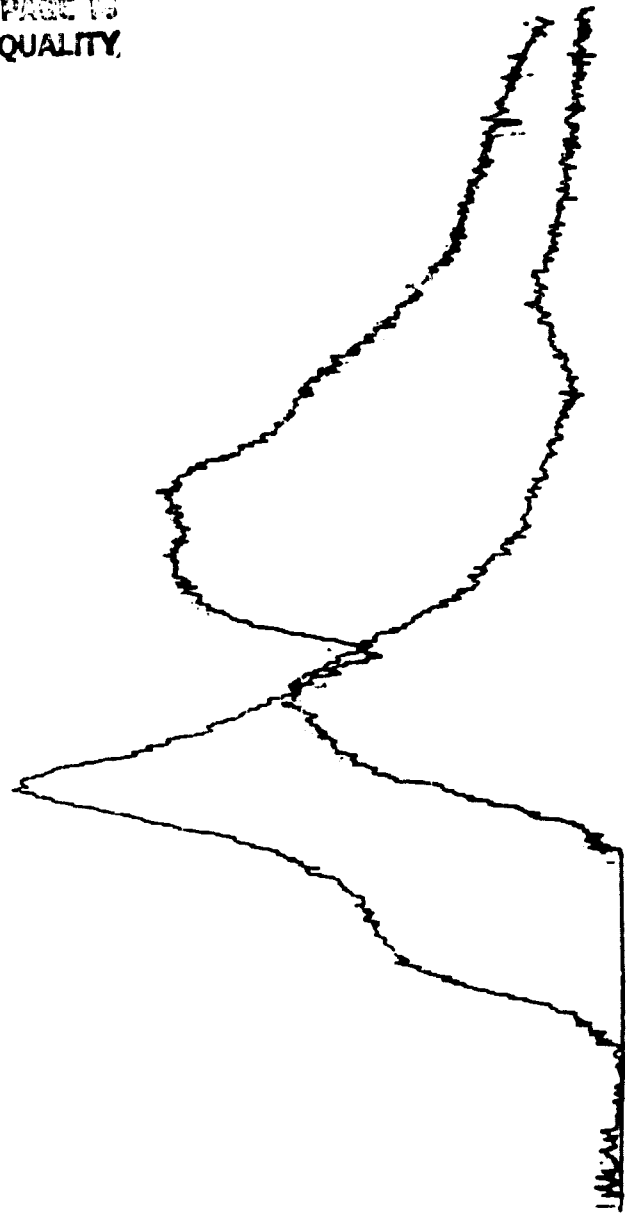
ORIGINAL PAGE IS
OF POOR QUALITY

Fig. 2B. SNYAL-2



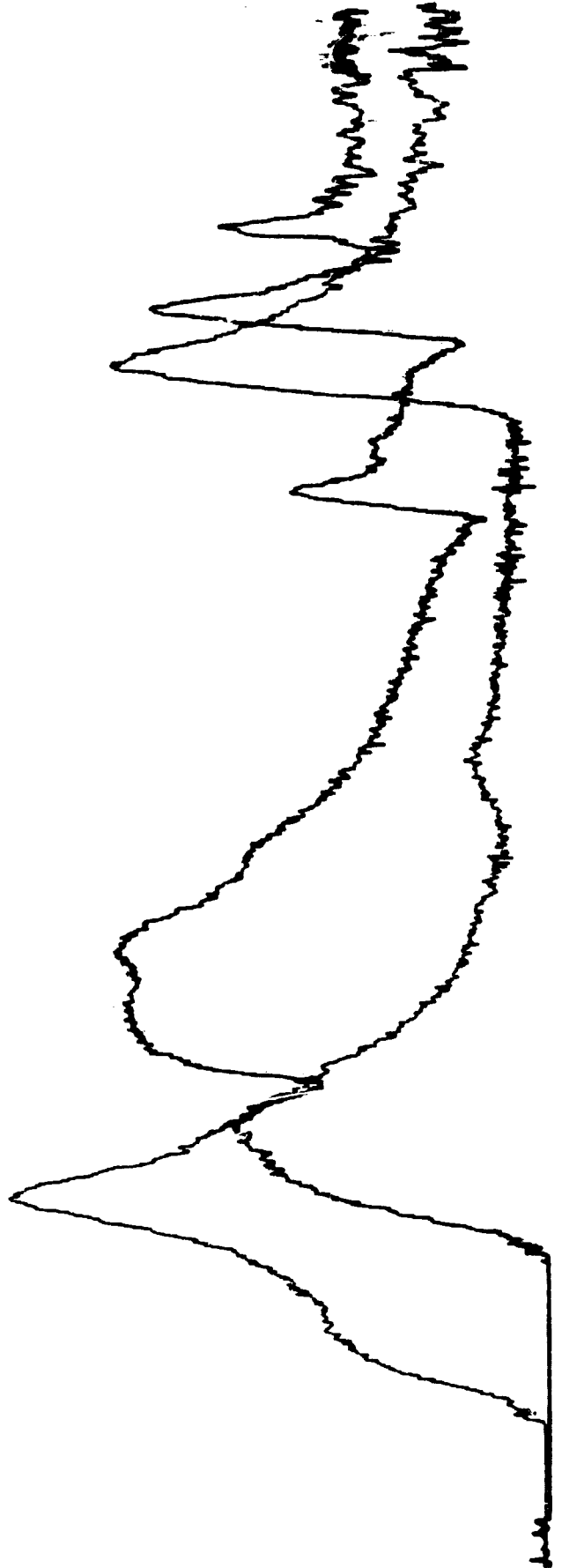
ORIGINAL PAGE IS
OF POOR QUALITY

Fig. 2C. SNYAL-3



ORIGINAL PAGE IS
OF POOR QUALITY

Fig. 2D. SNYAL-4



Results

X-ray analysis. Effects of the 1000°C and 1200°C, 10 hour heat treatments on the phases in the SNYAL series were determined by X-ray diffraction. Figures 2-3 and Table III summarizes the findings. The numbers shown in Table III for each 2θ value correspond to the relative intensity of the various X-ray peaks.

Prior to heat treatment only β Si_3N_4 was present in the samples containing 2, 4, and 6% Al_2O_3 along with an extensive glassy XRD hump from 24° - 36° 2θ . However even without heat treatment, the 8% Al_2O_3 material had significant quantities of $\text{Y}_2\text{Si}_2\text{O}_7$.

Heating for 10 hours at 1000°C induced formation of a very small amount of $\text{Y}_2\text{Si}_2\text{O}_7$ in the 2, 4, and 6% Al_2O_3 samples. The 8% Al_2O_3 material developed considerably more $\text{Y}_2\text{Si}_2\text{O}_7$ and also some 10-9-1 phase as a result of the 1000°C heat treatment. This large increase in devitrification was probably due to nucleation of the phases already being present in the unheated material.

The 1200°C heat treatment results in devitrification of all compositions, however the relative extent of crystallization depends considerably on the % Al_2O_3 present. Samples with 6% Al_2O_3 show extensive development of both $\text{Y}_2\text{Si}_2\text{O}_7$ and 10-9-1 phases (Fig. 5, Table III). The 2% Al_2O_3 composition also developed considerable amounts of both $\text{Y}_2\text{Si}_2\text{O}_7$ and 10-9-1 phases. The 4% Al_2O_3 material had more second phases after 1200°C/10 hr than after 1000°C/10 hr, but it was quite resistant to devitrification.

Heating at 1200°C seemed to reduce the extent of second phase crystallization for the 8% Al_2O_3 material. Figure 6 and Table III show that the relative intensities of both $\text{Y}_2\text{Si}_2\text{O}_7$ phases are decreased from

SNYAL - 2% Al_2O_3

ORIGINAL PAGE IS
OF POOR QUALITY

1200°C/10hr

1000°C/10hr

No Heat Treatment

20° 24° 28° 32° 36° 40°

Fig. 3

2θ

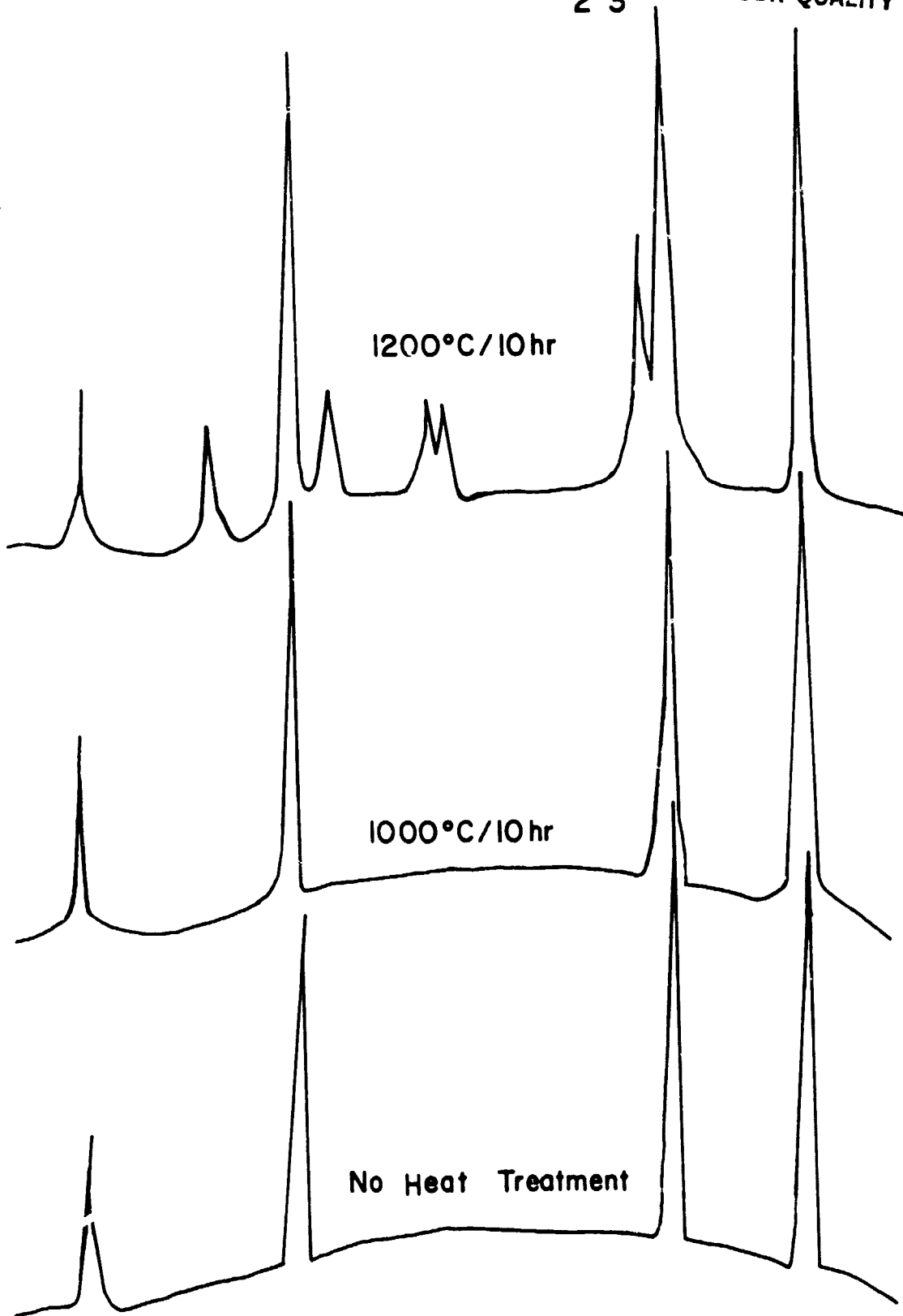


TABLE III. X-RAY DIFFRACTION ANALYSIS OF SNYAL SERIES

θ	d(A)	SNYAL-2%		SNYAL-4%		SNYAL-6%		SNYAL-8%					
		No H.T.	1000°C 10 Hr.	1200°C 10 Hr.	No H.T.	1000°C 10 Hr.	1200°C 10 Hr.	No H.T.	1000°C 10 Hr.	1200°C 10 Hr.			
23.4	3.79	23	35	28	20	40	19	25	32	33	25	27	28
25.7	3.47	-	-	8	-	-	15	-	-	8	-	15	3
26.5	3.35	-	-	-	-	-	-	-	-	-	16	15	-
27.2	3.28	64	84	97	88	95	85	80	93	96	85	81	70
27.8	3.20	-	-	18	-	-	8	-	-	39	-	-	5
29.6	3.02	-	-	-	-	-	-	-	-	29	-	22	81
29.9	2.99	-	-	15	-	10	-	-	6	11	-	8	9
32.8	2.73	-	-	-	-	-	-	-	-	1?	-	-	-
33.3	2.69	-	-	52	-	-	-	-	-	39	-	-	-
33.7	2.65	97	100	98	87	100	100	96	100	100	93	100	98
36.2	2.48	100	89	100	100	85	98	100	92	95	100	95	100
37.7	2.38	-	9	-	-	-	7	-	-	16	16	20	12

ORIGINAL PAGE IS
OF POOR QUALITY

ORIGINAL PAGE IS
OF POOR QUALITY

SNYAL - 4% Al_2O_3

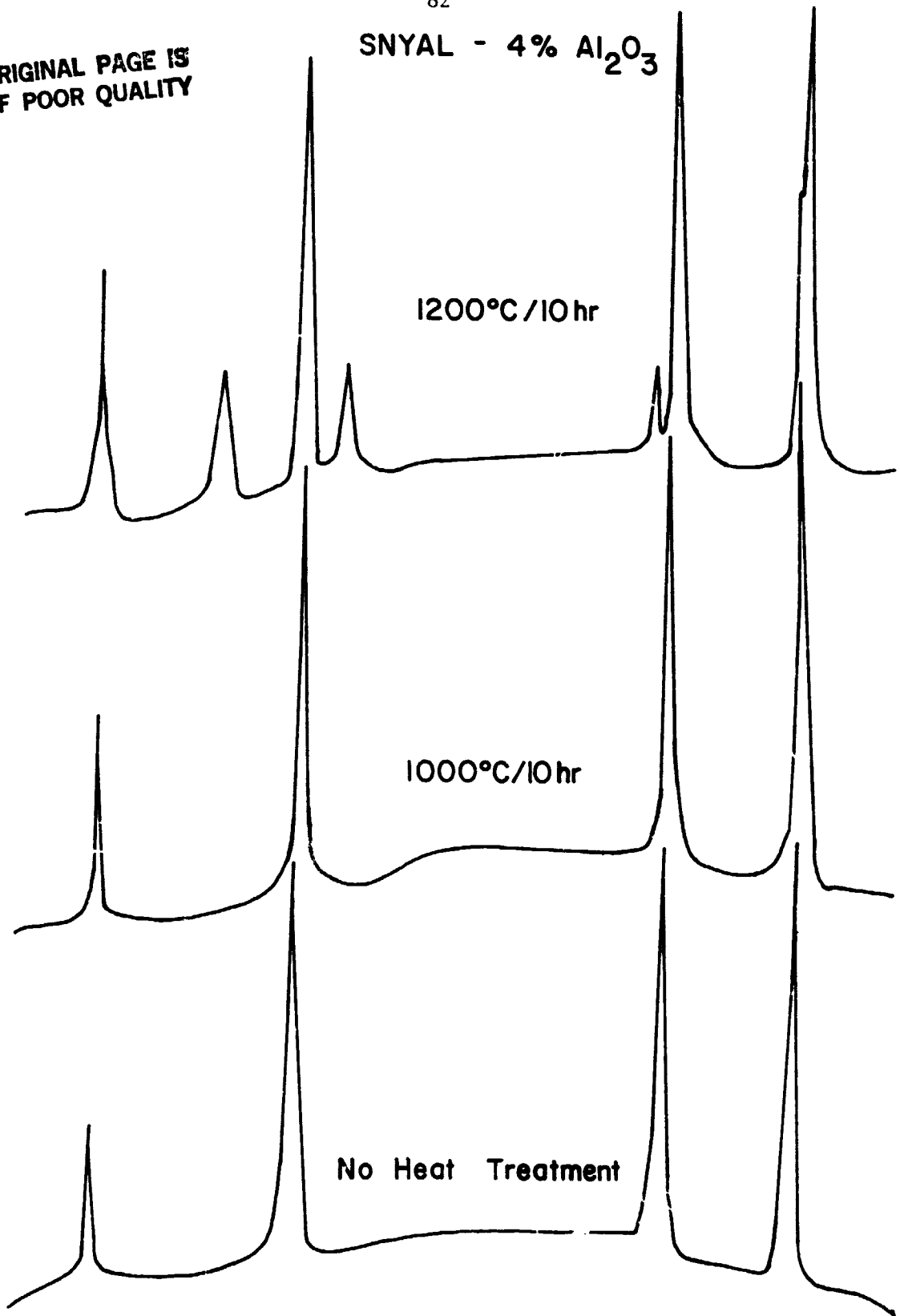
1200°C / 10 hr

1000°C / 10 hr

No Heat Treatment

20° 24° 28° 32° 36 40°

Fig. 4



ORIGINAL PAGE IS
OF POOR QUALITY

SNYAL - 6% Al_2O_3

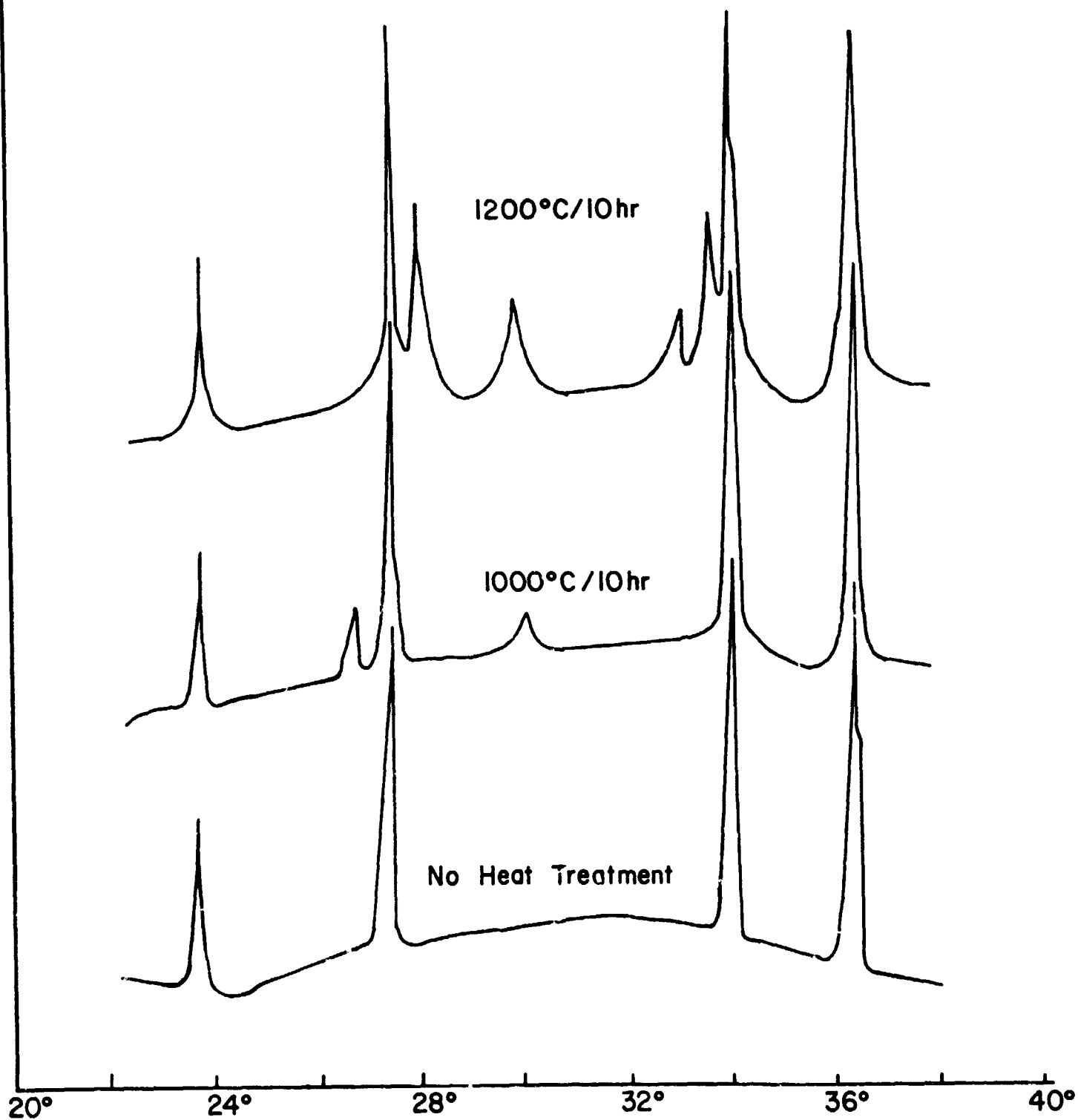


Fig. 5

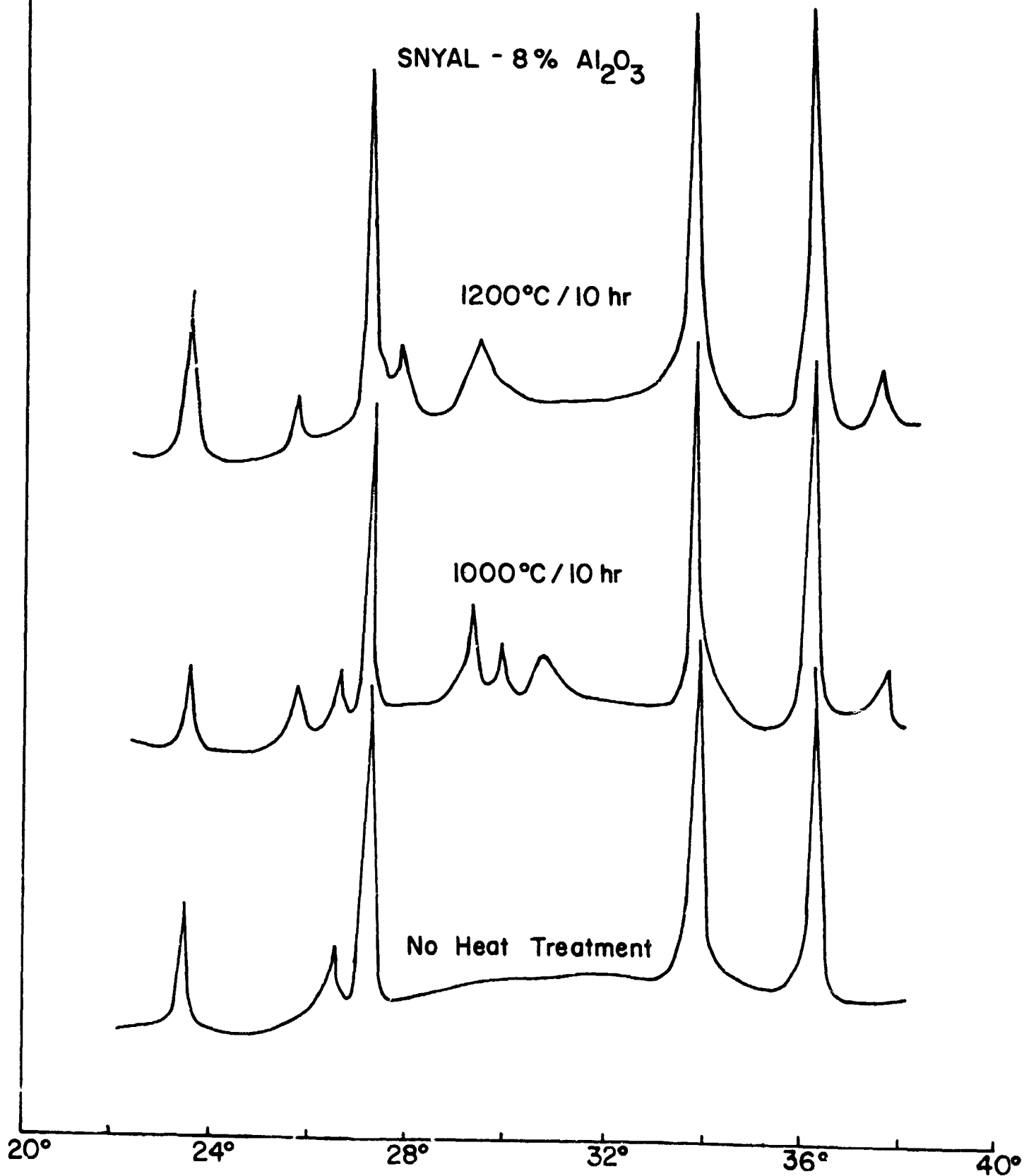


Fig. 6

those obtained after the 1000°C treatment. Some peaks are even less than observed without heat treatment. This suggests dissolution of the devitrified g.b. phase may be occurring.

Following room temperature fracture, the ends of the fracture samples were oriented incident to the X-ray beam. The objective was to determine whether the fracture surface had a different distribution of crystalline phases than the bulk material. Because of the very small area exposed to the X-rays there was very little diffraction intensity. Table IV summarizes the findings, even though the results must be considered inconclusive. Only β Si_3N_4 peaks were observed on any of the fracture surfaces. Changing the % Al_2O_3 or increasing crystallization did not show any additional peaks on the fracture surfaces. It is tempting to conclude that the heat treatment decreased the detection of Si_3N_4 on the fracture surface, see Table IV. However, the intensities were so low that such a conclusion is very tentative.

FTIRRS analysis. A Fourier transform IR spectrometer with a specular reflection stage was used to analyze the SNYAL series before and after heat treatment on both polished and fracture surfaces. Because of the roughness of a fracture surface there is considerable scattering of the incident IR beam. However, as discussed in previous papers from this investigation, (#3 and #4) an advantage in the Fourier transform IR reflection spectroscopy (FTIRRS) method is the ability to scan the same area on the sample for numerous times, store the digital spectral data in the computer, and plot a relatively noise free spectrum of the sample. In order to ascertain an optimal number of scans the fracture surfaces of the SNYAL-2% samples were analyzed for a total of 480, 960, 1440, and 1920 scans. It was found the 960 scans were sufficient to obtain reasonably noise free fracture surface spectrum.

TABLE IV. X-RAY DIFFRACTION ANALYSIS OF SNYAL FRACTURE SURFACES

Material	Heat Treatment			
SNYAL-2%	None	27° ($\beta\text{Si}_3\text{N}_4$)	33.7° ($\beta\text{Si}_3\text{N}_4$)	36° ($\beta\text{Si}_3\text{N}_4$)
SNYAL-2%	1000°C/10 Hr.	ND	33.7° ($\beta\text{Si}_3\text{N}_4$)	36° ($\beta\text{Si}_3\text{N}_4$)
SNYAL-2%	1200°C/10 Hr.	ND	ND	ND
SNYAL-4%	None	ND	ND	36° ($\beta\text{Si}_3\text{N}_4$)
SNYAL-4%	1000°C/10 Hr.	ND	ND	ND
SNYAL-4%	1200°C/10 Hr.	ND	ND	ND
SNYAL-6%	None	ND	ND	36° ($\beta\text{Si}_3\text{N}_4$)
SNYAL-6%	1000°C/10 Hr.	27° ($\beta\text{Si}_3\text{N}_4$)	34° ($\beta\text{Si}_3\text{N}_4$)	36° ($\beta\text{Si}_3\text{N}_4$)
SNYAL-6%	1200°C/10 Hr.	ND	ND	ND
SNYAL-8%	None	NA	NA	NA
SNYAL-8%	1000°C/10 Hr.	NA	NA	NA
SNYAL-8%	1200°C/10 Hr.	NA	NA	NA

Note: ND = No Peaks Detected
 NA = Not Analyzed

This procedure was followed in previous paper #4 and is the basis for the data presented herein for the other samples in the SNYAL series.

Results from the SNYAL-2% Al_2O_3 materials are shown in Fig. 7 over the spectral range of $1400\text{-}400\text{ cm}^{-1}$. The fracture surface spectra are shown only over the range $1300\text{-}600\text{ cm}^{-1}$ for sake of clarity. The FTIRRS spectrum of a fused, vitreous silica standard is also shown in Fig. 7 for comparison of the molecular vibrational modes on the Si_3N_4 surfaces. The two primary Si-N molecular stretching vibrations, SN_1 and SN_2 , are located at 1050 cm^{-1} and 900 cm^{-1} respectively whereas the Si-O molecular stretching vibration is at 1110 cm^{-1} .

Figure 7 shows that heat treatment of the SNYAL-2% Al_2O_3 material makes the fracture surface much more like the polished bulk surface, especially after 10 hours at 1200°C . The XRD analysis, Table III, provides the evidence that considerable crystallization has occurred with both $\text{Y}_2\text{Si}_2\text{O}_7$ and 10-9-1 phases appearing. The FTIRRS results show that the Si-O enriched spectral region from $1100\text{-}1000\text{ cm}^{-1}$ present in the fracture surfaces is eliminated by the crystallization treatment at 1200°C . Thus, the fracture mode which produces an oxide-enriched surface layer has been replaced by a fracture mode that has equivalence to the bulk Si_3N_4 structure.

There is much less devitrification of the SNYAL-4% Al_2O_3 material, Table III, at either heat treatment. The FTIRRS results, Fig. 8, also show no shift of the fracture surface spectra of the 4% material in contrast to that observed in the 2% Al_2O_3 samples with extensive devitrification. There is little change in the fracture surface spectra for the 4% Al_2O_3 material; if anything, the sample treated heated at 1200°C indicates more of a glassy phase on the fracture surface.

ORIGINAL PAGE IS
OF POOR QUALITY

FOURIER TRANSFORM INFRARED SPECTRA OF $\text{Si}_3\text{N}_4 + 15\%\text{Y}_2\text{O}_3 + 2\%\text{Al}_2\text{O}_3$

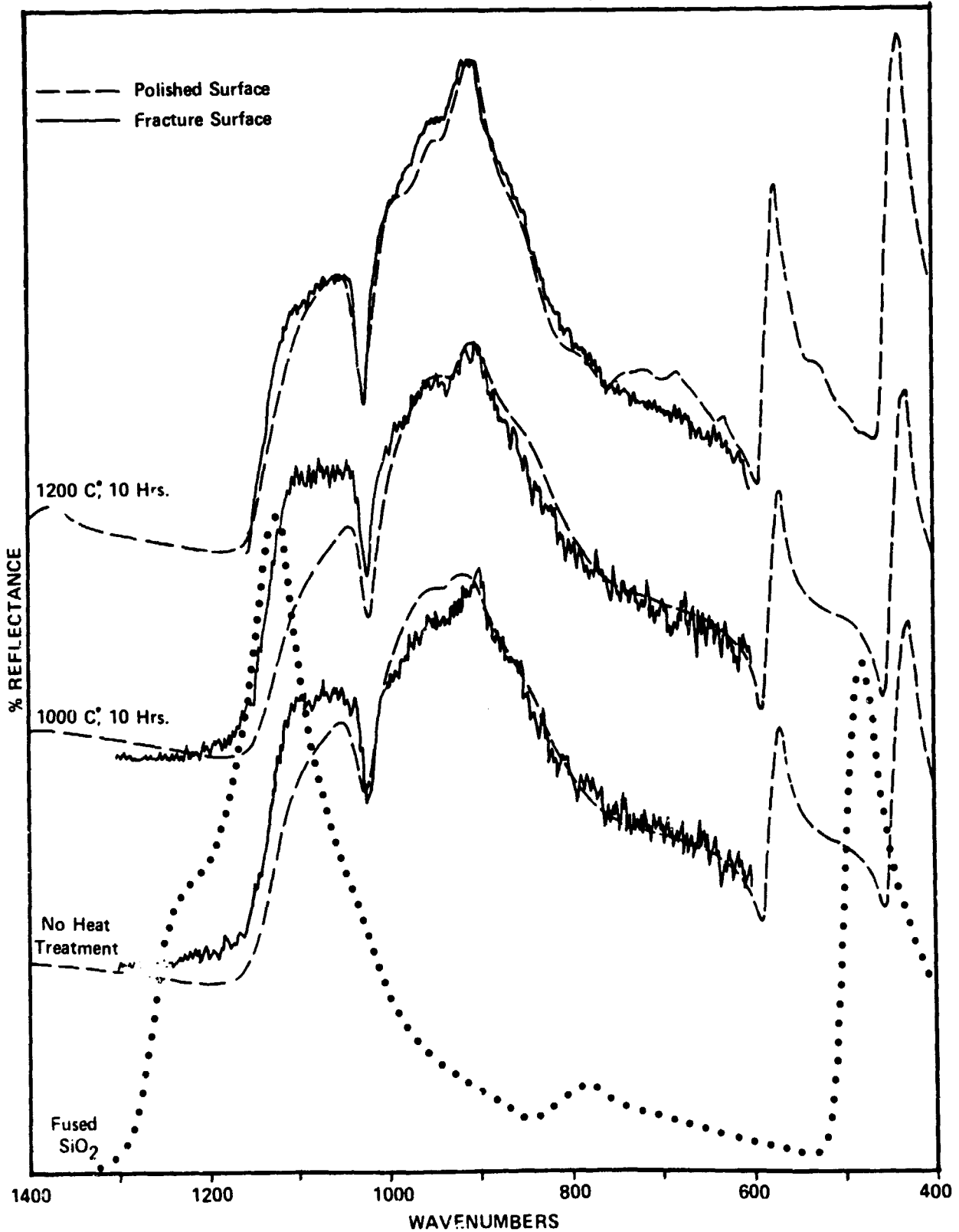
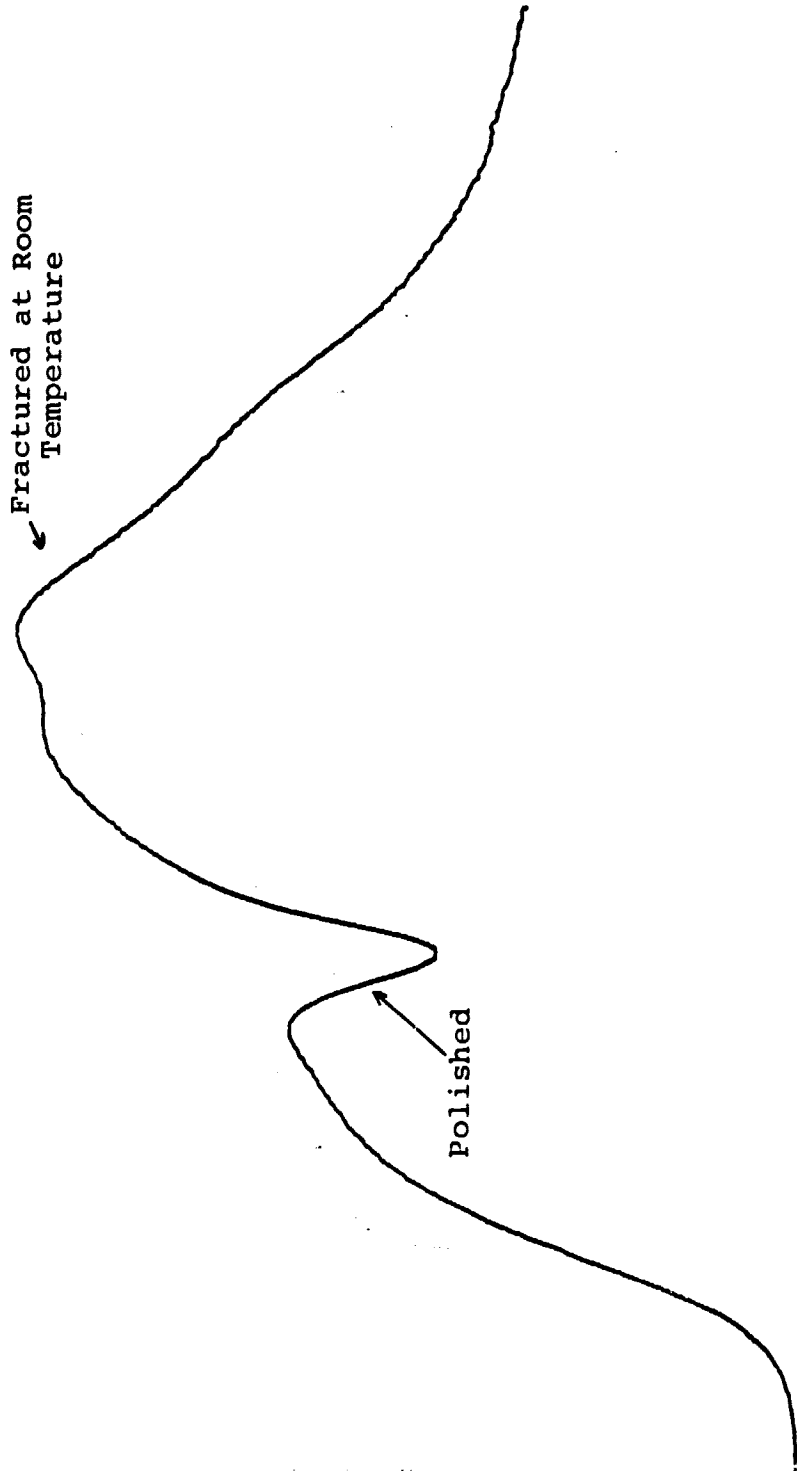


Fig. 7

ORIGINAL PAGE IS
OF POOR QUALITY

SNYAL-4% Al₂O₃, Non-Heat Treated



1000
100
10
1

Fig. 8A.

ORIGINAL PAGE IS
OF POOR QUALITY

SNYAL-48 Al₂O₃, 1000°C

Fractured at Room
Temperature

Polished

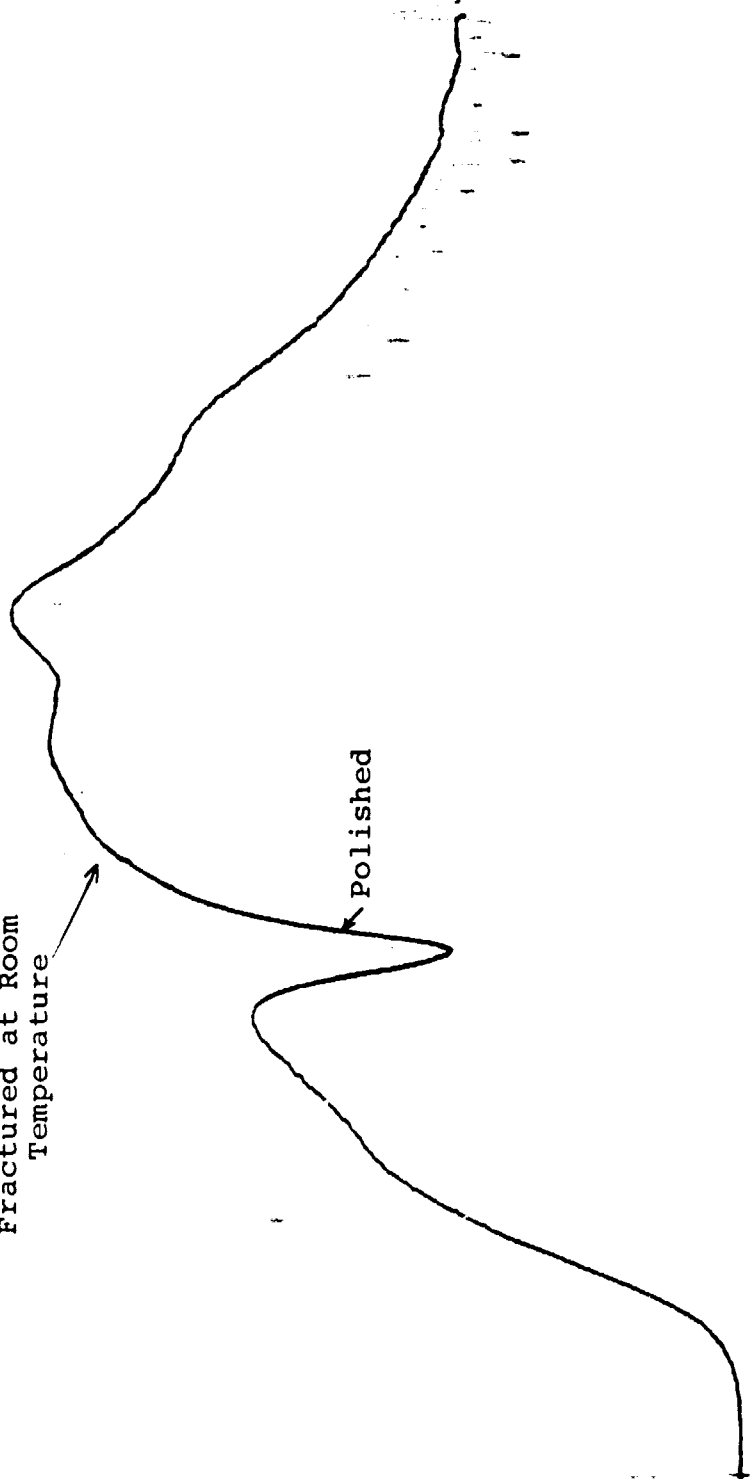


Fig. 8B

ORIGINAL PAGE IS
OF POOR QUALITY

SNYAL-48 Al₂O₃, 1200°C

Fractured at Room
Temperature

Polished

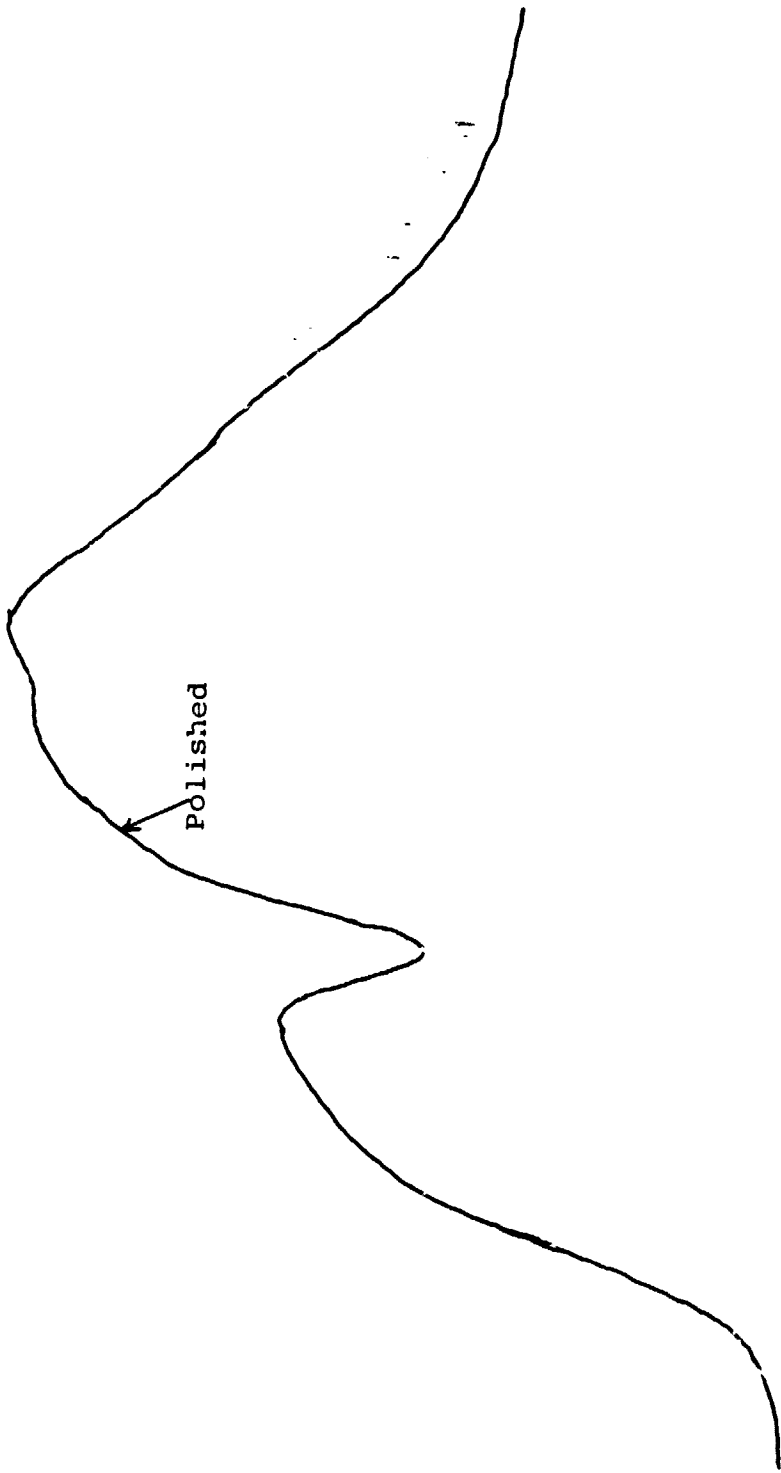


Fig. 8C

Neither the 6% Al_2O_3 series or the 8% Al_2O_3 series shows an obvious correlation of the FTIRRS results with the change in crystal phases shown in Table III. There is no appreciable difference between the polished and fracture surfaces in the unheat treated, 6% sample or the 1000°C/10 hr sample (Fig. 9). The extensive devitrification of the 6% Al_2O_3 sample produces a major change in the SN_2 vibrational mode. It has split into two peaks with one at 975 cm^{-1} and the other other at 900 cm^{-1} . The structural origin of this spectral splitting is not known at this time. There is much less evidence of the peak splitting on the fracture surface which is more like the unheattreated Si_3N_4 spectrum.

The 8% Al_2O_3 series, Fig. 10, also shows little evidence of the fracture surface having a major change in g.b. crystallinity. Splitting of the SN_2 Si-N molecular stretching vibrations is much more extensive for the heat treated material. There is a substantial change of the relative proportion of the split SN_2 peaks for the fracture surface. In contrast, the non-fracture surface of the 8% series changes only a small amount with heat treatment. This finding confirms that the crystallization occurring from the 1000°C and 1200°C heating is primarily located in the g.b. phase and alters the fracture mode for the material.

Fracture at 1370°C in air results in both oxidation of the bulk surface of the Si_3N_4 samples and the fracture surface. Figure 11 is an example of the FTIRRS spectra obtained from the SNYAL 1370°C fracture series. The sample is SNYAL-4% Al_2O_3 heat treated for 1200°C for 10 hrs. Comparison with Fig. 8 shows that almost none of the original Si-N vibrational modes are present. Instead a significant peak has developed at 1090 cm^{-1} due to formation of Si-O molecular vibrations. The remainder of the spectrum is complicated and will require additional systematic studies of Si_3N_4 oxidation to establish the mechanisms of the surface alteration.

ORIGINAL PAGE IS
OF POOR QUALITY

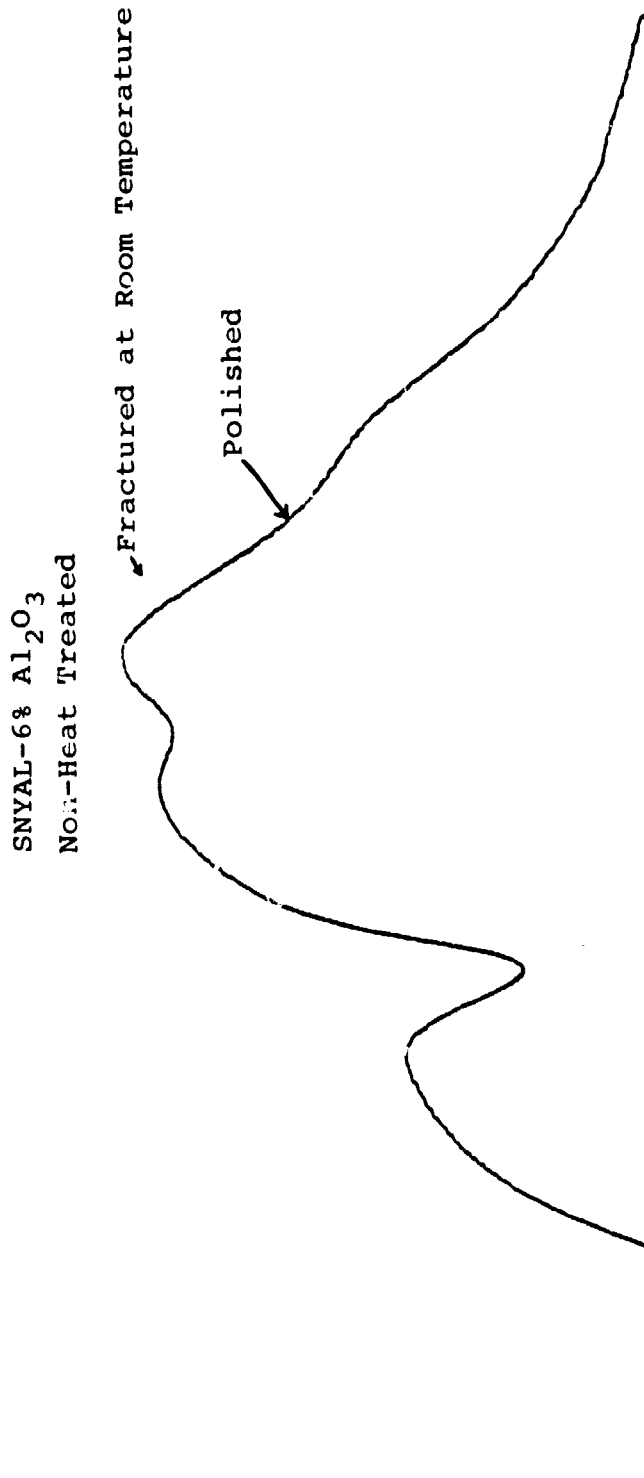


Fig. 9A.

ORIGINAL PAGE IS
OF POOR QUALITY

SNYAL-68 Al₂O₃, 1000°C

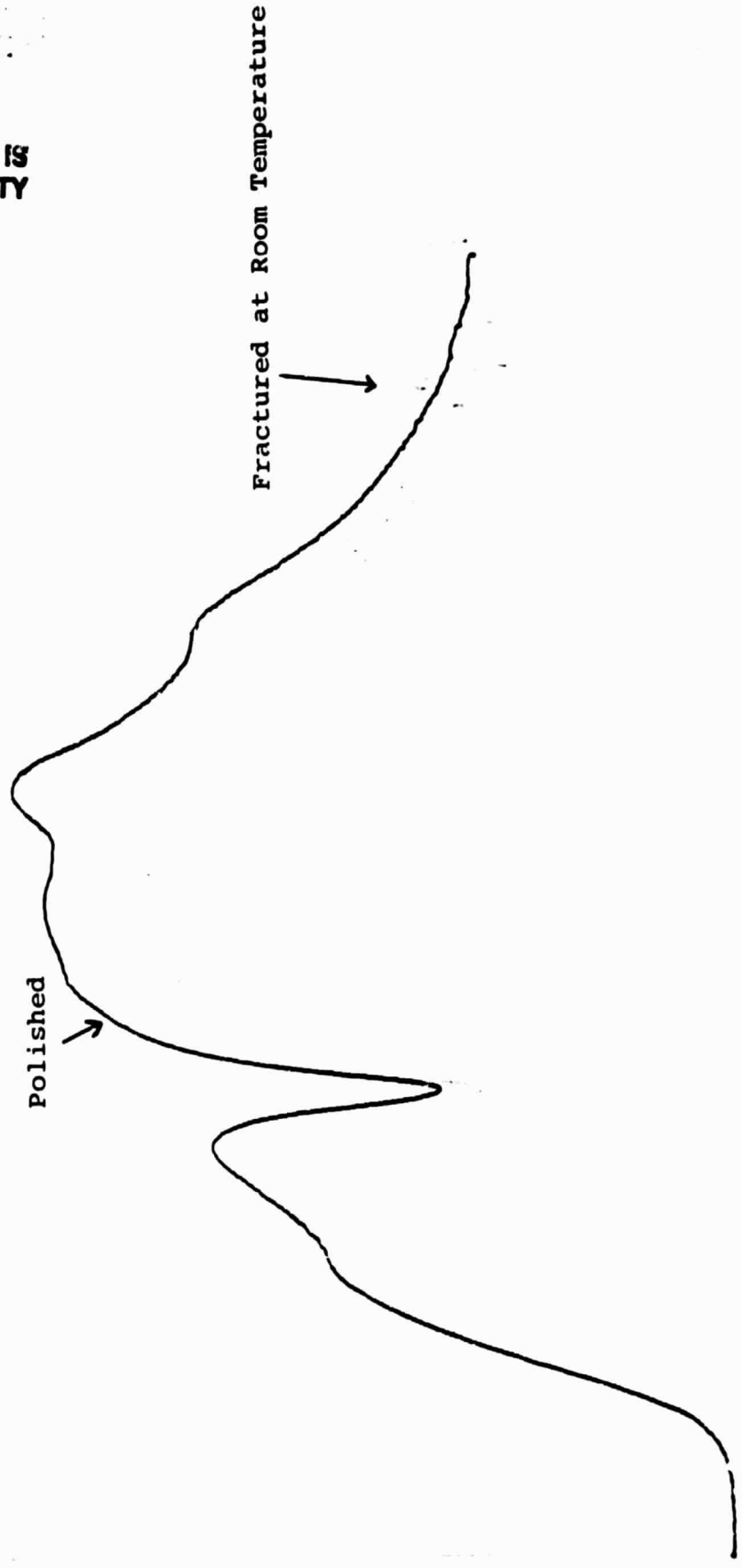
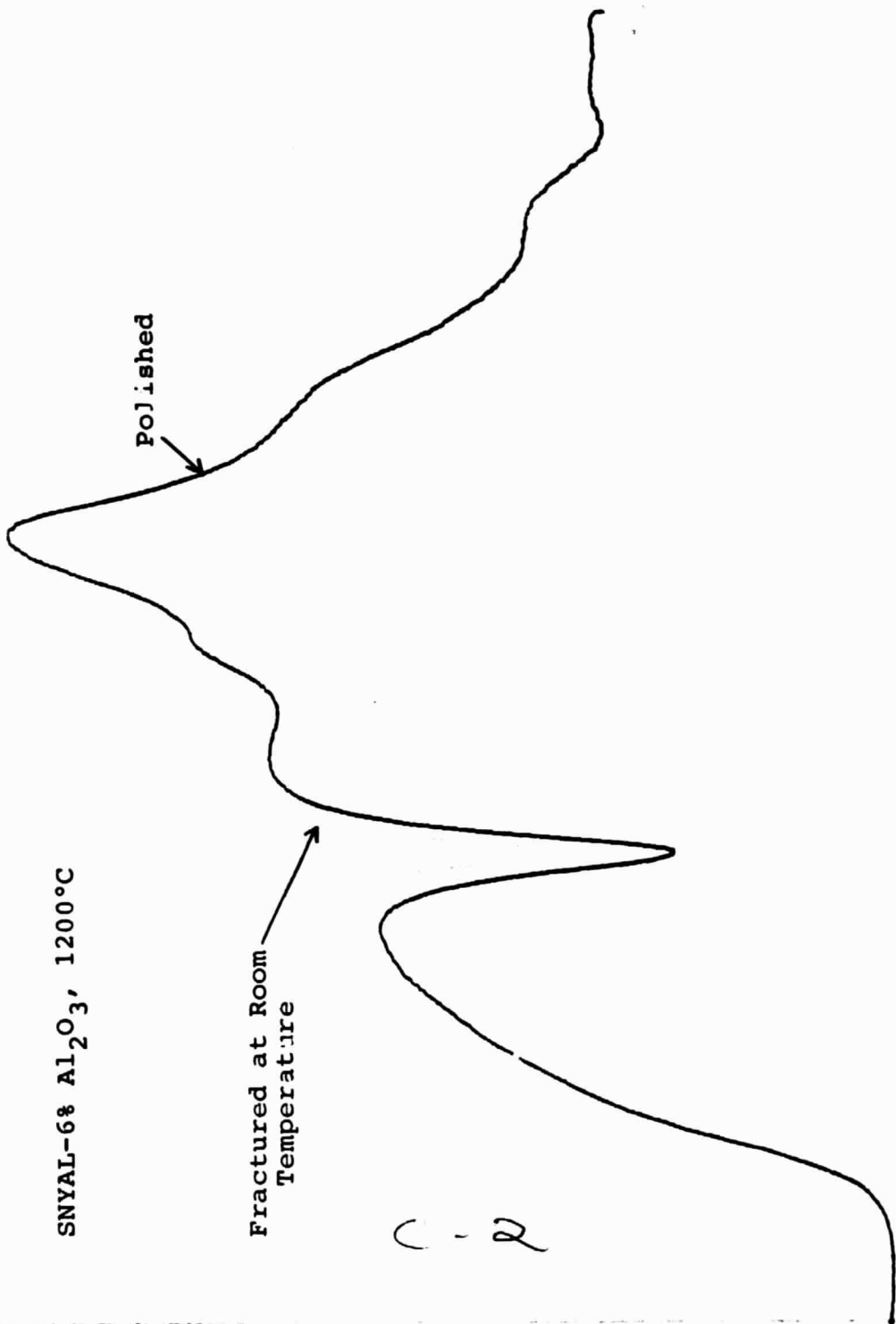


Fig. 9B.

ORIGINAL PAGE IS
OF POOR QUALITY



SNYAL-6% Al₂O₃, 1200°C

Polished

Fractured at Room
Temperature

C-2

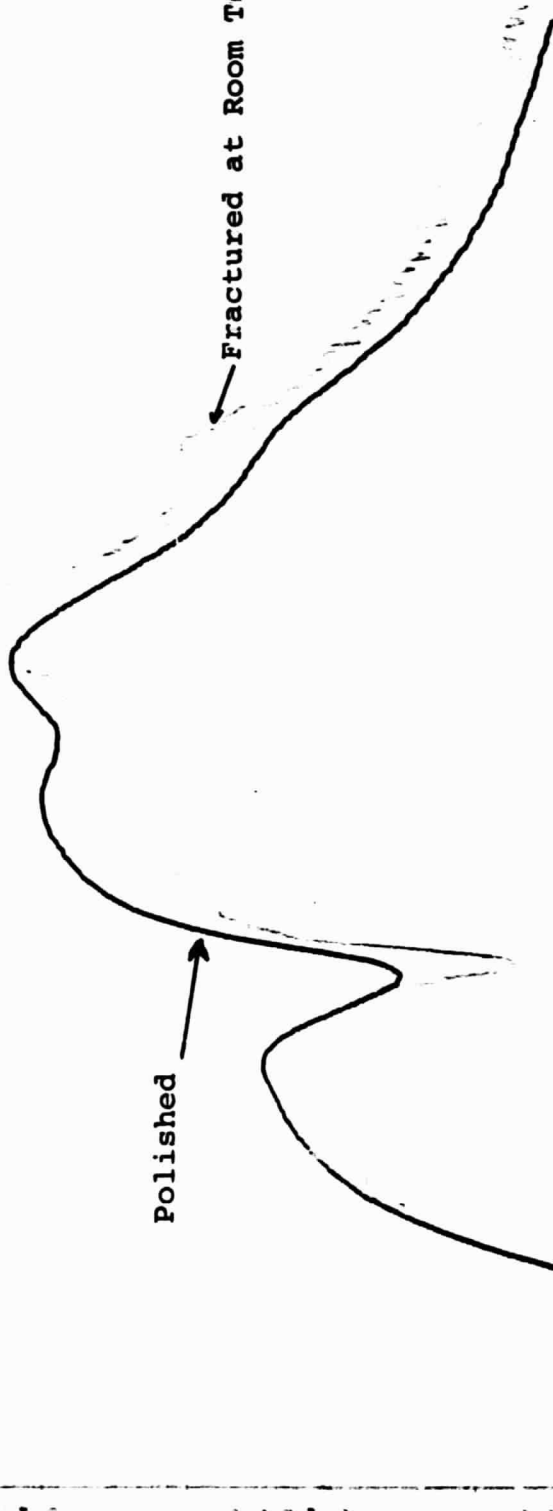
Fig. 9C

ORIGINAL PAGE IS
OF POOR QUALITY

SNYAL-8% Al_2O_3
Non-Heat Treated

Polished

Fractured at Room Temperature



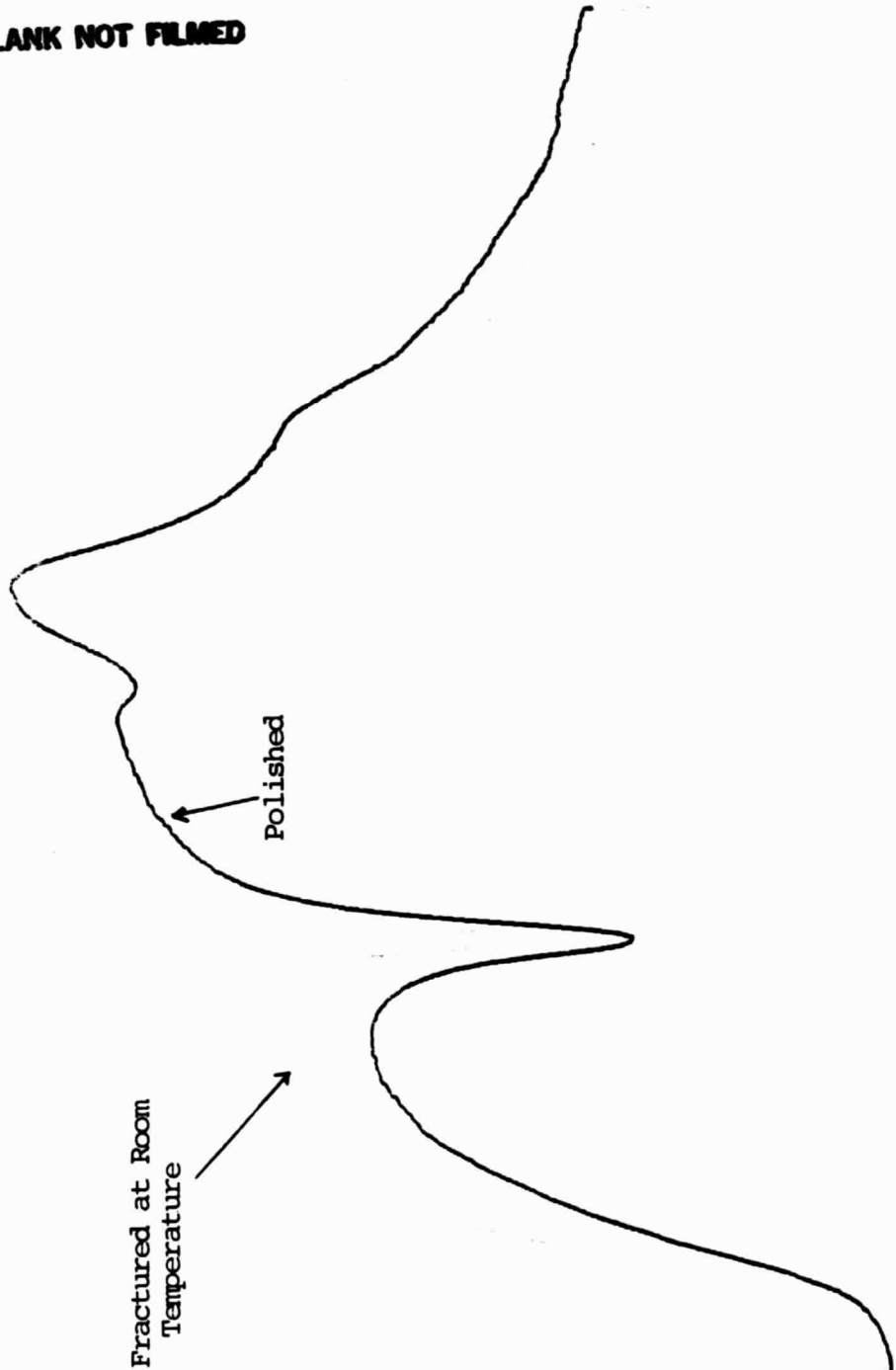
700

Fig. 10A

ORIGINAL PAGE IS
OF POOR QUALITY

PRECEDING PAGE BLANK NOT FILMED

SNYAL-8% Al_2O_3 , 1200°C



Fractured at Room
Temperature

Polished

Handwritten notes and markings on the right side of the page, including a vertical line and some illegible text.

Fig. 10C

NICOLET MX-1 SAMPLE

NS= 960
SC= 0
PF= 100
DF= 1.00
GAN B

ORIGINAL PAGE IS
OF POOR QUALITY

SNYAL-2, 80%, 1200°C

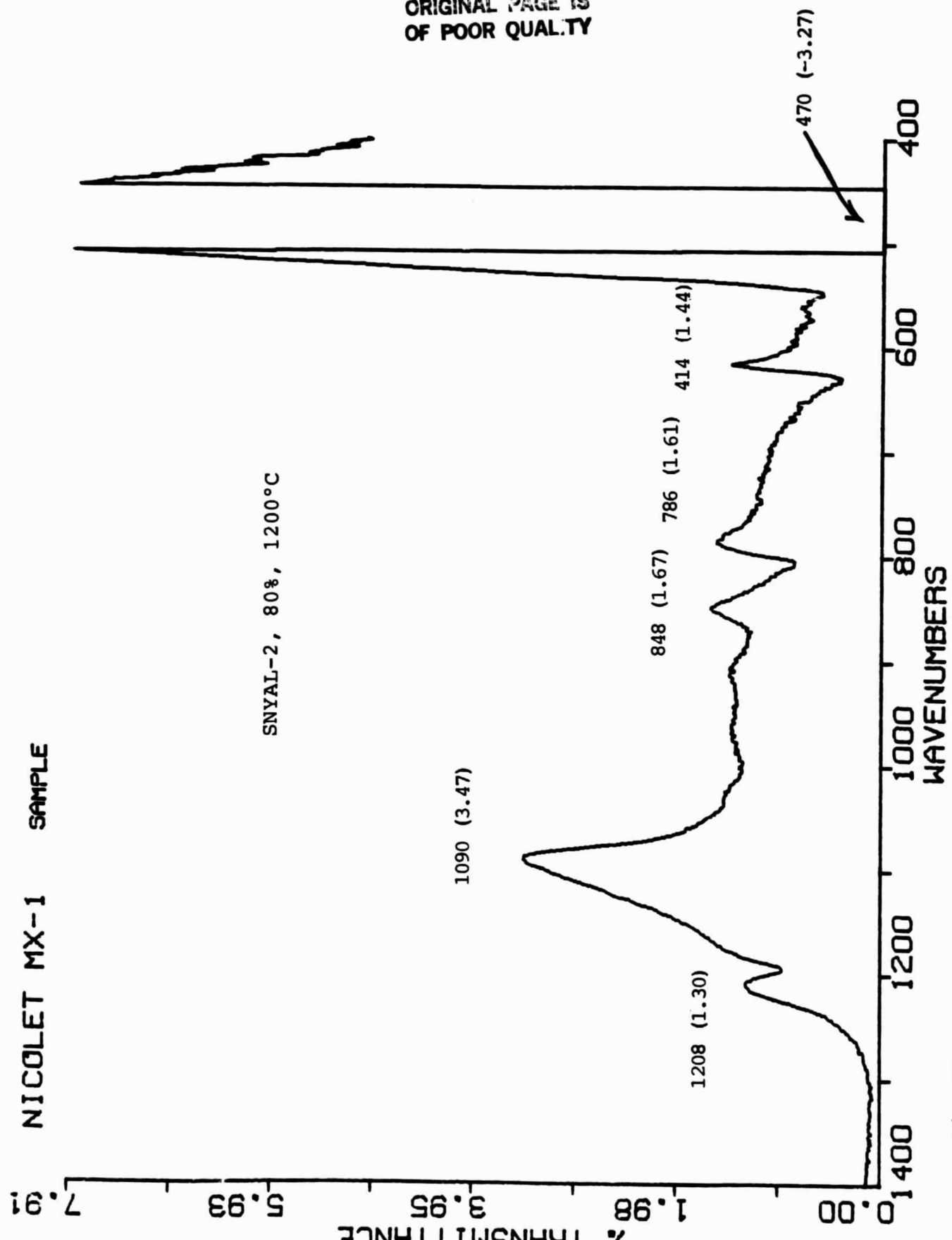


Fig. 11.

NS= 960
SC= 0
PF= 100
DF= 1.00
GAN 8

ORIGINAL PAGE IS
OF POOR QUALITY

PRECEDING PAGE BLANK NOT FILMED

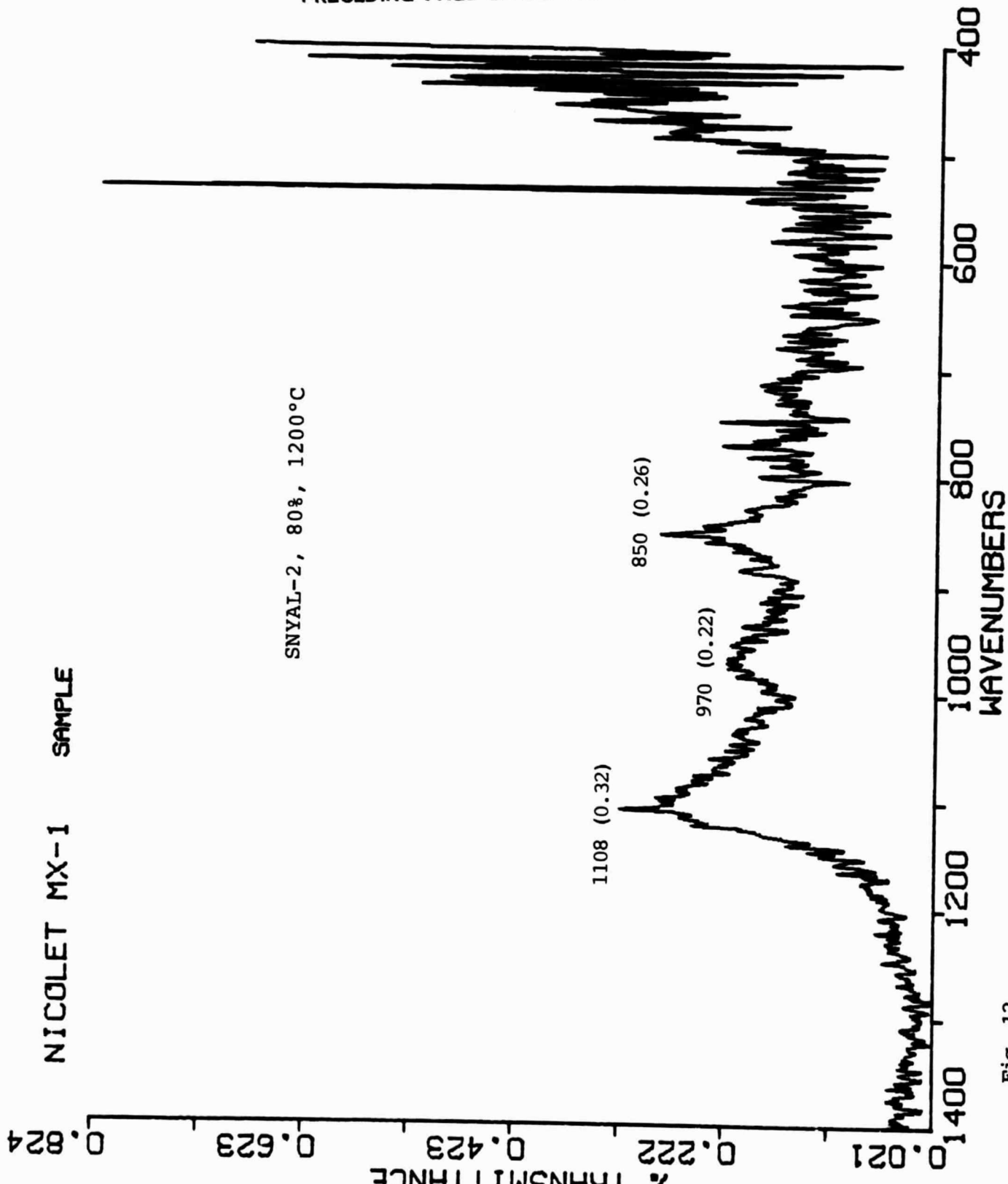


Fig. 12

NS= 960
SC= 0
PF= 100
DF= 1.00
GAN 8

ORIGINAL PAGE IS
OF POOR QUALITY

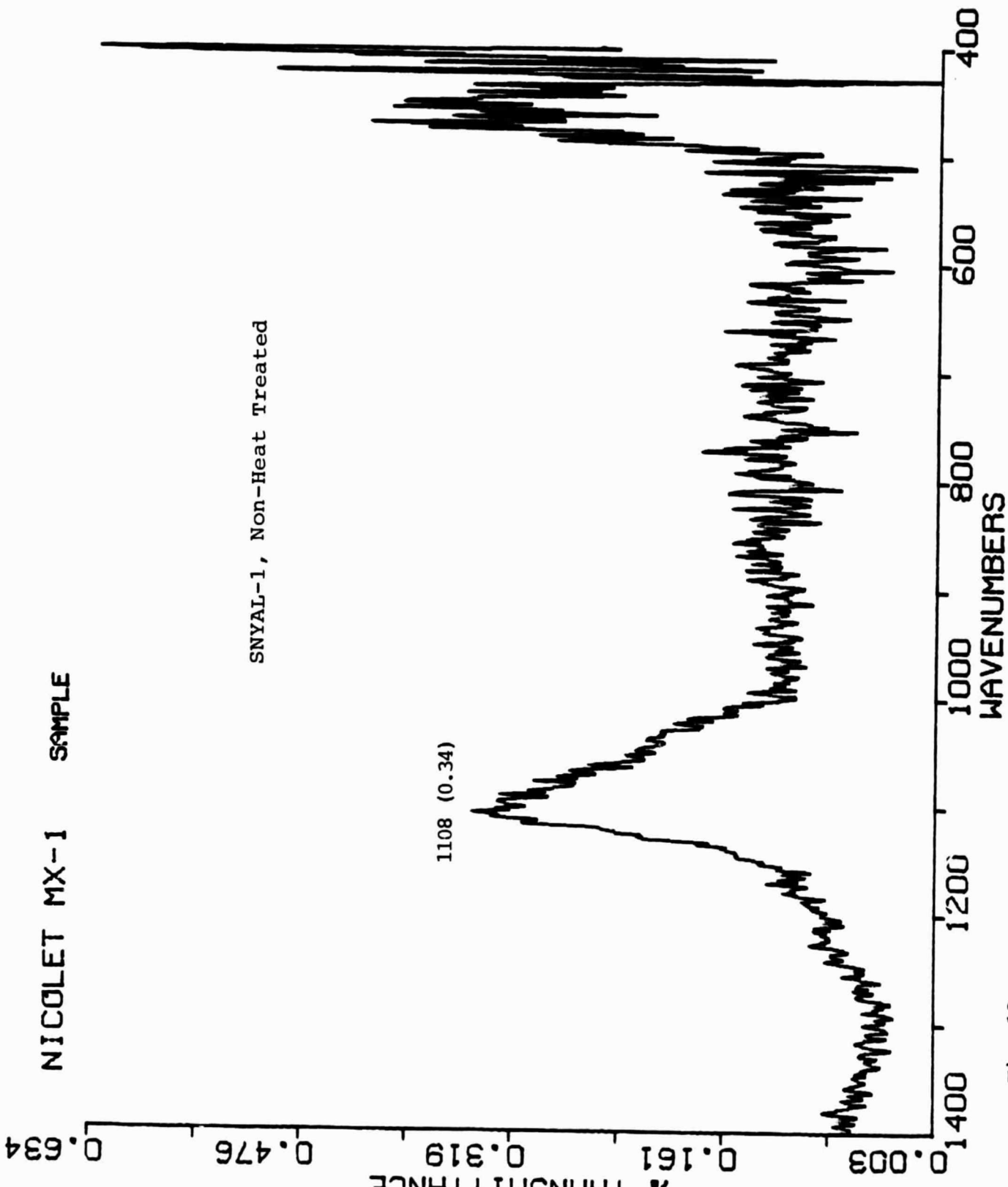


Fig. 13

TABLE V. 4-PT BEND STRENGTH OF SNYAL SERIES

Material	Room Temperature Strength (psi)			1370°C Strength		
	No Heat Treatment	1000°C 10 Hrs.	1200°C 10 Hrs.	No Heat Treatment	1000°C 10 Hrs.	1200°C 10 Hrs.
SNYAL-2%	70,080 (483 MPa)	79,680 (550 MPa)	48,000 (331 MPa)	3,045 (21 MPa)	2,393 (16 MPa)	3,335 (23 MPa)
SNYAL-4%	98,880 (682 MPa)	77,760 (536 MPa)	85,440 (589 MPa)	6,924 (48 MPa)	7,903 (54 MPa)	7,830 (54 MPa)
SNYAL-6%	95,040 (655 MPa)	88,320 (609 MPa)	88,320 (609 MPa)	13,050 (90 MPa)	8,338 (58 MPa)	12,108 (84 MPa)
SNYAL-8%	69,120 (477 MPa)	21,120* (146 MPa)	113,280 (781 MPa)	16,095 (111 MPa)	18,705 (129 MPa)	20,010 (138 MPa)

*Specimen contained crack prior to loading

ORIGINAL PAGE IS
OF POOR QUALITY

TABLE VI. RATIO OF HIGH TEMPERATURE (1370°C)
TO ROOM TEMPERATURE BEND STRENGTH

Material	No Heat Treatment	1000°C 10 Hrs.	1200°C 10 Hrs.
SNYAL-2%	.04	.03	.07
SNYAL-4%	.07	.10	.09
SNYAL-6%	.14	.09	.13
SNYAL-8%	.23	-	.17

TABLE VII. RATIO OF HIGH TEMPERATURE (1370°C) STRENGTH
AFTER HEAT TREATMENT TO UNHEAT TREATED ROOM
TEMPERATURE STRENGTH.

Material	1000°C 10 Hrs.	1200°C 10 Hrs.
SNYAL-2%	.03	.05
SNYAL-4%	.08	.08
SNYAL-6%	.09	.13
SNYAL-8%	.27	.29

8% Al_2O_3 material. Heat treatment at 1200°C did not enhance the strength of the other compositions. The most important finding is the improved high temperature strength of the heat treated samples with 8% Al_2O_3 , Table V. There is almost a 7X improvement in high temperature strength for the 1200°C/10 hr heat treated 8% Al_2O_3 samples over the values for the 2% Al_2O_3 material. This finding indicates that an optimization of the devitrification schedule of the 8% Al_2O_3 -15% Y_2O_3 material may yield even more significant advances in the high temperature performance of this material. Other work in this program (paper #6) shows that oxidation resistance is also greatly improved with this material. Consequently, extension of this work should be pursued in order to optimize thermal induced devitrification on the oxidation resistance 8% Al_2O_3 material.

References

1. G. E. Gazza, "Effect of Yttria Additions in Hot-Pressed Si_3N_4 ," Am. Ceram. Soc. Bull., 54(9) 778-81 (1975).
2. A. Tsuge, H. Kudo, and K. Komeya, "Reaction of Si_3N_4 and Y_2O_3 in Hot-Pressing," J. Am. Ceram. Soc. 57(6) 269-70 (1974).
3. J. Thomas Smith and Carr Lane Quackenbush, "Phase Effects in Si_3N_4 Containing Y_2O_3 or CeO_2 ": I and II, Am. Ceram. Soc. Bull. 59(5) 529-532 and 533-536 (1980).
4. A. Tsuge, K. Nishida, and M. Komatsu, "Effects of Crystallizing the Grain-Boundary Glass Phase on the High Temperature of Hot-Pressed Si_3N_4 Containing Y_2O_3 ," J. Am. Ceram. Soc. 58(7-8) 323-26 (1975).
5. R. E. Loehman and D. J. Rowcliffe, "Sintering of Si_3N_4 - Y_2O_3 - Al_2O_3 ," J. Am. Ceram. Soc. 63(3-4) 144-148 (1980).
6. R. K. Willis, S. Holmquist, J. M. Wimmer, and J. A. Cunningham, "Phase Relations in the System Si_3N_4 - Y_2O_3 - SiO_2 ," J. Mater. Sci. 11(7) 1305-1309 (1976).

EFFECT OF Y_2O_3 and Al_2O_3 ON THE OXIDATION
RESISTANCE OF Si_3N_4

by

L. L. Hench*, P. N. Vaidyanathan*, and Sunil Dutta**

ABSTRACT

Oxidation of cold pressed and sintered Si_3N_4 containing 15 w/o Y_2O_3 and 2, 4, 6 and 8% Al_2O_3 is observed at temperatures as low as 1000°C with infrared reflection spectroscopy. Concentrations of Al_2O_3 >4% greatly retard the rate of oxidation and alter the mechanism of surface attack by promoting formation of a glassy layer on the surface containing mixed oxynitride bonds. The glassy layer retards heterogeneous attack and reduces the effect of an oxidation transition temperature between 1000°C and 1100°C for these materials.

*Ceramics Division, Department of Materials Science and Engineering,
University of Florida, Gainesville, Florida.

**NASA Lewis Research Center, Cleveland, Ohio

Introduction

A number of investigations have shown that use of Y_2O_3 as a densification aid in Si_3N_4 materials can improve high temperature strengths relative to Si_3N_4 containing MgO ¹⁻⁷. However, instability of certain grain boundary compositions make some $Si_3N_4 + Y_2O_3$ materials susceptible to structural degradation under oxidizing conditions.^{8,9} The accelerated oxygen attack occurs at or below a transition temperature (T_c)¹⁰. Above T_c the oxidation kinetics are parabolic with time and the oxide layer formed is dense, coherent and protective¹⁰. Below T_c , oxidation kinetics are linear, the oxide layer has open, connected porosity and is nonprotective¹⁰.

Additions of Al_2O_3 to the $Si_3N_4 + Y_2O_3$ materials suppresses the destructive low temperature oxidation¹⁰. It is proposed that this is due to formation of a glassy surface phase which spreads at a low temperature to form a dense, pore-free surface layer¹⁰.

The objective of this study is to examine the effects of Al_2O_3 content on the low temperature oxidation of $Si_3N_4 + 15\% Y_2O_3$. This composition is in the $Si_3N_4-Y_2O_3$ compositional field which shows minimal oxidation resistance due to formation of the deleterious $YSiO_2N$ phase¹⁰. However, addition of Al_2O_3 both aids in the formation of a grain boundary liquid^{9,11,12} and inhibits crystallization of the g.b. phase⁷. Thus, a study of the effects of progressive concentrations of Al_2O_3 to $Si_3N_4 + 15\% Y_2O_3$ may yield an understanding of the protective mechanism for low temperature oxidation proposed by Quackenbush and Smith¹⁰ if a glassy surface phase is involved.

The experimental approach used is analysis of the oxidized surface with infrared reflection analysis (IRRS). Previous investigation of oxidized silicon nitride with this method showed that two major modes of attack were present. Si_3N_4 with MgO additives generally showed a uniform degradation of the IRRS spectrum whereas Si_3N_4 with ZrO_2 showed that a glassy surface layer developed which inhibited oxidation and preserved the strength of the material^{13,14}.

Experimental Procedure

Four compositions of $\text{Si}_3\text{N}_4 + \text{Y}_2\text{O}_3$ and Al_2O_3 (Table I) were prepared as follows:

Commercial grade Si_3N_4 , Y_2O_3 , and Al_2O_3 powders were used in the fabrication studies. An impurity analysis and the sources of the "as-received" powders are shown in Table II. Si_3N_4 and Al_2O_3 powders were a higher purity with respect to metal contaminants. Y_2O_3 powder contained Al, Si and Fe as major impurities. The Si_3N_4 powder had an oxygen content of 2.7 wt% and a specific surface area of $11.84\text{m}^2/\text{g}$ (3-point BET method). The Si_3N_4 powder was totally amorphous; the powder particles were spherical and often agglomerated, with individual particle sizes ranging from 0.05 to 1.0 μm . Mixtures for 100 - g batches were wet milled in polyethylene bottles for 17 - 20 h. using high alumina grinding media and ethanol. The starting compositions were adjusted to allow for pick up of Al_2O_3 from the mills. After the powders were milled, the slurry was dried on a heated aluminum plate and sieved through a 60 mesh sieve to

TABLE I

MATERIAL COMPOSITIONS (WEIGHT %)

SNYA1-1	83% Si_3N_4 + 15% Y_2O_3 + 2% Al_2O_3
SNYA1-2	81% Si_3N_4 + 15% Y_2O_3 + 4% Al_2O_3
SNYA1-3	79% Si_3N_4 + 15% Y_2O_3 + 6% Al_2O_3
SNYA1-4	77% Si_3N_4 + 15% Y_2O_3 + 8% Al_2O_3

TABLE II - TRACE IMPURITY ANALYSIS OF
RAW POWDERS (ppm)

Element	Si ₃ N ₄ * SN402	Al ₂ O ₃ ⁺	Y ₂ O ₃ ⁺⁺
Al	--	Major	640
Co	50	-----	---
Cu	--	-----	---
Cr	--	-----	90
Fe	70	70	160
Mg	--	110	90
Mn	--	-----	---
Mo	--	-----	---
Ni	--	-----	---
Si	Major	154	230
Ti	--	-----	---
V	--	-----	---
W	--	-----	---
Zr	--	-----	---

----- = not determined

*GTE, Sylvania, Towanda, PA

+Lande A, Union Carbide Corporation, New York, NY

++United Mineral & Chemical Corporation, New York, NY

break up agglomerates. Seventeen grams of mixed powder was cold pressed into rectangular blocks 7.6 by 2.5 by 0.64 cm followed by cold isostatic pressing at a total pressure of 414 Mn/m^2 . The compacts were pressureless sintered in a "cold-wall" furnace at 1750°C for 2 h under nitrogen pressure of 1 atm.

Sintered specimens were machined into test bars (2.54 by 0.64 by 0.32 cm), and the surfaces were subsequently ground with a 220-grit wheel to a surface roughness of 10-15 μm in rms.

The samples were oxidized in ambient laboratory air at 1000°C and 1100°C for the following times: 5, 10, 15, 30, 45, 60, 90, 120 minutes.

Before and after oxidation all samples were examined with infrared reflection spectroscopy (IRRS) over the spectral range from 1400 cm^{-1} to 200 cm^{-1} . The spectra were calibrated to a vitreous silica standard by adjusting a shutter in the IR beam such that the peak for the Si-O-Si molecular stretching vibration at 1120 cm^{-1} was 80% reflectance.

Results

All four compositions showed nearly identical IRRS spectra, Fig. 1. Multiple scans along the four sides of each sample showed no more than $\pm 2\%$ variation in IRRS intensity, evidence of excellent homogeneity. Previous investigations of samples with varying degrees of homogeneity showed variations in IRRS intensity of as much as 60% reflection¹⁵. Thus, the present series of specimens gave highly reproducible oxidation results because of their excellent homogeneity.

Five peaks characterize the IRRS spectra of the silicon nitride samples (Fig. 1). There are two Si-N-Si molecular stretching vibrations, labeled SN_1 and SN_2 , and three Si-N-Si molecular rocking vibrations, SNR_1 , SNR_2 and SNR_3 . The location and relative intensity of these peaks is independent of the concentration of Al_2O_3 . Figure 1 also shows the IRRS spectrum of vitreous SiO_2 which consists of two primary peaks. The peak at 1120 cm^{-1} , designated S, is assigned to the Si-O-Si molecular stretching vibration¹⁶. A single peak (R) at 470 cm^{-1} is assigned to the Si-O-Si molecular rocking vibration. Thus uniform coherent oxidation of a Si_3N_4 surface should result in a gradual replacement of the five SN and SR peaks with a broadened spectrum containing only S and R peaks.

Figure 2 shows however that oxidation at 1000°C for the sample with 2% Al_2O_3 results in a gradual deterioration of the Si_3N_4 spectrum with no S or R peaks appearing. The progressive decrease in intensity of both molecular stretching and molecular rocking peaks with no shift in peak location can generally be ascribed to increased scattering of the IR beam incident on the surface^{17,18}.

Increasing the Al_2O_3 content to 4 weight % or greater provides a remarkable increase in protection of the surface, Fig. 3. Very little reduction in the relative intensity of the spectrum of samples with 4, 6 and 8% Al_2O_3 is observed after 120 minutes oxidation at 1000°C . In fact the major SN_2 stretching peak is increased, due to a reduction in scattering from surface features that are covered with the glassy oxidation layer.

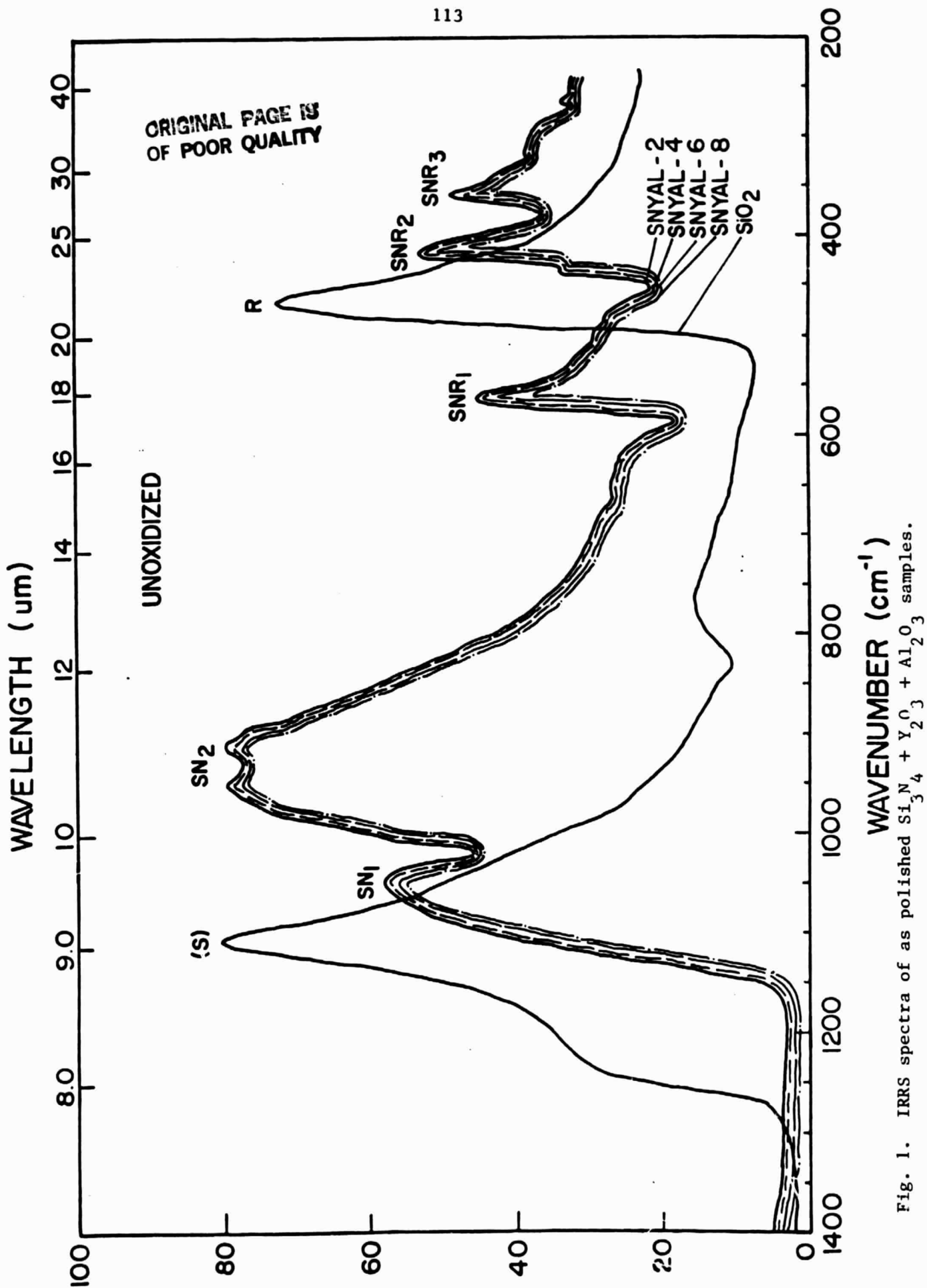


Fig. 1. IRRS spectra of as polished $\text{Si}_3\text{N}_4 + \text{Y}_2\text{O}_3 + \text{Al}_2\text{O}_3$ samples.

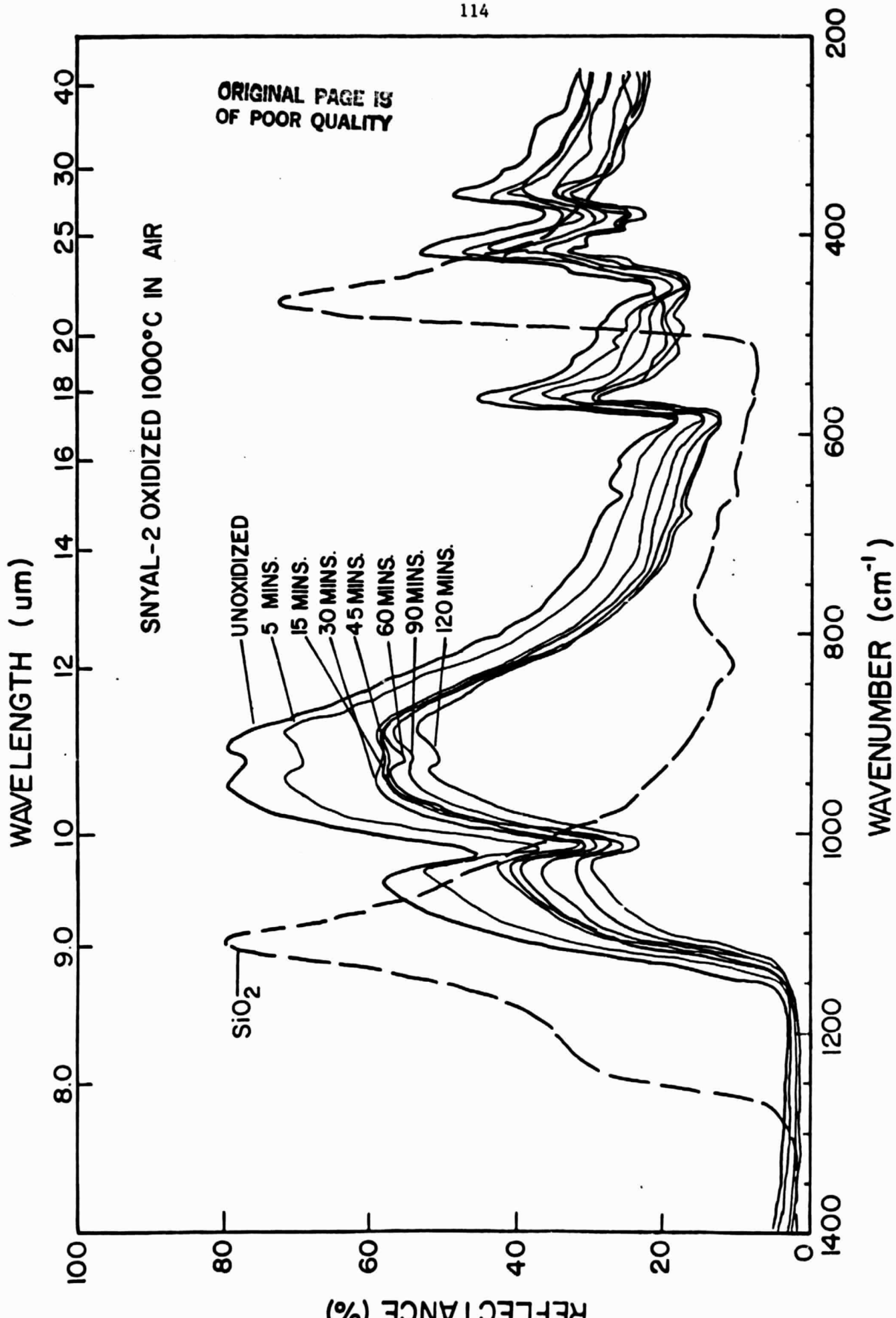


Fig. 2. IRRS spectra of $\text{Si}_3\text{N}_4 + \text{Y}_2\text{O}_3 + 2\% \text{Al}_2\text{O}_3$ sample oxidized at 1000°C .

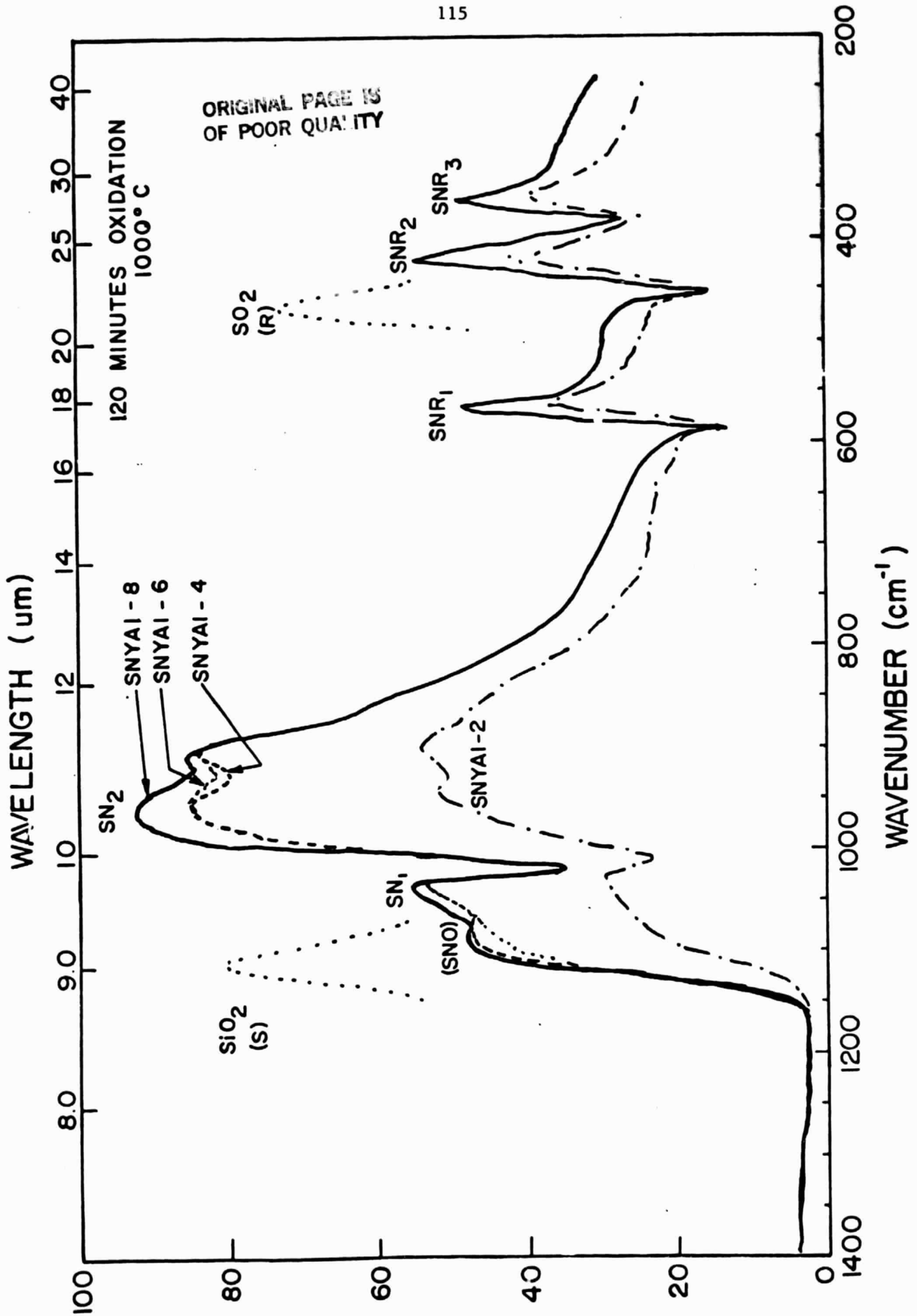


Fig. 3. IRRS spectra of $\text{Si}_3\text{N}_4 + \text{Y}_2\text{O}_3 + \text{Al}_2\text{O}_3$ samples oxidized at 1000°C for 120 mins.

An important difference is present in the SN_1 peak for the 6% and 8% Al_2O_3 samples 1000°C after oxidation. A second peak located at $1100cm^{-1}$ to $1140cm^{-1}$ has developed, Fig. 3. This change occurs between 90 and 120 minutes at 1000°C. Note however that a new peak at $470 cm^{-1}$ has not appeared during the 1000°C oxidation for any of the compositions. Consequently it is unlikely that the new peak developing near $1120 cm^{-1}$ is due to formation of Si-O-Si bonds. It is more likely to be due to mixed silicon, oxynitride vibrational species, similar to that observed for low temperature oxidized Si_3N_4 with either MgO or ZrO_2 additives¹⁹. Thus this peak is labeled SNO, in Fig. 3.

The time dependent changes of the intensity of the SN_2 (normalized to pre-oxidation intensity) and the SNO peaks for the four compositions are shown for the first 90 minutes of oxidation in Fig. 4. There is a rapid reduction of the SN_2 peak for the 2, 4 and 6% Al_2O_3 samples followed by a slower rate of attack. The 8% Al_2O_3 sample exhibits only the slower rate of attack of the SN_2 peak. For all four compositions there is no evidence of either the SNO peak, S, or R peaks during the 90 minute time period of 1000°C oxidation. After 120 minutes only the 8% Al_2O_3 sample shows a SNO peak.

Increasing the oxidation temperature to 1100°C greatly accelerates the attack of the composition containing 2% Al_2O_3 (Fig. 5). After just 15 minutes severe degradation of SN_1 , SN_2 and all three SNR peaks has occurred. In contrast, the major SN_2 peak of the 4, 6 and 8% Al_2O_3 samples has increased in reflection intensity and the $SNR_{1,2,3}$ peaks show very little alteration. The SN_1 peak of the higher Al_2O_3 samples

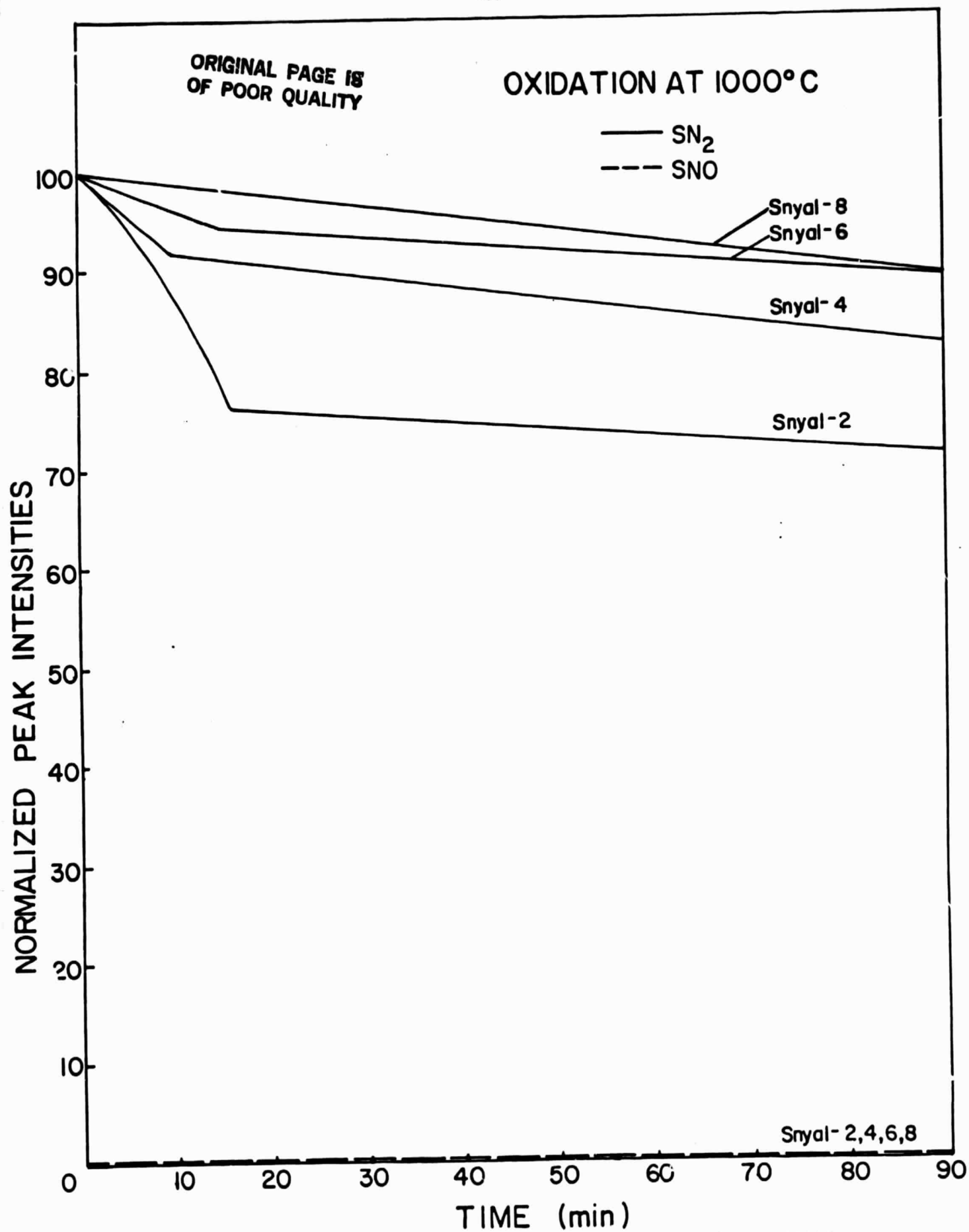


Fig. 4. Time dependent change of IRRS SN₂ peak and SNO peak due to 1000°C oxidation.

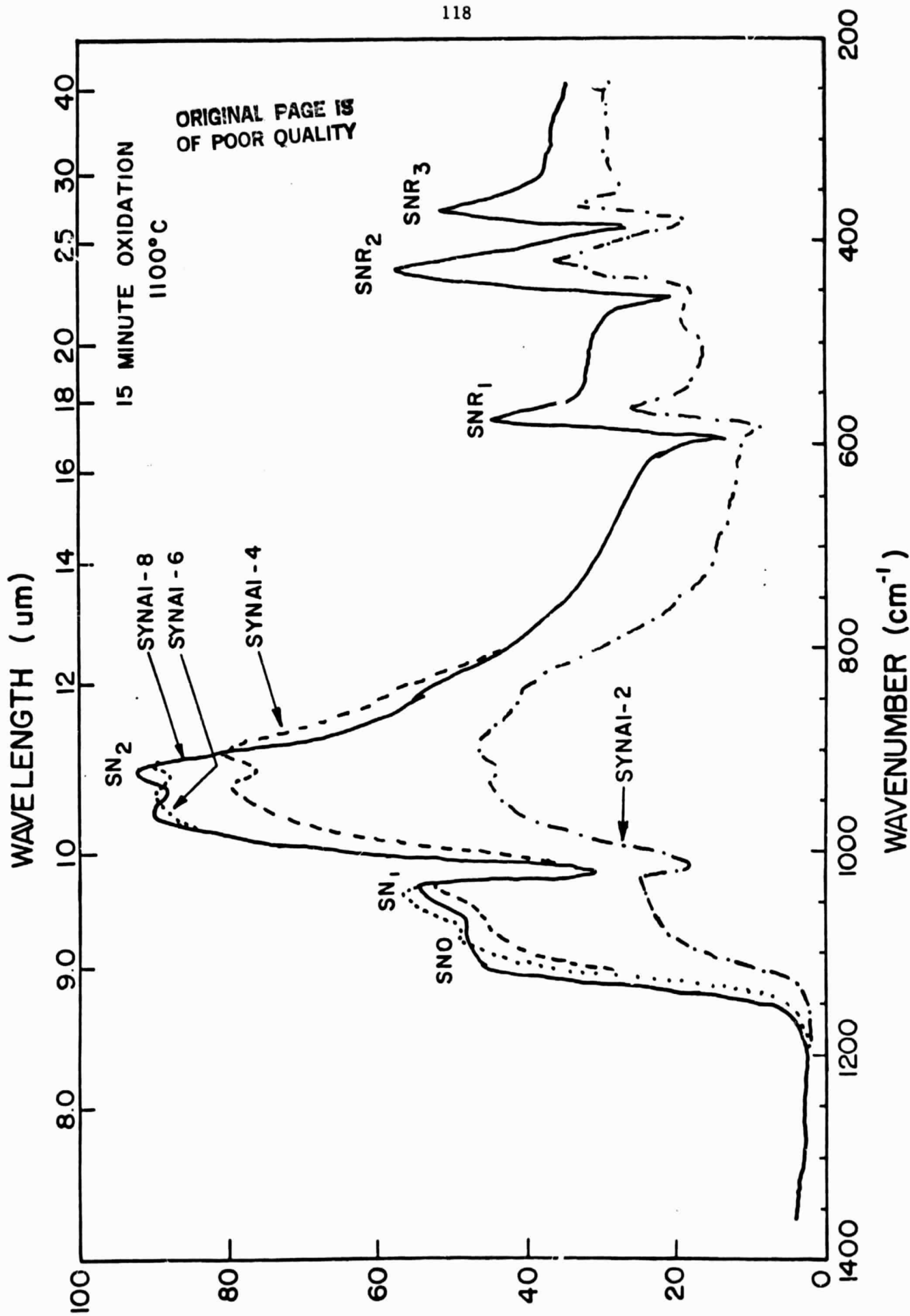


Fig. 5. IRRS spectra of $\text{Si}_3\text{N}_4 + \text{Y}_2\text{O}_3 + \text{Al}_2\text{O}_3$ samples oxidized at 1100°C for 15 mins.

has developed into a doublet due to formation of the SNO silicon-oxynitride bonds in the surface. These bonds appear within 5 minutes of 1100°C oxidation of the 8% Al₂O₃ sample (Fig. 6) and are associated with the longer term protection of the surface. After 60 minutes some deterioration of the SN₂ peak has occurred for the 8% Al₂O₃ material (Fig. 7) but the rate of attack is very low (Fig. 6). The intensity of the SNO peak remains approximately constant as the SN₁ peak is completely replaced by the SNO peak as discussed in a subsequent paper on high temperature oxidation of Si₃N₄¹⁹.

The materials with 4% and 6% Al₂O₃ also show appearance of the SNO peak by 15 minutes oxidation (Fig. 5). The peak remains stable for a short period of time for these compositions (Fig. 6) but is eventually decreased in intensity (Figs. 6,7) along with the SN₂ peak. This is due to a increase in roughness and scattering of the IR beam by the surface and is an index of overall surface attack for these compositions.

Discussion

These results show that Al₂O₃ significantly increases the oxidation resistance of Si₃N₄ materials containing a high percentage of Y₂O₃. The effectiveness of the Al₂O₃ additions appears to be related to enhanced formation of a surface silicon oxynitride or mixed silicon dioxide-silicon nitride layer, associated with the SNO peak in the IRRS spectra. The fact that an SiO₂ related R peak does not develop at 470cm⁻¹ during formation of the SNO peak favors the assignment of the new 1100cm⁻¹ and 1140cm⁻¹ is a mixed silicon oxynitride species.

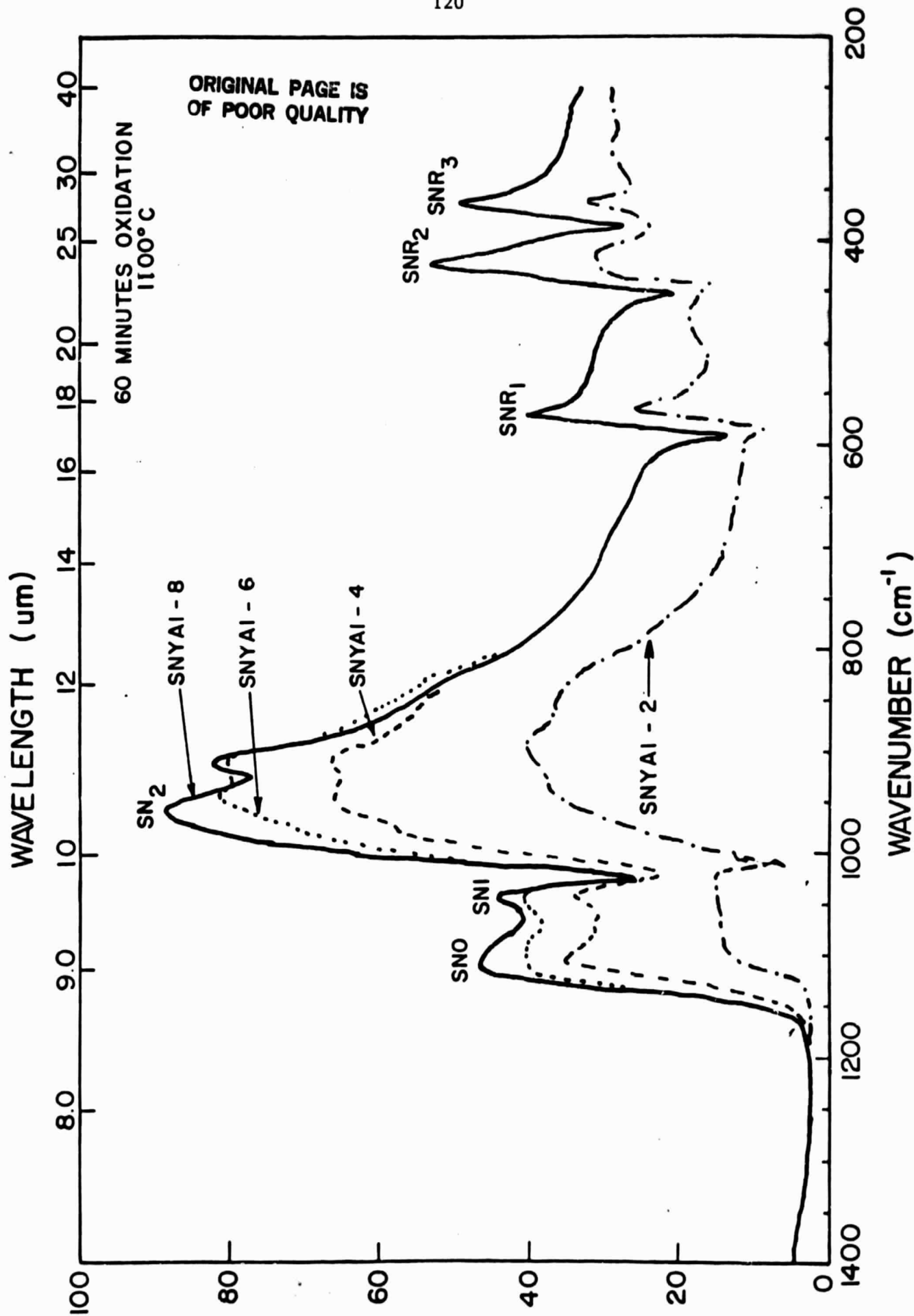


Fig. 6. Time dependent change of IRRS SN₂ peak and SNO peak due to 1100°C oxidation.

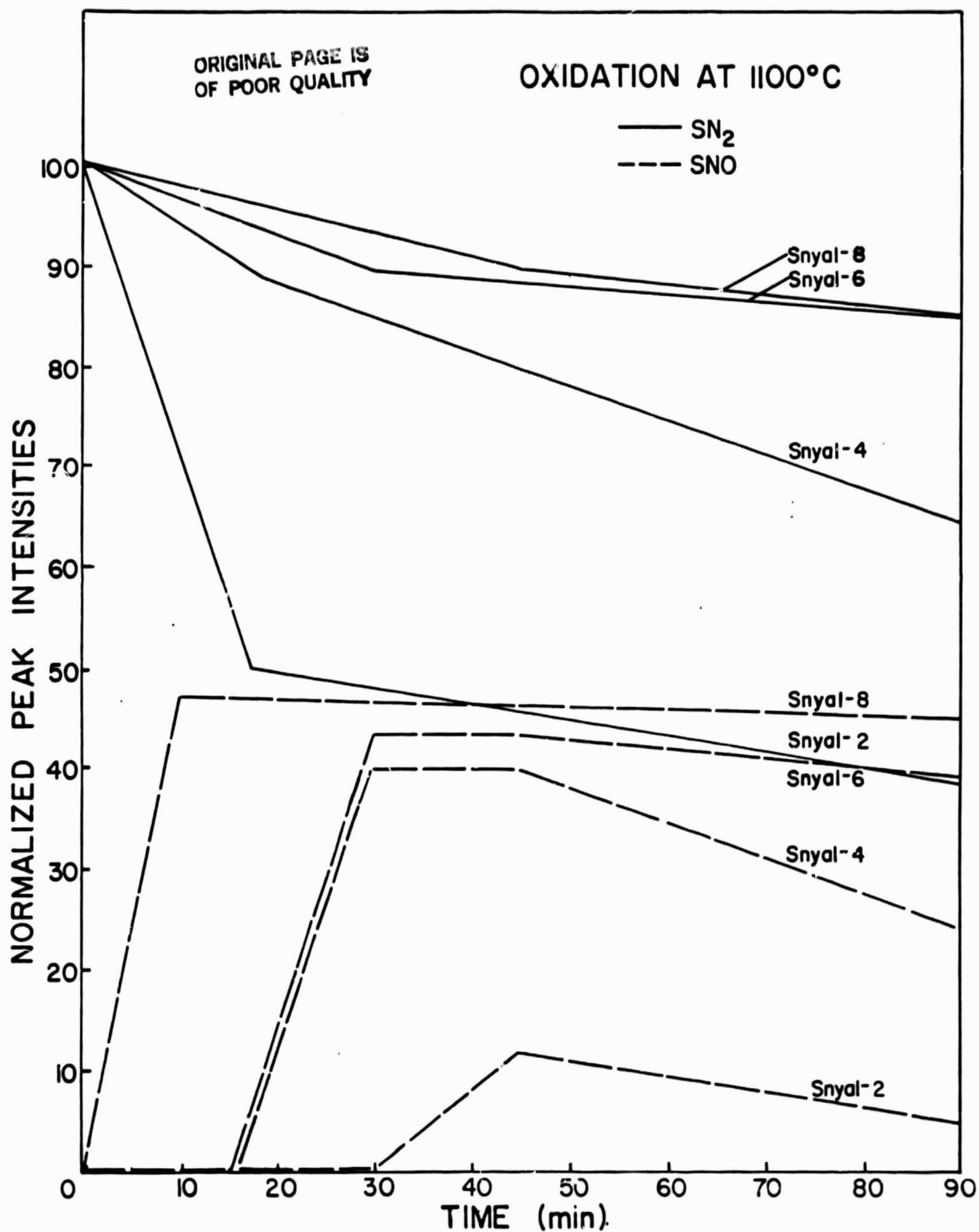


Fig. 7. IRRS spectra of $\text{Si}_3\text{N}_4 + \text{Y}_2\text{O}_3 + \text{Al}_2\text{O}_3$ samples oxidized at 1100°C

A critical concentration of Al_2O_3 is necessary to form the SNO peak and provide protection against attack of the Si_3N_4 structure. Without the critical (>4%) amount of Al_2O_3 , surface attack is observed, Fig. 2, as quickly as 5 minutes at 1000°C . The general deterioration of the IRRS spectra is concluded to be due to roughening of the surface indicative of heterogeneous attack of grain boundaries and formation of the porous surface layer described by Quackenbush and Smith¹⁰. When this mode of attack is initiated, it is rapid. Subsequent surface damage is a much slower process (Figs. 4 and 7).

Thus, it is proposed that the region of low temperature linear oxidation kinetics results from the onset of the heterogeneous surface attack. Addition of a critical amount of Al_2O_3 greatly retards this process even in compositions containing sufficient Y_2O_3 to be in the $\text{Si}_3\text{Y}_2\text{O}_3\text{N}_4$ field.

These processes and compositional effect appear to be the same at both 1000°C and 1100°C confirming previous the conclusion¹⁰ that development of surface glassy phases greatly reduces the importance of an oxidation transition temperature for these materials.

Conclusions

Al_2O_3 additions of 4% or greater greatly retard oxidation of Si_3N_4 + 15% Y_2O_3 even though this composition is in the field where the destructive $\text{Si}_3\text{Y}_2\text{O}_3\text{N}_4$ phase can form. The oxidation protection is due to formation of a surface layer containing mixed silicon oxynitride bonds which retards a heterogeneous mode of attack of the Si_3N_4

structure. The mechanisms and compositional effects are the same for both 1000°C and 1100°C indicating that any oxidation transition temperature is masked by the formation of the protective surface layer.

Acknowledgement

The authors gratefully acknowledge partial financial support of NASA Grant No. NSG 3254.

REFERENCES

1. G. E. Gazza, "Hot-Pressed Si_3N_4 ", "J. Am. Ceram. Soc. 56 [12] 662 (1973).
2. G. E. Gazza, "Effect of Yttria Additions on Hot-Pressed Si_3N_4 " "Am. Ceram. Soc. Bull., 54 [9] 778-81 (1975).
3. A. Tsuge, H. Kudo, and K. Komeya, "Reaction of Si_3N_4 and Y_2O_3 in Hot-Pressing," "J. Am. Ceram. Soc., 57 [6] 269-70 (1974).
4. A. Tsuge, K. Nishida, and M. Komatsu, "Effect of Crystallizing the Grain-Boundary Glass Phase on the High-Temperature Strength of Hot-Pressed Si_3N_4 Containing Y_2O_3 " *ibid.*, 58 [7-8] 323-26 (1975).
5. G. Q. Weaver and J. W. Lucek, "Optimization of Hot-Pressed Si_3N_4 - Y_2O_3 Materials," "Am. Ceram. Soc. Bull., 57 [12] 1131-34, 1136 (1978).
6. G. E. Gazza, H. Knoch, and G. D. Quinn, "Hot-Pressed Si_3N_4 with Improved Thermal Stability," *ibid.*, [11] 1059-60.
7. J. T. Smith and C. L. Quackenbush, "Purity Effects in Si_3N_4 Containing Y_2O_3 or CeO_2 : I, Strength," "J. Am. Ceram. Soc. Bull., 59 [5], pp. 529-32, 537 (1980).
8. F. F. Lange, S. C. Singhal, and R. C. Kuznicki, "Phase Relations and Stability in the Si_3N_4 - SiO_2 - Y_2O_3 Pseudoternary System," "J. Am. Ceram. Soc., 60 [5-6] 249-52 (1977).
9. J. T. Smith and C. L. Quackenbush, "A Study of Sintered Si_3N_4 Compositions with Y_2O_3 and Al_2O_3 Densification Additives"; pp. 426-42 in Proceedings of the International Symposium on Factors in Densification and Sintering of Oxide and Non-oxide Ceramics, Hakone, Japan, October 3-6, 1978.

10. J. T. Smith and C. L. Quackenbush, "Phase Effects in Si_3N_4 Containing Y_2O_3 or CeO_2 :II, Oxidation," *J. Am. Ceram. Soc. Bull.*, 59 [5], pp. 533-6 (1980).
11. A. Tauge and K. Nishida, "High Strength Hot-Pressed Si_3N_4 with Concurrent Y_2O_3 and Al_2O_3 Additions," *Am. Ceram. Soc. Bull.*, 57 [4] 424-26, 431 (1978).
12. M. Mitomo, "Sintering of Si_3N_4 with Al_2O_3 ," *Yogyo Kyokai Shi.* 85 [8] 50-54 (1977).
13. J. M. Barrett, L. L. Hench, S. Bernstein, D. E. Clark and S. W. Freiman, "Effect of Heat Treatment on the Oxidation of Hot Pressed Si_3N_4 as Determined by Infrared Reflection Analysis," *Proceedings 2nd and 3rd Annual Conferences on Composites and Advanced Materials*, Am. Cer. Soc., Columbus, Oh, pp. 481-488, (1980).
14. L. L. Hench, F. Ohuchi, S. W. Freiman, C. C. Wu and K. R. McKinney, "Infrared Reflection Analysis of Si_3N_4 Oxidation," *Proceedings of Composites and Advanced Materials Conference*, Am. Ceram. Soc. (1980), Cocoa Beach, Florida.
15. L. L. Hench, "Non-destructive Analysis of Si_3N_4 Structural Variability", to be published.
16. D. M. Sanders, W. B. Person and L. L. Hench, "Quantitative Analysis of Glass Structure Using Infrared Reflection Spectra," *Appl. Spectroscopy*, 28 [3] (1974) 247-255.
17. D. M. Sanders and L. L. Hench, "Surface Roughness and Glass Corrosion," *Bull. Am. Cer. Soc.*, 52 [9] (1973) 666-669.

18. D. E. Clark, E. C. Ethridge, M. F. Dilmore and L. L. Hench,
"Quantitative Analysis of Corroded Glass Using IRRS Frequency
Shifts," *Glass Technol.*, 18 [4] (1977) 637-656.
19. L. L. Hench, "Use of New Surface Physics for Controlling the
Physical Properties of Ceramics," *Proceedings Science of Ceramics*
10, September 2-4, 1979, Munich, Germany.